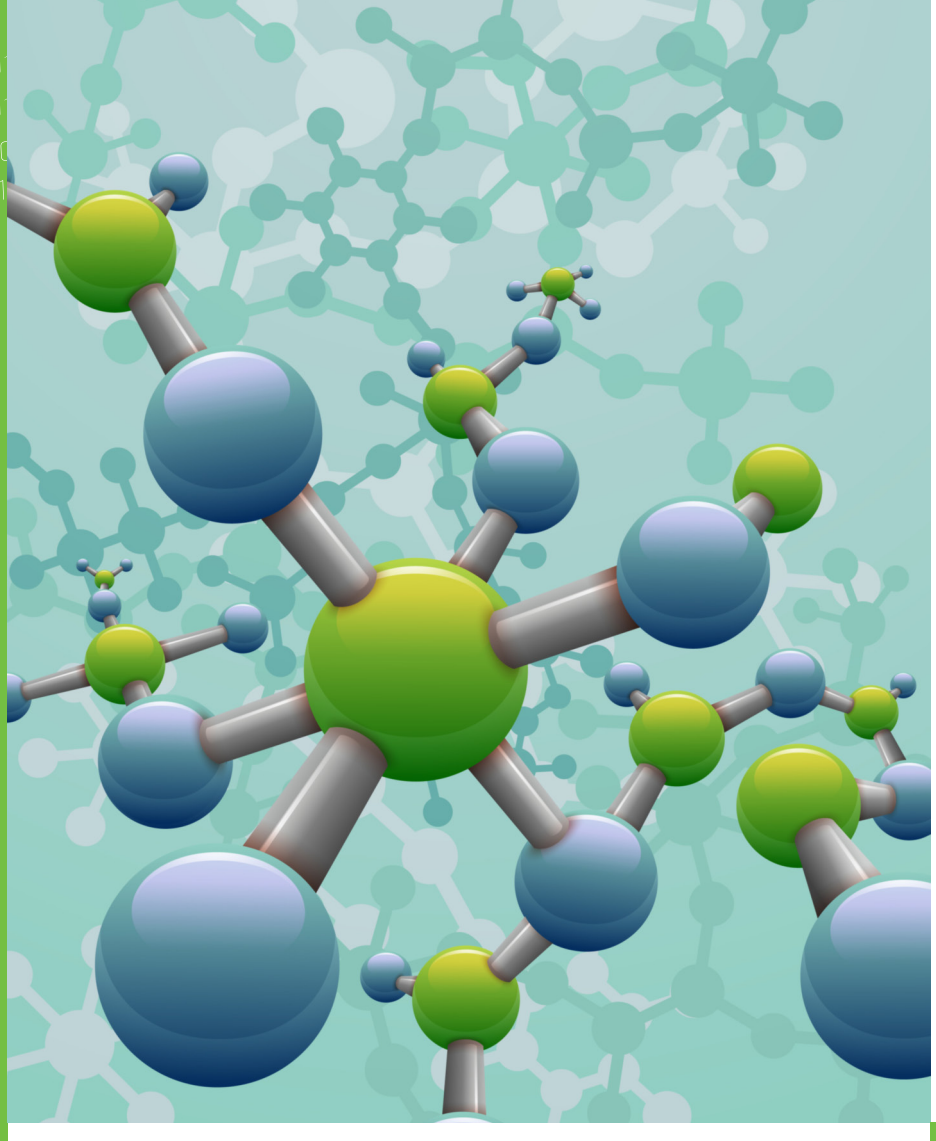

SCIENCE • TECHNOLOGY • RESEARCH HIGHLIGHTS • VISIONS •

Dissertation
97

Improving sealing, electrical contacts, and corrosion resistance in solid oxide fuel cell stacks

Markus Rautanen

VTT

VTT SCIENCE 97

Improving sealing, electrical contacts, and corrosion resistance in solid oxide fuel cell stacks

Markus Rautanen

Thesis for the degree of Doctor of Science to be presented with due permission of the Aalto University School of Science for public examination and criticism in Auditorium K216, at Aalto University (Espoo, Finland), on the 8th of June, 2015 at 12 noon.

ISBN 978-951-38-8313-3 (Soft back ed.)
ISBN 978-951-38-8314-0 (URL: http://www.vtt.fi/publications/index.jsp)

VTT Science 97

ISSN-L 2242-119X
ISSN 2242-119X (Print)
ISSN 2242-1203 (Online)

JULKAISIJA – UTGIVARE – PUBLISHER

Teknologian tutkimuskeskus VTT Oy
PL 1000 (Tekniikantie 4 A, Espoo)
02044 VTT
Puh. 020 722 111, faksi 020 722 7001

Teknologiska forskningscentralen VTT Ab
PB 1000 (Teknikvägen 4 A, Esbo)
FI-02044 VTT
Tfn +358 20 722 111, telefax +358 20 722 7001

VTT Technical Research Centre of Finland Ltd
P.O. Box 1000 (Tekniikantie 4 A, Espoo)
FI-02044 VTT, Finland
Tel. +358 20 722 111, fax +358 20 722 7001

Juvenes Print, Tampere 2015

Preface

The work presented in this thesis has been carried out in VTT Technical Research Centre of Finland between 2008 and 2014. Financial support from VTT Technical Research Centre of Finland, the Fuel Cells and Hydrogen Joint Undertaking and TEKES – the Finnish Funding agency for Innovation is acknowledged.

The work presented in this thesis has been completed with the help of many persons. I would like to thank my instructors Jari Kiviaho and Olli Himanen for encouraging me in starting doctoral studies in the first place and for the support that I have received over the years. I would also like to thank Peter Lund for accepting me as a student in the department of applied physics and being very flexible with my studies. I want to thank the whole fuel cell team at VTT, especially Jari Kiviaho, Olli Himanen, Olivier Thomann, Kari Koskela, Johan Tallgren and Valtteri Pulkkinen for close collaboration and for the relaxed atmosphere.

For my parents, Marja-Leena and Pentti: thank you for always encouraging me to study while never pushing me towards any particular profession or career. Certainly the most efficient person in taking my mind of work has been my son Otso – thank you for that. The most grateful I am to my wife Tanja. With you I have had the privilege to share many of the best moments in my life. Hopefully there is still many more awaiting behind the horizon.

Espoo, 14.5.2015
Markus Rautanen

Academic dissertation

Supervising professor

Professor, Dr. Peter Lund
Department of Applied Physics
Aalto University School of Science
Espoo, Finland

Thesis advisors

Dr. Jari Kiviaho
Chief Research Scientist
Fuel Cells
VTT Technical Research Centre of Finland Ltd
Espoo, Finland

D.Sc. Olli Himanen
Senior Research Scientist
Fuel Cells
VTT Technical Research Centre of Finland Ltd
Espoo, Finland

Reviewers

Dr. Tero Hottinen
General Manager
Business Innovation
Wärtsilä
Helsinki, Finland

Dr. Bin Zhu
Assosiate Professor
Advanced fuel cell and solar cell group
Royal Institute of Technology (KTH)
Stockholm, Sweden

Opponent

Professor, PhD Alan Atkinson
Department of Materials
Imperial College
London, United Kingdom

List of publications

This thesis is based on the following original publications, which are referred to in the text as I–VI. The publications are reproduced with kind permission from the publishers.

I. **Rautanen, Markus**; Himanen, Olli; Saarinen, Ville; Kiviaho, Jari
Compression properties and leakage tests of mica-based seals for SOFC stacks
Fuel Cells. Vol. 9 (2009) No: 5, 753–759

II. **Rautanen, Markus**; Pulkkinen, Valtteri; Tallgren, Johan; Himanen, Olli; Kiviaho, Jari
Effects of the first heat up procedure on mechanical properties of solid oxide fuel cell sealing materials
Journal of Power Sources. Elsevier. Vol. 284 (2015), 511–516

III. Hoyes, John; **Rautanen, Markus**
SOFC sealing with Thermiculite 866 and Thermiculite 866 LS
ECS Transactions. Electrochemical Society. Vol. 57 (2013) No: 1, 2365–2374

IV. **Rautanen, Markus**; Thomann, Olivier; Himanen, Olli; Tallgren, Johan; Kiviaho, Jari
Glass coated compressible solid oxide fuel cell seals
Journal of Power Sources. Elsevier. Vol. 247 (2014), 243–248

V. Thomann, Olivier; Pihlatie, Mikko; **Rautanen, Markus**; Himanen, Olli; Lagerbom, Juha; Mäkinen, Maija; Varis, Tommi; Suhonen, Tomi; Kiviaho, Jari
Development and application of HVOF sprayed spinel protective coating for SOFC interconnects
Journal of Thermal Spray Technology. ASM; Springer. Vol. 22 (2013) No: 5, 631–639

VI. Thomann, Olivier; **Rautanen, Markus**; Himanen, Olli; Tallgren, Johan; Kiviaho, Jari
Post-experimental analysis of a SOFC stack using hybrid seals
Journal of Power Sources. Elsevier. Vol 274 (2015), 1009–1015

Author’s contributions

For Publications I and IV, the author had primary responsibility for all parts of the publication.

For Publication II, the author had primary responsibility for the design of experiments, interpretation of results, and writing.

For Publication III, the author conducted part of the measurements and actively participated in the writing process.

For Publications V and VI, the author actively participated in analysis of the results and in the writing process.

Contents

List of symbols

A	Anode
AFC	Alkaline fuel cell
ASR	Area specific resistivity
BSE	Back scattered electron imaging
c	Concentration
C	Cathode
CEV	Chemically exfoliated vermiculite
cross	Cross leak between anode and cathode
D	Diffusion coefficient
EDS	Energy dispersive spectroscopy
F	Faraday constant
ΔG	Change in Gibbs free energy
H_2	Hydrogen molecule
H_2O	Water/steam molecule
HVOF	High velocity oxygen flame
I	Electrical current
J	Diffusion flux
LSCF	Lanthanum strontium cobalt ferrite, $La_xSr_{1-x}Co_yFe_{1-y}O_{3-\delta}$
LSM	Lanthanum strontium manganite, $La_{1-x}Sr_xMnO_3$
NASA	National Aeronautics and Space Administration
NTP	Normal temperature and pressure (273.15 K, 1013.25 mbar)
OCV	Open circuit voltage

p	Pressure
$\dot{Q}$	Flow
R	Gas constant
t	Time
T	Temperature
PAFC	Phosphoric acid fuel cell
PEMFC	Proton electrolyte membrane fuel cell
SEM	Scanning electron microscopy
SOFC	Solid oxide fuel cell
TEC	Thermal expansion coefficient
TOT	Total
V	Volume
X	Fraction
YSZ	Ytria stabilized zirconia

1. Introduction

1.1 Background

Today's world is dominated by fossil fuel-based energy production. It is at the moment under debate when exactly these non-renewable sources of energy will run out, but it is very clear that sooner or later an energy system based on renewable energy sources needs to be established. Before the balance of energy production shifts to renewable energy sources, energy production efficiency should be of high concern, to make sure that both renewable and non-renewable energy is utilized with the highest possible efficiency. Fuel cells can contribute to energy production during and after this change: they can directly convert chemical energy of fuel and oxidant to electricity with high efficiency and low emissions. Fuel cells can operate with a variety of fuels such as natural gas, biogas or hydrogen.

The fuel cell is an invention first mentioned in 1839 by German physicist William Schönbein in The London and Edinburgh Philosophical Magazine and Journal of Science [1]. However, it took more than a century for the technology to reach sufficient maturity for the first significant applications to emerge. Since the 1950s, fuel cells have played a part in, for example, NASA's space flight programmes, producing electricity and water during space missions [2]. Development of fuel cell-powered vehicles started in the early 1990s, and several manufacturers have now completed field trials, and market entry is expected during 2015 [3]. In the field of stationary power production, fuel cells are also gaining more ground and installations of fuel cell power plants have exceeded 180 MW with a fast growth rate of about 50 MW of new installations in 2013 [4].

Fuel cells are commonly divided into different groups based on their operating temperature and electrolyte. Low-temperature fuel cells such as the polymer electrolyte fuel cell (PEMFC) and alkaline electrolyte fuel cell (AFC) are used in automotive and mobile applications. High-temperature fuel cells such as the phosphoric acid fuel cell (PAFC) and solid oxide fuel cell (SOFC) are used mostly in stationary heat and power generation, mostly due to their ability to utilize hydrocarbon fuels such as natural gas. The work presented in this thesis is focused on the solid oxide fuel cell.

Current challenges of SOFCs can be easily summarized: insufficient lifetime and high capital costs. At the moment, capital expenditure on a stationary SOFC system such as a 100 kW system offered by Bloom energy Ltd is in the order of $7000/kW, and the cost of residential CHP systems in the range of 1…10 kW is around $25000/kW [5]. This figure needs to be reduced to around $1000/kW to allow entry to non-subsidized markets [6]. At the same time, the high operating temperature of SOFCs creates challenges for the materials, causing performance degradation over the operating time. Currently, state-of-the-art SOFC stacks have a lifetime of around 5000…10000 h, which needs to be expanded to the range of 20000…40000 h [7]. The heart of any SOFC power system is a stack in which the electrochemical reactions take place. Stack cost is estimated to be around 40…60% of the total system cost [8]. Therefore, this is the area where most of the performance gains and cost reduction needs to take place.

1.2 Objectives of this thesis

The goal of the work presented in this thesis was to achieve performance and lifetime enhancement in SOFC stacks. Four major targets were set for this work:

1. A SOFC stack sealing material capable of 20% compression using maximum of 1 MPa compressive stress
2. Sealing material capable of maintaining leak levels below 1% of inlet fuel flow using a maximum of 1 MPa compression
3. A decrease in-stack electrical contact losses below 1% at 0.3 Acm^{-2} current density
4. A target stack lifetime of 10 000 h with reduction of chromium evaporation from interconnect steels and no significant corrosion between other stack materials.

The compression of the sealing materials affects stack design and manufacturing of other components around the seal. For example, if the sealing material's ability to compensate for manufacturing variation of other components is high, this increases the manufacturing yield of other components, as their dimensional tolerances can be wider. This naturally has a direct influence on the manufacturing costs of the whole stack. For example, the anode support of the SOFC cell manufactured via tape casting route has a thickness variation of the order of 1…5% [9,10]. To be sure that cell-to-cell thickness variation within a stack does not significantly affect the apparent stress on the seal and therefore gas tightness, the compressibility of the seals needs to be significantly higher than the cell-to-cell thickness variation. As shown in chapter three of this work, compressibility of conventional compressible sealing materials such as mica papers is only in the order of 3% per megapascal of applied stress. This calls for stress levels of at least several megapascals, which are impractical as material thicknesses should

be reduced to gain cost savings. Therefore a target of 20% compression at 1 MPa was set for the sealing development work.

Any loss of electrical power capability inside the fuel cell stack is away from the actual net power production of the whole system. The second goal of this work is related to decreasing in-stack leakage which directly influences the electrical efficiency of the cell, as less fuel is wasted in leakage-induced burning. Therefore an overall target for the sealing material to be developed was a leak rate of less than 1% of inlet fuel with 1 MPa of compression and 20% of compressibility.

The third goal also focuses on improving the electrical efficiency of the stack by decreasing resistive losses inside the stack. These can occur, for example, by contact losses or corrosion-related growth of insulating oxide layers. Diminishing these contact losses below 1%, at a typical 0.3 Acm^{-2} current density of SOFC stacks, would have a beneficial effect on the electrical efficiency of the stack. The fourth goal targets an enhanced stack lifetime. If the lifetime can be improved, this will also have a beneficial impact on cost, as stack changes in a system will become less frequent. In total, these performance and lifetime improvements will lower the cost per produced energy unit of SOFC technology, making it more competitive in the energy markets.

This thesis starts with a short introduction to the field in chapter two. Chapters 3–5 summarize Publications I–VI. Chapter 6 presents the conclusions of the work and the outlook for future research in the field.

2. SOFC stack technology

2.1 Basics of solid oxide fuel cell stacks

A fuel cell is a device that converts the chemical energy of fuel and oxidant directly into electricity and heat. This is achieved by the electrochemically active cell, which can operate at electrical efficiency in excess of 60%. A solid oxide fuel cell consists of three main components: a dense electrolyte and anode and cathode electrodes. Figure 1 shows the basic operating principle of a SOFC cell. Oxygen (air) is fed into the cathode and oxygen ions move through the electrolyte to the anode, reacting there with fuel. Electrons move through the outside circuit from anode to cathode. Typical layouts are anode supported and electrolyte supported cells. In an anode supported structure, the anode layer is usually 100…500 µm thick and used as a substrate, over which thin electrolyte and cathode layers are constructed by, for example, screen printing. In an electrolyte supported structure, the electrolyte is relatively thick (100…200 µm) and used as a mechanical support, over which the porous electrodes are constructed.

SOFC electrolyte materials, such as zirconia doped with yttria, require operating temperatures in excess of 500 °C to reach sufficient ionic conductivity. Typical, modern SOFC stacks operate at temperatures of 600…850 °C. This is seen as an optimum operating area where sufficient cell-level performance is achieved, internal reforming of methane is still possible [11], while the relatively low operating temperature allows the use of ferritic stainless steels as interconnects. Table 1 presents a few SOFC cell manufacturers and the main characteristics of their cells.

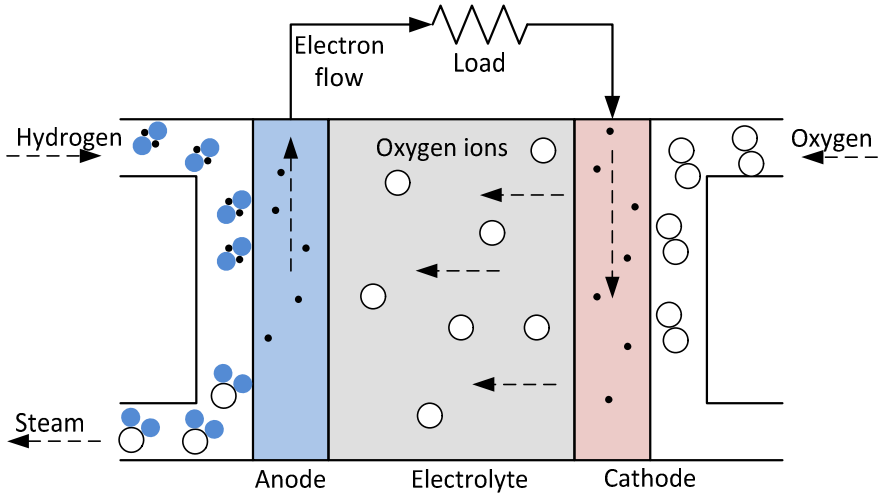

Figure 1. Principle of solid oxide fuel cell.

Table 1. Common manufacturers of SOFC cells.

Manufacturer	Mechanical support	Typical operating temperature / °C	Typical cell size / cm^2	Reference
Elcogen AS	Anode	600…800	100	[10]
SOFCMAN	Anode	700…800	100	[12]
SOFCMAN	Electrolyte	850	100	[12]
Kerafol/HCStarck	Electrolyte	750…950	100	[13]
Versa Power Systems	Anode	650…800	550	[14]

The power of a single cell is often insufficient, so a number of cells are incorporated into a stack assembly. Other main components of a typical SOFC stack are interconnects and seals, which are used to direct gas flows and electricity through the stack [15]. There are two main fields of SOFC stacks: planar and tubular designs. Typical advantages associated with tubular design are rapid start-up times and ease of sealing, whereas a planar design holds more promise for cheaper mass manufacturing costs and higher power density [15]. The focus of this thesis is on the planar type of fuel cell stacks with metallic interconnect plates.

Stack designs vary considerably from one manufacturer to another, but commonly the cell is located roughly in the centre of the interconnect, and inlet and outlet gas streams flow at the perimeter of the interconnect in separate manifolds. The cell and manifolds are sealed to prevent anode and cathode gases from mixing with each other. Figure 2 shows an example of an SOFC stack construction. Cells, interconnects, and seals of different geometries are stacked into a tower-like structure to increase the total power. At both ends of the stack are endplates that seal the manifolds from the surroundings and provide means to connect the stack to fuel and air pipelines. Electrical current is either collected from the endplates or from specific current collector plates near both ends of the stack.

Stacks are often described according to their flow configuration, meaning the direction of anode and cathode flows over the cell. The usual flow configurations are cross-flow, co-flow, and counter-flow [16]. There are also more complicated flow geometries or mixtures of the previous three basic types (see e.g. [17]).

While still a few years ago, stacks were mostly based on cells of around 100 cm^2 with a total power range around 1 kW, currently there are several stack designs based on larger cell areas offering electrical power in the range of 5…10 kW [18,19].

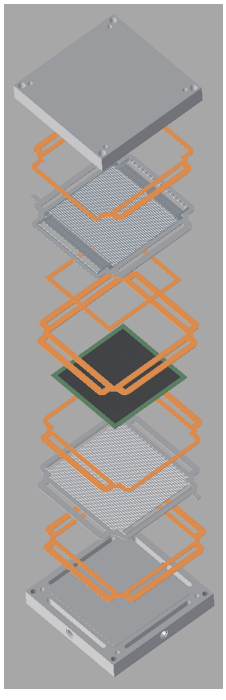

Figure 2. Typical SOFC stack construction (only a single repetitive unit shown for clarity).

2.2 Interconnects

Interconnect plates need to provide good electrical connection from cell to cell and separate anode and cathode atmospheres. It is also beneficial if the interconnects can offer mechanical support to the stack structure. In the SOFC stack, heat is generated in the cells, and therefore it is also beneficial if the heat conduction capability of interconnects is high so that they can help in transferring heat from the cell.

In the early stage of SOFC technology, interconnects were often made of ceramics such as $LaCrO_3$ based materials. The downsides of $LaCrO_3$ materials include their low electrical conductivity at temperatures below 800 °C and relatively expensive manufacturing [20]. Lanthanum chromites also exhibit swelling in reducing atmospheres leading to internal stresses and possibly cracking (see e.g. [21] for more details). Advancements made in the cell technology have made it possible to lower the operating temperature from 900…1100 °C of early SOFC cells to the 600…900 °C range. This allows relatively cheap metallic interconnects to be used.

A typical interconnect plate has gas channels against the cell to provide space for the reactants to flow along the cell and enough contact area for a good electrical conductivity. Figure 3 shows an example of an SOFC interconnect. The ribs and valleys in the middle of the plate form contact areas against the cell and gas channels respectively. At the perimeter of the interconnect are gas manifolds for air and fuel.

The main drivers in using ferritic stainless steels are ease of manufacturing, price, and the thermal expansion coefficient (TEC), which closely matches that of the SOFC cell [22]. Metallic interconnects are usually manufactured of ferritic high-temperature steel. The most common steel grades used as interconnects are Crofer 22 H [23], AISI 441 [24], ZMG232L [25], Sanergy HT [26], E-Brite [27], and CFY [28].

Table 2 contains the main elements present in these materials. The five first materials are all ferritic stainless steels, with AISI 441 having the lowest chromium content of 18% compared to 26% of E-Brite. The last material (CFY) is a chromium-based alloy manufactured through a powder metallurgical route. The high chromium content and low aluminium and silicon content of these alloys results in the formation of chromium rich oxide scales. This is beneficial as the conductivity of chromium oxide is in the range of 0.1…1 Ωm, which is about 10^5 times higher compared to alumina [29].

Metallic interconnects can be manufactured from bare steel by, for example, machining, punching, coining, hydro-forming, or laser-cutting methods. Typically in the case of thin (<1 mm) interconnects, forming techniques such as stamping or hydroforming are common, while thicker interconnects are often machined into shape. As the cost of the material is directly related to its weight, thin interconnects are of primary interest. However, decreasing material thickness usually has

an effect on the durability as well, so this needs to be balanced with cost-saving potential. For example, Huczkowski et al. have observed that doubling the thickness of uncoated Crofer 22 APU or ZMG232 steels roughly doubles their lifetimes [30].

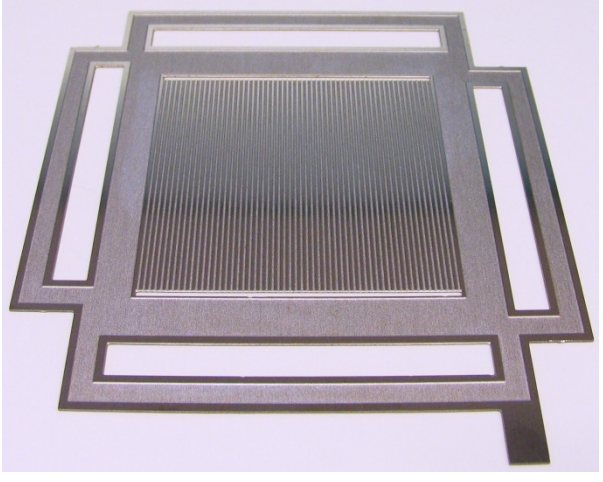

Figure 3. Interconnect.

Table 2. Chemical compositions of typical metallic interconnect materials in mass percentages.

Material	Fe	Cr	Ni	C	Si	W	Nb	Ti	Y	Al	Mn
Crofer 22 H	bal	22		0.015	0.3	1.5	0.6	0.01			0.6
AISI 441	bal	18		0.02	<1		0.3	0.3			
ZMG232L	bal	22	<0.7	<0.1	<0.1						
Sanergy HT	bal	21.2		0.040	<0.3		0.71			0.017	
E-Brite	bal	26	0.15	0.002	0.20						0.05
CFY	5	bal		<0.025	<0.12				0.1	<0.12	

2.3 Interconnect coatings

In SOFC stacks, interconnects are subjected to a reducing atmosphere on one side and an oxidizing atmosphere on the other side. This, together with a cost-driven need to use thinner interconnects, creates severe material challenges. Corrosion of interconnects can lead to mechanical failure of the stack, poisoning of the cell by volatile species, an increase of contact resistance between cell and interconnect, or short-circuiting over one or more cells. A number of coating methods have been developed to mitigate these corrosion effects.

One of the most significant reasons for the cell performance degradation is chromium poisoning. This happens when the chromium oxide scale of the metallic interconnect is subjected to humidity and oxygen. In the presence of humidity, chromium oxyhydroxide is the dominant species [31,32] and formed according to equation (1) [33].

$$Cr_2O_3(s) + 2H_2O(g) + 3/2O_2(g) \rightarrow 2CrO_2(OH)_2(g) \qquad (1)$$

The gaseous chromium oxyhydroxide can reduce at the cathode, and the chromium deposited there causes loss of electrochemical performance [34]. To minimize the effect of cell performance degradation due to chromium poisoning, metallic interconnects are usually coated with either perovskites [35,36,37], spinels [38] [39], or metals [26]. The purpose of these coatings is to form a barrier layer that inhibits chromium evaporation from the interconnect steels.

Common methods of application of chromium barrier coatings are wet powder spraying [15], thermal spraying [40,41,42], chemical vapour deposition processes [43,44] such as atomic layer deposition [45], and physical vapour deposition processes [26]. Coating is usually carried out by the stack manufacturer, although, for example, Sandvik offers steels such as Sanergy HT already pre-coated with cobalt or ceria and cobalt [26].

2.4 Stack sealing

An ideal SOFC stack-sealing material should be gas tight and have good compressibility and conformability. It should naturally also be resistant to SOFC operating temperatures and be chemically stable with gas atmospheres, as well as with neighbouring components. Sealing that is placed between different electrical potentials within a stack also needs to be electrically insulating. The requirement of gas tightness is quite severe, as any leak will directly decrease the electrical efficiency of the stack and also cause a local hot spot that could induce material

degradation. Localized leak also increases the local fuel and/or air utilization which can lead to e.g. oxidation of the anode.

Stack seal should also function as a spacer between adjacent components. It is often the case that the seals are practically the only flexible components in a stack, so they need to be able to take up any manufacturing or assembly-related tolerances.

Traditionally, SOFC stacks have been sealed with glass- and glass-ceramic materials (see e.g. [46,47,48]). Glass-based seals bond to the adjacent surfaces and can offer very gas tight sealing if properly designed, heat-treated, and operated. The downsides can include a need for a well-controlled joining procedure during the first heat up [49], cracking under mechanical stress, chemical reactions at interfaces to be joined, and brittleness at low temperatures. As an example, Figure 4 shows a SEM cross section of a typical glass-ceramic material, H.C. Starck HSC3 after 100 h at 700 °C. Two different phases and black pores can be identified from the micrograph. A lot of work has concentrated on manufacturing glass-based sealing materials that have a similar coefficient of thermal expansion compared to SOFC cells. For more details, see [50,51,52,53,54].

Another group of sealing materials is compressible seals. Stacks with compressible seals can usually be easily assembled, and they require no special joining procedure. Traditionally, materials from a group called mica have been used to seal SOFC stacks. Mica is a group of silicate minerals with a general structure of $AB_{2\text{-}3}(Al,Si)\text{-}Si_3O_{10}(OH)_2$ in which A is either K, Na, Ca, or Ba, and B is either Al, Fe, Mg, or Li [55]. Micas can also contain other elements such as F^- replacing some of the OH^- ions [56]. Of this group, phlogopite ($KMg_3(AlSi_3O_{10})(OH)_2$) mica is by far the most common. Phlogopite mica papers are being sold under different brands, such as Statotherm HT by Burgmann Industries [57] and Cogemica by Cogebi. Figure 5 shows the cross sectional SEM-image of Statotherm HT. Vertical, interleaving phlogopite platelets are clearly seen in the image. The drawback of these types of compressible materials is the requirement of compressive stress in excess of several MPa to form a gas tight seal. Their leak rates are usually higher compared to bonding seals and the leak rates are dominated by the interfacial leak paths, especially at low compressive stresses [58,59,60,61,62].

Flexitallic Ltd. has developed a series of materials under a trade name Thermiculite, which are claimed to lower compressive stress requirements. Thermiculite 866 and Thermiculite CL87 consist of only chemically exfoliated vermiculite and steatite, also known as talc; there is no other component and no organic binder. The sheets of the CEV act as a binder to hold the whole together to form a flexible sheet that is robust enough to be cut into complex shapes [63,64]. Figure 6 shows the cross-section of Thermiculite 866. Horizontal vermiculite platelets (light grey) are seen between steatite filled areas (dark grey).

In recent years, some attention has been generated by a solution known as hybrid seals. These seals have a compressible core with conformable layers on both sides of the core to provide enhanced sealing at the interfaces. The interfacial

layers are usually made of glass or metal foil. These materials are targeted to be used under low (<2 MPa) compressive stresses while maintaining the easy handling and assembly associated with compressible seals (see e.g. [65,66] for more details).

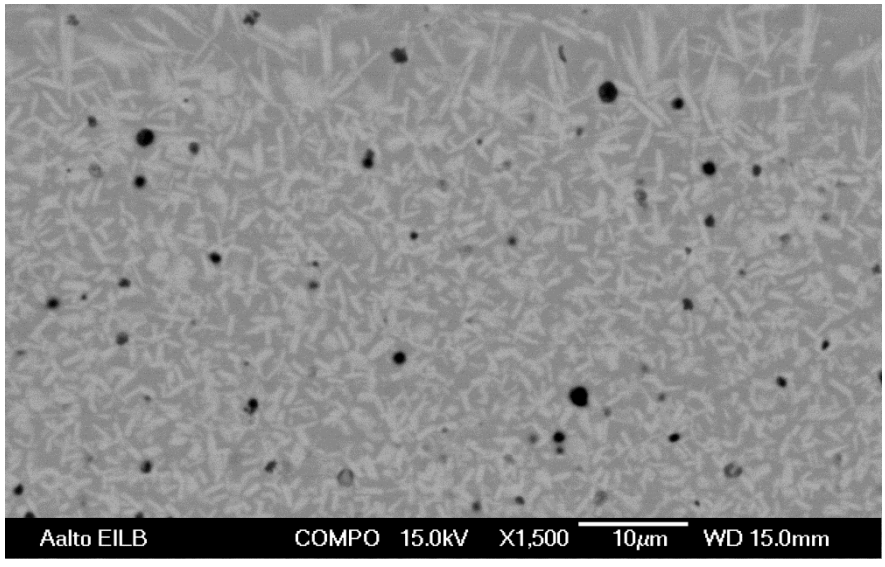

Figure 4. SEM image of H.C. Starck Ampergy HSC3 glass-ceramic sealing material.

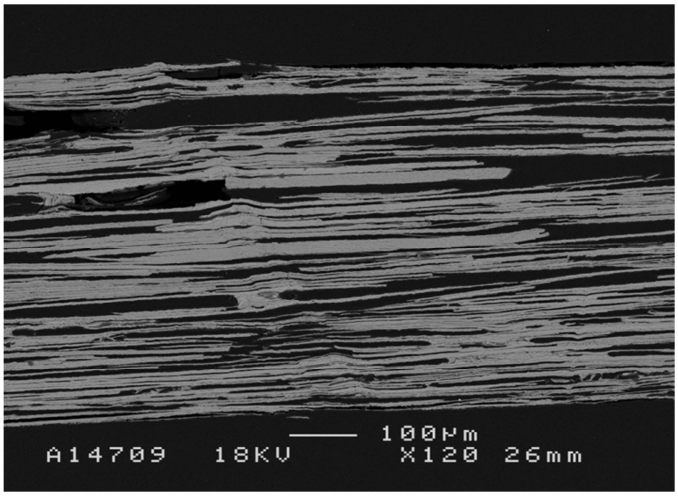

Figure 5. SEM image of Statotherm HT (phlogopite mica paper).

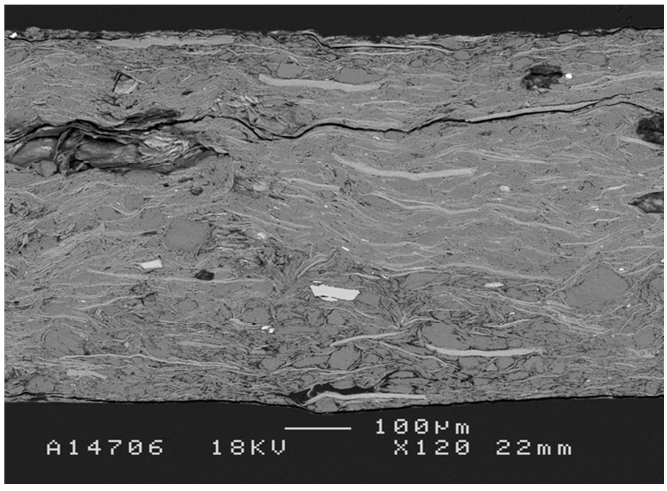

Figure 6. Cross-sectional SEM image of Thermiculite 866.

3. Mechanical properties of SOFC sealing materials

3.1 Background

The primary function of SOFC stack seals is the ability to effectively separate cathode and anode gases from each other and from the surroundings. As the seal is often the only non-rigid component within a stack, it needs to take up the manufacturing and assembly tolerances of other components. To this end, the sealing material needs to have a sufficient amount of compressibility. Figure 7 displays a simplified sealing arrangement of a typical SOFC stack. In a perfectly engineered sealing solution, the seal provides a gas-tight barrier between adjacent components (a). If the seals are too thick, the gas tightness of the stack might be good, but this would often result in poor electrical contact between interconnects and cells, as the compressive stress is mostly on the seals and not on the cell (b). On the other hand, if the seals are too thin, electrical contact might be good but the gas tightness is poor, at least in the case of compressible seals, due to the cell carrying most of the compressive stress (c). In the last two cases, mechanical stresses on interconnects are usually also higher due to uneven stress distribution. Therefore, an optimal sealing solution needs to balance between achieving low contact resistance between cell and interconnect, and gas tightness to obtain maximum stack performance.

The progress in manufacturing SOFC cells is leading to an increase in cell area. Increasing the cell size is intriguing for the stack manufacturer, as the number of components needed in a stack is decreased for the same amount of power. From the perspective of compressible seals, the increase in cell area presents a challenge: the higher the cell area, the higher the required compressive force for the stack. Increasing the external forces to the stack includes a risk of either deforming or breaking stack components should the forces not be optimally distributed. Higher external forces will also result in more bulky components both inside the stack and in the stack compression mechanism. The mechanical compression of a stack is often needed at a lower temperature than the operating temperature,

as, for example, steel springs cannot be relied upon at SOFC operating temperatures, leading to heat loss from the stack along the compression rods or structures.

Typically, SOFC stacks are assembled at room temperature, then heated up and conditioned, and then operated at temperatures in the range of 600…900 °C. This creates a need to understand the mechanical properties of the seals not only at room temperature or at operating temperature, but throughout the whole operating region. Of special interest are the mechanical properties of materials during the first heat up, in which the stack is sealed, reduced, and tested.

In publications I-III, the mechanical properties of SOFC sealing materials were studied. Compressibilities of the materials were analysed as a function of temperature. Especially the mechanical behaviour of compressible sealing materials, as well as a glass material, was studied during the first heat-up procedure.

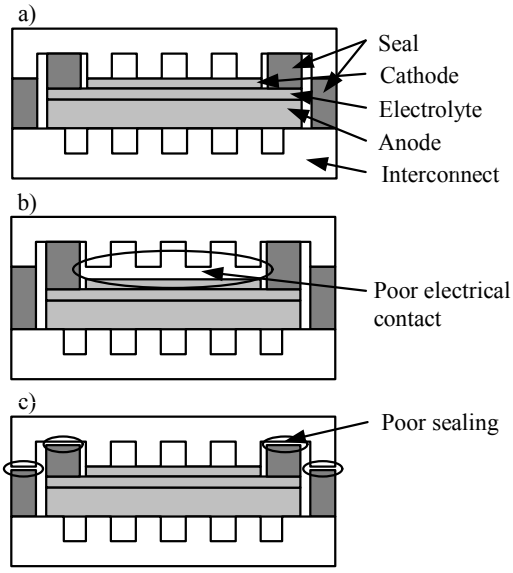

Figure 7. Stack sealing challenges with different seal thicknesses. Low contact-stress areas have been indicated with circles.

3.2 Experimental

Mechanical properties of sealing materials were evaluated as a function of compressive stress and temperature. Figure 8 shows a schematic of the equipment used in the low compressive stress (<1 MPa) measurements. A sample is inserted between the measurement rods, and a weight is clamped on the top of both rods. The thickness of the sample is read off a dial gauge mounted at the top of the push-rods. The lower part of the assembly can be inserted in a dedicated furnace to control the temperature of the sample. The accuracy of the device is ±10 µm in a temperature range of 0…700 °C. For more details on the test equipment, see [67]. The high stress (>1 MPa) measurements were carried out using commercially available fatigue testing devices (e.g. Instron 8801).

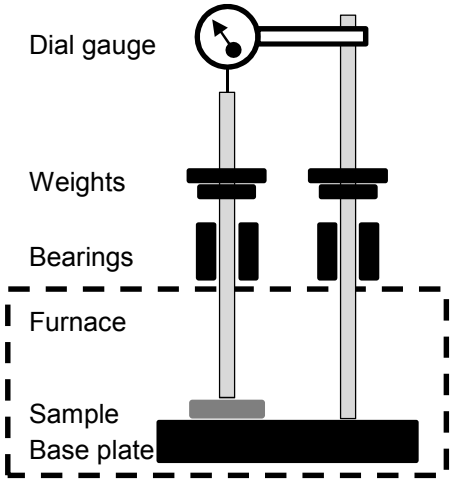

Figure 8. Schematic of the measurement setup

3.3 Results

The thickness of different materials as a function of compressive stress was analysed. Figure 9 shows the effect of temperature on the compressibility of Thermiculite CL87. It can be noted that heating the material significantly reduces the compressibility: already at 200 °C, the compressibility is the same as at 700 °C. If the compressive stress is applied at room temperature before the first heat up, Thermiculite CL87 compresses about 42% between 0.1…0.9 MPa. If full compression to 1.0 MPa is applied after first heat up, the compressibility between 0.1…0.9 MPa is limited to 4%. Most probably the loss of compression is related to drying of the sealing material, and therefore it is likely that any heating above room temperature will result in partial loss of compressibility. Therefore, it is very beneficial to carry out as much of the first compression as possible at room temperature before first heat up. This would allow for the maximum amount of deformability in the sealing materials, therefore allowing for the highest ability to compensate for stack manufacturing and assembly tolerances, leading to a gas-tight stack with low electrical contact resistances.

To compare mechanical properties of Thermiculite CL87 to conventional compressible sealing materials, Figure 10 shows the compressibility of Statotherm HT (phlogopite mica paper) material. It can be noted that this material only compresses about 3% per megapascal of applied stress. This leads to the conclusion that any significant amount of compressibility requires a compressive stress of several megapascals.

Figure 11 shows Schott GM31107 glass sealing material thickness as a function of temperature and time using two different heat-up procedures. The grey curve corresponds to heating under 0.44 MPa of compressive stress, and the black curve to heating under no compressive stress. The weight of the measurement rod corresponds to 0.04 MPa of compressive stress on the sample, so this is the actual stress in a “no compression” case. It is noticed that there is only very little thickness change until about 570 °C. Above that temperature, two distinct changes are noticed, the first at 570…615 °C and the second at 660…700 °C. It should be noted that these are furnace temperatures, so the temperature of the sample lags behind during heating. Based on hot-stage microscopy data [46], the first of these changes relates to binder burnout and sintering, and the second change to glass softening and wetting of the surfaces. The final thickness of the glass was about 12 µm at 0.44 MPa. Further compression to 1.0 MPa at 700 °C did not reduce this thickness. The difference throughout the heating using 0.44 MPa of compressive stress and no stress at all is minimal. Based on these results, the behaviour of the Schott GM31107 glass does not depend greatly on the compression procedure during first heat up. However, if a significant amount of compression is applied at room temperature where the glass tape is very thick compared to its final thickness, the stress distribution within a stack structure should be analysed to be sure that stresses are within acceptable limits.

The methodology and results presented here and in articles I-III are directly applicable to designing SOFC stacks. In the past, methods such as hot-stage microscopy have often been used to gain information on the mechanical properties of glass materials. While this is a reliable method, it is very remote from the actual SOFC stack environment: there is only one (bottom) surface for the glass to wet, no compressive stress, and usually large glass samples are used. With the methodology presented in publications I-III, the measurements are closer to stack conditions: the compressive stress can be varied, the glass has two surfaces to wet, and sample sizes can be realistically dimensioned. The same arguments apply naturally for measuring compressible seals. The measurement data also shows that there is a significant difference in the compressibility of Thermiculite 866 as a function of temperature, which should be taken into account in the assembly and first heat up of stacks.

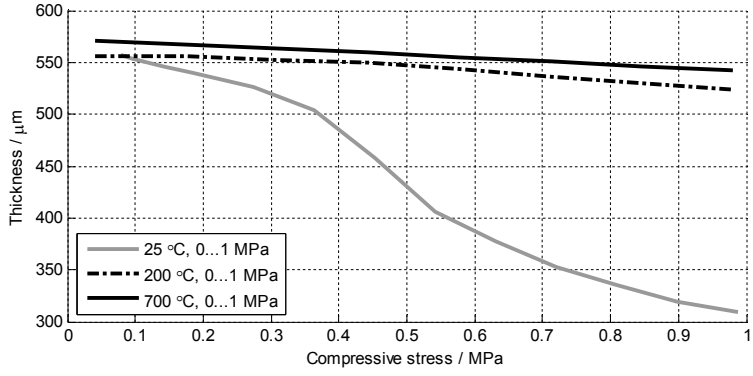

Figure 9. Compressibility of Thermiculite CL87 at room temperature, 200 °C, and 700 °C.

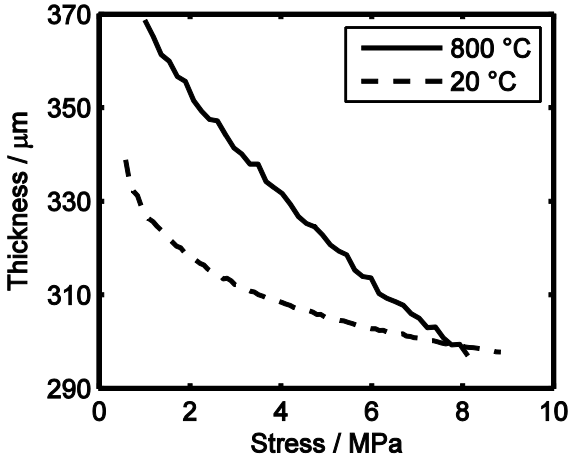

Figure 10. Thickness of Statotherm HT as a function of compressive stress.

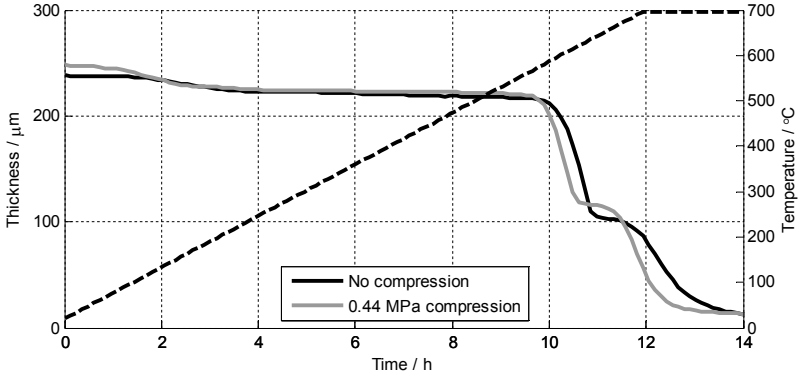

Figure 11. Thickness of Schott GM31107 glass seal (250 µm green tape) as a function of temperature with no compression (0.04 MPa) and with 0.44 MPa compression.

4. Analysis and reduction of stack leakages

4.1 Background

Any fuel burning before the electrochemically active cell does not take part in the electrochemical reactions and therefore decreases the electrical efficiency of the stack. Therefore, reducing leakages is beneficial, as it directly enhances the electrical efficiency of the stack. Leakages can also induce hot-spots or local fuel or air starvation inside the stack. These can cause re-oxidation of the anode or material degradation thus decreasing stack performance and lifetime. Cross leakages between anode and cathode also have an effect on the oxygen to carbon ratio at fuel side, which needs to be taken into account in the process control system. Monitoring leakages through testing is also important, as it gives insight into the lifetime of the seals. In Publication IV, the methodology for ex-situ and in-situ leakage measurements and calculations is presented.

Reducing the required surface stress of the seal diminishes the necessary compression of the stack, which in turn leads to simpler and less expensive compression systems. This also allows more freedom for the stack designer, as thinner, less robust components such as interconnects can be used. A general problem with compressible seals is that lowering the compressive stress increases the leak rate, as the leakage paths along the interfaces tend to dominate the total leak rate. Therefore, using glass seals at low compressive stresses has been a common solution. However, glass seals are usually more difficult to handle and assemble, and require a specific heat treatment procedure. Their electrical resistivity is also usually lower compared to compressible seals, and can be more easily affected by chemical reactions between the glass and adjacent components [68]. Glass seals are also prone to cracking due to thermomechanical stresses generated during thermal cycling [69]. To overcome these challenges, a solution known as a hybrid seal has been presented. In this type of seal, a substrate such as mica paper and conformable interlayers are brought together to form a composite seal. The purpose of the substrate is to provide mechanical properties comparable to compressible seals, while the conformable interlayers diminish interfacial leak-

ages. In Publications III and IV, a glass-based coating was developed to suppress interfacial leakages.

4.2 Experimental

4.2.1 Surface coating

The goal of the experimental work was to design a sealing material that could be operated at low compressive stress (<1 MPa) while still maintaining a leak level below 1% of the stack inlet fuel flow. To this end, a hybrid sealing concept with compressible core substrate and compliant surface layers was chosen. The substrate material for the seal was chosen to be Thermiculite 866, manufactured by Flexitallic Ltd. The glass layer was chosen to be very thin (<20 µm) so that the seal would inherit its mechanical properties from the Thermiculite 866 rather than the glass layer. A thin glass layer also allows the glass to have low viscosity, which helps to seal the interfaces. The glass powder was suspended in an organic carrier consisting of terpineol, ethanol, and ethylene cellulose. Table 3 contains the typical compositions of the coating. By mechanical coating means, the organic content and the viscosity of the suspension were tailored to be much higher (~40 cSt) than when using spray coating (14 cSt) [70]. The results presented here were obtained with a spray-coating method using a U-POL Maximum HVLP mini spray gun with a 1.0 mm nozzle. After applying the coating, the coated Thermiculite 866 sheets were dried at 75 °C for 2 h and then cut to the required shape. All the seals were heated from room temperature up to 700 °C using a 60 $°Ch^{-1}$ ramp rate. For more details on the coating process, see [71] and [72], and for more details on the mechanical properties of the coated seals, see [67].

Table 3. Typical compositions of various coatings.

Coating method	terpineol / w%	ethanol / w%	ethyl cellulose / w%	Glass to organic – ratio / w/w	Viscosity / cSt
Brush/spatula/roller	81	15	4	2:1	40
Wet spraying	24	75	1	1:2	14

4.2.2 Leak rate measurements

Leak rate measurements were conducted on the manufactured hybrid seals, as well as for the non-coated core material (Thermiculite 866). Ring-shaped seals of 40 mm outer diameter and 5 mm landwidth were placed between Crofer 22 H plates (Figure 12). The bottom plate was 20 mm thick and the top plate 1 mm thick. The gas was fed into the seal via a hole in the middle of the bottom plate. A chosen gas flow was fed to the seals with mass flow controllers, and a pressure controller kept the gas pressure at a set level.

After heat up in air, the samples were exposed to 50/50 H_2/N_2. Leak rate measurements were conducted periodically by closing the valve V1 and logging the pressure decay. The leak rate measurement and calculation procedure were based on measuring the pressure decay and calculating the leak rate as a function of pressure from that. For more details on the methodology, see Chapter 4.3.

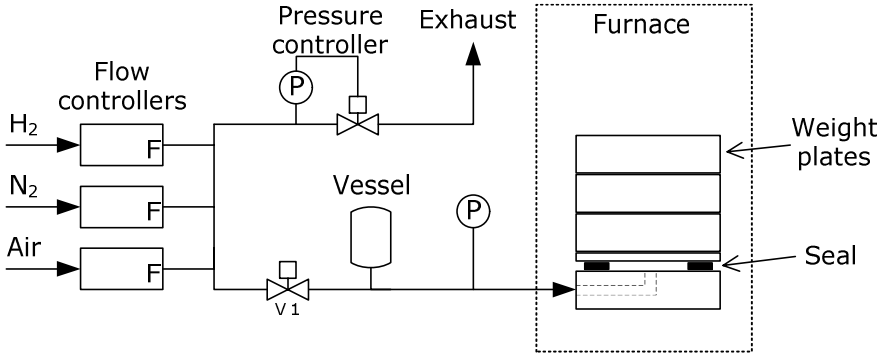

Figure 12. Leak test setup.

4.2.3 Stack test

To further verify the sealing solution, a test stack was manufactured and tested. The stack contained 30 cells by Elcogen AS. Table 4 presents the main features of the stack. Figure 13 shows a picture of the stack before the start of the test. The pipe coils at the bottom provided pre-heating for the air and fuel. The two vertical rods at the right are the current rods. Compression was provided through the thick vertical pipes at the bottom and top of the picture. The smaller pipes at the left are the impulse lines of the pressure transducers.

During heat up, air was fed to both the anode and cathode sides of the stack, to ensure that all the organic binders of the coating on seals were burned off. After heat up, the anode side was reduced with hydrogen in nitrogen. Cross leaks were measured before reduction, after reduction, and during operation.

Table 4. Nominal operating conditions of the stack.

Cells	30 pcs Elcogen ASC-10B
Flow configuration	Co-flow
Active area	81 cm^2
Cathode inlet temperature	590 °C
Cathode outlet temperature	700 °C
Current density	0.25 Acm^{-2}
Air utilization	22%
Fuel utilization	46%
Cathode outlet pressure	ambient
Flows during heat up	Anode: 4.5 NLPM air Cathode: 4.5 NLPM air
Flows before reduction	Anode: 4.5 NLPM N_2 Cathode: 4.5 NLPM air
Flows at OCV	Anode: 0.5 NLPM H_2, 8.5 NLPM N_2 Cathode: 8.5 NLPM air
Flows at nominal operating conditions	Anode: 9.0 NLPM H_2, 8.5 NLPM N_2 Cathode: 50 NLPM air

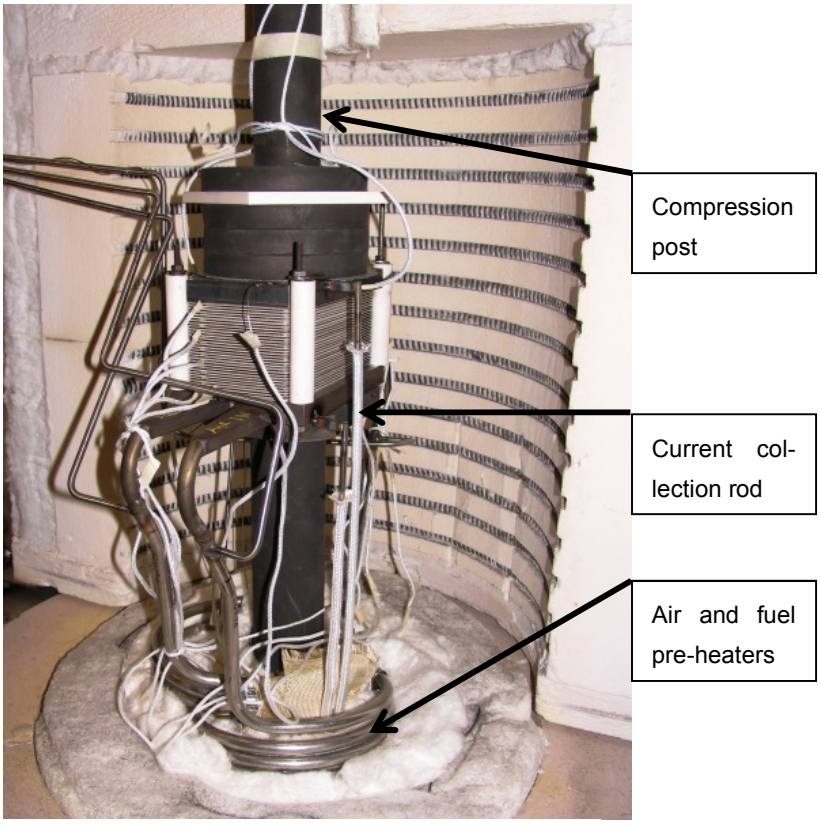

Figure 13. The 30-cell stack in a furnace before testing.

4.3 Leak rate analysis

4.3.1 Pressure drop methodology

Ex-situ leak test results in this thesis have been calculated by analysing pressure versus time curves while the sample and its associated volume have been isolated. This allows for calculation of the leak rate as a function of pressure between the starting pressure and the end pressure of the decay, resulting in a large amount of data based on a single measurement. Based on the ideal gas assumption, the leak rate is proportional to the slope of the pressure decay curve, and therefore the leak rate can be written as a function of pressure

$$\dot{Q}_{NTP} = V \frac{T_{NTP}}{T p_{NTP}} \frac{dp}{dt} , \quad (2)$$

where V is the combined volume of the vessel and the sample, T is the average temperature of the gas in the volume, and T_{NTP} and p_{NTP} are normal temperature and pressure.

From the equation above, it can be noted that the accuracy of the result depends on accuracies of volume, temperature, and dp/dt. The volume of the system can be determined with high accuracy, so that can be neglected. The average temperature of the gas inside the system volume is more prone to errors. It is estimated that this error is less than ±15 °C, corresponding to a leak rate uncertainty of 5%. For evaluation of the derivative dp/dt, there are several options. If one wants to calculate leak rate at a specific pressure from the data, which is a set of points taken at regular intervals, one could approximate dp/dt by a difference in pressure and time of the consecutive steps

$$\frac{dp}{dt} \cong \frac{p_i - p_{i-1}}{t_i - t_{i-1}} . \quad (3)$$

If the sampling rate has been sufficient, the difference p_i-p_{i-1} is bound to be small. Therefore, any random uncertainty of the pressure measurement will induce a large relative error in the pressure measurement. To overcome this, a third degree polynomial was fitted to the pressure versus time data using the least squares method, thus minimizing the random uncertainty of the pressure measurement. The fitted polynomial was then differentiated to obtain the leak rate as a function of pressure. Figure 14 presents this methodology in graphical format. On the top left, there is raw pressure data and below it, there is leak rate as a function of pressure, calculated using consecutive points in the data (the equation above). It can be noted that even a small amount of noise in the pressure data results in very noisy leak rate data. On the top right is the same pressure data fitted with a third degree polynomial, and below it is leak rate as a function of pressure, calculated

by differentiating the polynomial. The resulting data through this processing method is much more usable.

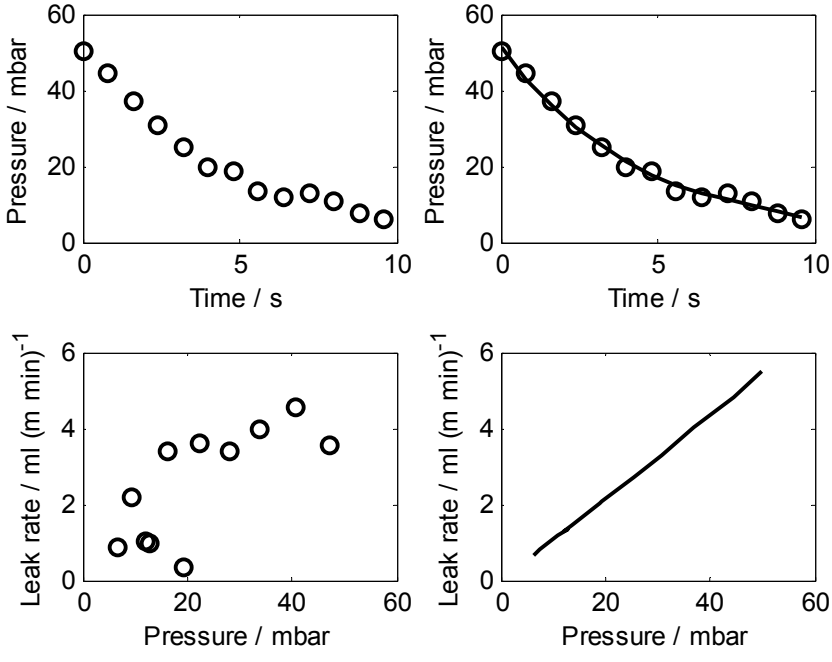

Figure 14. Example of the pressure decay methodology. Leak rate calculated using individual data points (left) and polynomial fit (right).

4.3.2 Stack tests

During stack tests, cross leak between anode and cathode is an important parameter to monitor. An increase in cross leak directly decreases electrical efficiency and it may also be an indication of a developing mechanical failure such as a cracked cell or seal. An easy way of measuring cross leak is to observe the open circuit voltage (OCV) and compare this value against the theoretical value given by the Nernst potential

$$E = -\frac{\Delta G}{2F} + \frac{RT}{2F}\ln\left(\frac{p_{H2}p_{O2}^{0.5}}{p_{H2O}}\right), \quad (4)$$

where ΔG is the change of Gibbs energy, F is the Faradic constant, R is the gas constant, T is the temperature and terms denoted with p are partial pressures of the reactants. This is only applicable at OCV and not during operation. It should also be noted that any leak taking place after cell cannot be detected with this method. Figure 15 presents theoretical Nernst potential as a function of anode side humidity (induced by cross leak of oxygen) and temperature. As cell voltage can easily be measured accurately, and cell temperature is also usually known at OCV, at least within 100 °C, this method can be used for a rough check on the leakages. For example, a cell voltage of 1.2 V at 700 °C yields a humidity of 0.2% at the anode. It should be noted that since according to

$$H_2 + \frac{1}{2}O_2 \rightarrow H_2O \quad (5)$$

only half a mole of oxygen is needed per mole of steam. Therefore, 0.2% steam content at the anode corresponds to 0.1% of leaked oxygen molecules compared to anode inlet flow.

In the stack test presented in this chapter, cross leakages were quantified by measuring steam and oxygen content from cathode and anode outlets. Oxygen cross leak was calculated before cell reduction as

$$\dot{Q}_{O_2}^{cross} = X_{O_2}^{A,out}\dot{Q}_{N_2}^{A,in}. \quad (6)$$

By this methodology, one is able to measure the stack cross leak before introducing reducing gases (hydrogen) to the stack. The hydrogen cross leak after reduction was calculated as

$$\dot{Q}_{H_2}^{cross} = (X_{H_2O}^{C,out} - X_{H_2O}^{C,in})(\dot{Q}_{air}^{C,in} - n_{cells}\frac{I}{4F}\frac{RT_{ntp}}{p_{ntp}}), \quad (7)$$

where terms denoted with X are measured oxygen and steam volumetric fractions, n_{cells} is the number of cells in the stack (30), I is the current drawn from the stack, and F is the Faradic constant. These calculations are based on the assumption

that the leak rates between ambient and anode/cathode and the nitrogen cross leak are small compared to total flow rates.

As partial pressure measurements of oxygen and steam at stack outlets can be used in all operating conditions, these were used as a primary means to assess stack leakages.

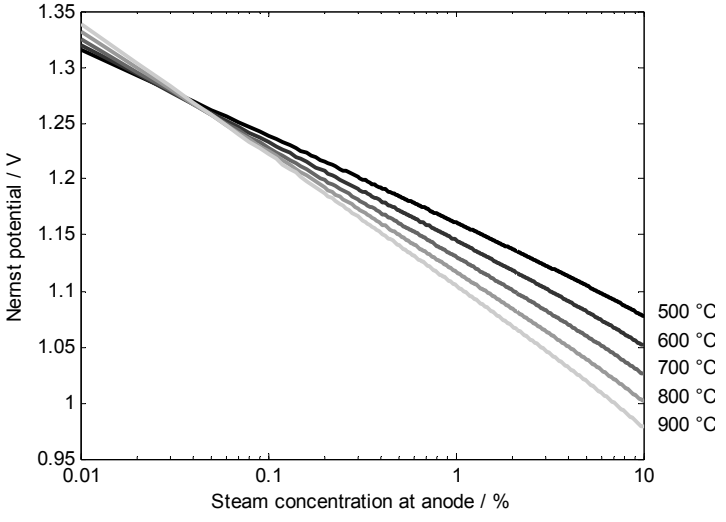

Figure 15. Nernst potential of 50/50 H_2/N_2 fuelled fuel cell as a function of temperature and anode steam concentration (leak).

4.4 Results

4.4.1 Surface coating

Hybrid seals were manufactured by coating glass layers with an organic carrier on top of compressible Thermiculite 866 substrate. Figure 16 shows a SEM cross-section of Crofer 22 APU / seal / Crofer 22 APU structure after heat-treating 50 h at 700 °C. It can be noticed that the glass interlayers are well adhered to the Thermiculite structure, even penetrating slightly in between vermiculite/steatite slits. Figure 17 shows another cross-section of the coated seal. The bottom steel plate had been intentionally scratched before assembly with ~15 µm scratches, to observe the filling properties of the coating. It can be noted that the glass coating has filled the scratch fully and formed clearly a gas tight seal also in this area.

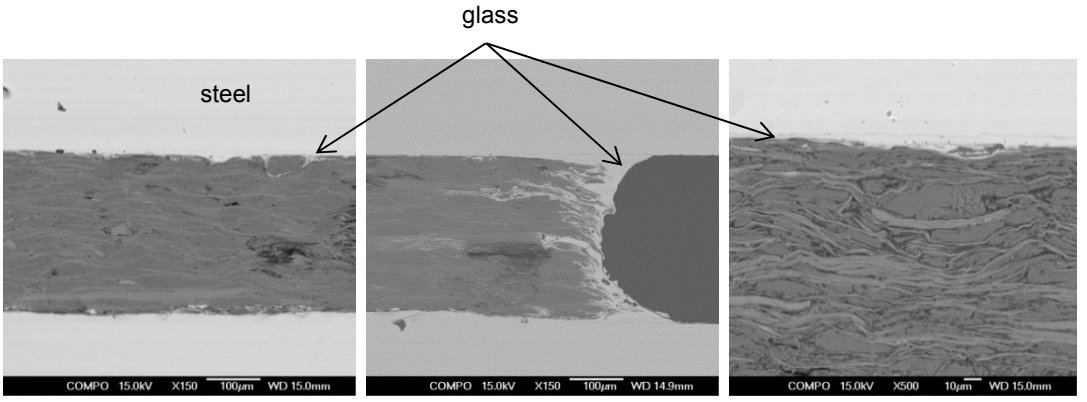

Figure 16. SEM cross-sections of the manufactured seals.

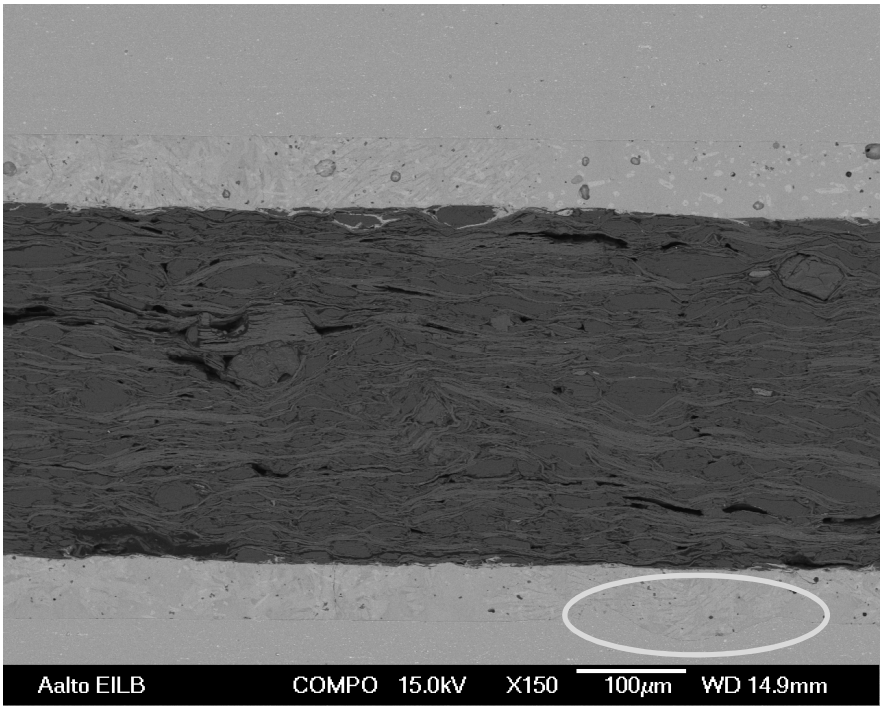

Figure 17. Cross-section of coated seal. Scratches in the Crofer 22 APU have been filled.

4.4.2 Ex-situ leakage tests

Leak rates of the manufactured hybrid seals and of core material (Thermiculite 866) were measured. Figure 18 presents leak rates of the samples as a function of gas pressure at 0.1 MPa and 0.4 MPa compressive stresses. From this figure, it can be noticed that the surface coating decreases the leak rate of Thermiculite 866, especially at low compression stress levels. The coated Thermiculite 866 seals show leak rates of 0.1…0.3 ml (m min)$^{-1}$, which is a reduction of 60…90% compared to uncoated samples, which showed leak rates of 0.3…3 ml (m min)$^{-1}$.

Figure 19 shows the leak rate as a function of pressure using different test gases. There is a difference in slopes of the leak rate versus pressure curves between coated and uncoated samples. The coated samples show almost constant leak rate as a function of pressure with H_2/N_2 mixtures, while leak rates of uncoated samples are more pressure dependent. This suggests that with the coated samples, the primary driving force is concentration gradient rather than pressure gradient, as with the uncoated samples. The negligible dependency of the overpressure on the diffusive leak rate can be understood by considering Fick's law of diffusion, using total concentration c_{TOT}, total pressure p_{TOT}, and the molar fraction x:

$$J = -D\nabla c = -c_{TOT} D\nabla x = -\frac{p_{TOT}}{RT} D\nabla x \qquad (8)$$

where D is diffusion coefficient, c is concentration, x is fraction, p is pressure, R is the gas constant and T is temperature. From this equation, one can notice that varying the absolute overpressure p_{TOT} in a range of ~1000…1030 mbar induces very little effect on the concentration-driven leak rate. Although the real situation is more complex, the concentration dependency of the leak rates should be carefully considered, as different research groups use very different gas compositions and overpressures for leak tests, such as 3% H_2 in nitrogen or argon, 100% H_2 or 100% He.

The effectiveness of the surface coating was further tested by thermally cycling the seals and observing leak rates. Figure 20 shows the leak rate data before and after five thermal cycles for coated and uncoated seals. The leak rate of the hybrid seal remains stable at around 0.2 ml/m/min level at 25 mbar overpressure, while the uncoated seal shows a leak rate of about 3 ml/m/min. It can be noticed that the leak rates of the compressible and hybrid seals do not change during thermal cycling, and the leak rate of the hybrid seal is about 90% less than that of the compressible seal.

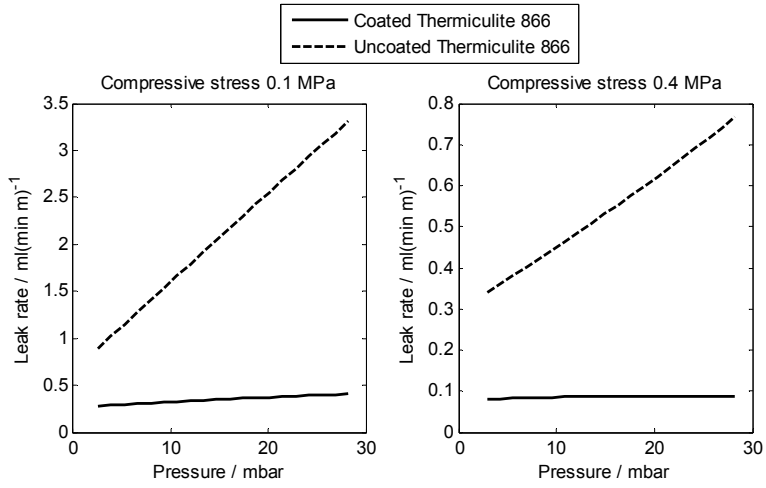

Figure 18. Leak rate comparison of coated and uncoated seals (50/50 N_2/H_2).

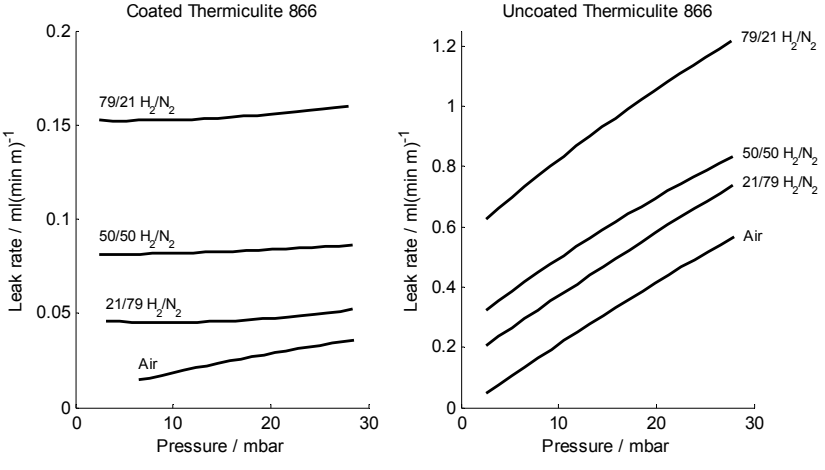

Figure 19. Leak rate comparison of coated and uncoated seals with different gas atmospheres.

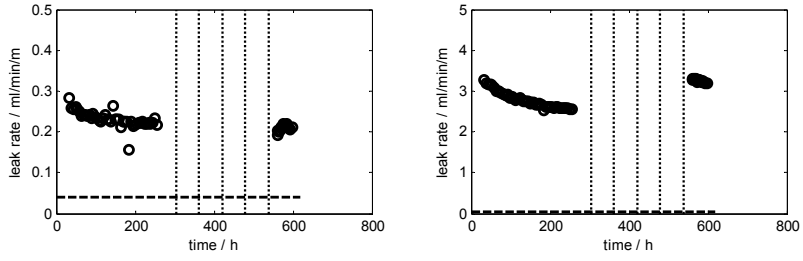

Figure 20. Leak rates of coated seal (left) and uncoated seal (right) before and after five thermal cycles.

4.4.3 Stack test

A 30-cell stack was assembled and tested using the manufactured hybrid seals. The oxygen cross leak of the stack was measured before reduction, and hydrogen cross leak at purge gas and during operation. Table 5 shows the calculated leak rates in different operating conditions, along with the measured quantities. The hydrogen leak rates have been analysed by measuring steam concentration at cathode out. The oxygen leak has been analysed by measuring oxygen concentration at anode out before reduction, and by measuring OCV at 50/50 H_2/N_2. It can be noted that leakages with air and with 5% hydrogen in nitrogen mixture (purge gas) are significantly lower than with higher hydrogen concentration (nominal operating conditions). This is further illustrated in Figure 21, where hydrogen cross leak of the 30-cell stack is plotted as a function of average hydrogen concentration between anode inlet and outlet. It can be observed that the leak rate is directly proportional to the hydrogen concentration. This behaviour corresponds well with the ex-situ observations presented in the previous chapter. The hydrogen cross-leak at nominal operating conditions corresponds to about 0.7% of inlet hydrogen flow, which is well below the 1% target set for this thesis work.

Table 5 also contains leak rates per unit length, allowing comparison between leak rate tests. During nominal operating conditions, the hydrogen cross leak was 4 ml/m/min. In this condition, anode gas composition was 49% H_2 in N_2, which is almost identical to the 50/50 H_2/N_2 mixture used in most of the ex-situ tests. At 0.1 MPa of compressive stress, ex-situ tests showed leak rates of 1…3 ml/m/min, and at 0.4 MPa of compressive stress the leak rates were 0.3…0.8 ml/m/min. It can be noted that the stack leakages and values measured fall in the same order of magnitude. The difference between these values could be explained by inhomogeneous stress distribution on the stack seals.

Table 5. Summary of the measured leak rates and flow rates. The cathode inlet humidity was constant at 0.08%.

	Direction of leak	Measured quantity	Calculated leak	
			ml min^{-1}	ml (m $min)^{-1}$
Before reduction	Ambient, cathode => anode	0.18% O_2 (anode out)	8±2 (O_2)	0.3±0.1
Purge gas	Anode => cathode	0.20% H_2O (cathode out)	10±2 (H_2)	0.7±0.2
OCV (50/50 H_2/N_2)	Ambient, cathode => anode	Average cell volt-age 1163 mV	46±15 (O_2)	1.5±0.5
Nominal	Anode => cathode	0.20% H_2O (cathode out)	60±12 (H_2)	4±0.9

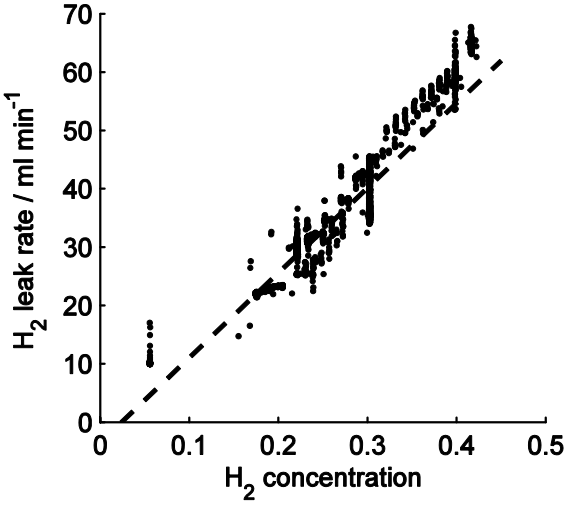

Figure 21. Hydrogen cross leak of the 30-cell stack as a function of average hydrogen concentration between anode inlet and outlet.

5. Analysis of corrosion phenomena and protective coatings in SOFC stacks

5.1 Background

The high operating temperatures of SOFC stacks in combination with both oxidizing and reducing atmospheres presents a challenging environment for materials. Corrosion of materials can take place due to interfacial reactions as well as by gas/solid reactions. Of special importance is to avoid any corrosion mechanism that can lead to deactivation of the electrochemical cell. One typical example of these deactivation mechanisms is chromium evaporation from interconnect steel materials. The evaporated chromium is transported in the gas phase to the electrochemically active cell, where it can solidify to chromium oxide, causing loss of performance [73]. The transported chromium can also react with strontium in SOFC cathode materials and for strontium chromate ($SrCrO_4$). The electrical resistivity of strontium chromate is in the order of 60 Ωm at 800 °C and increases with decreasing temperature [74]. This corresponds to area-specific resistivity of 0.6 Ωcm^2 at a thickness of only 1 µm. Therefore, it is clear that formation of strontium chromate can cause significant ohmic losses in stack performance. These phenomena can be mitigated with, for example, chromium barrier coatings on interconnect steels. A variety of protective coatings are reported in the literature, see e.g. review of Shaigan et al [75]. Coatings based on $(Mn,Co)_3O_4$ spinels have been of high interest due to their good performance, see e.g. [76]. More recently, $MnCo_{2-x}Fe_xO_4$ has been tested for its' higher electrical conductivity [77].

Publication V deals with development and application of a protective coating for SOFC interconnects. Publication VI presents corrosion analysis of different interfaces within a stack.

5.2 Experimental

5.2.1 Manufacturing of protective coatings

To mitigate effects of chromium evaporation from interconnects, two different protective coatings were prepared and tested. The first one was manufactured from a commercially available $MnCo_2O_4$ powder, and the second one ($MnCo_{1.8}Fe_{0.2}O_4$) was manufactured in-house via a solid carbonate synthesis route. The coatings were deposited on Crofer 22 APU plates by a high-velocity oxygen flame (HVOF) method. See [78] for more details on the HVOF process. As using thin, formed steel interconnects is of interest from a cost savings point-of-view, coatings were also deposited on corrugated 0.2-mm-thick Crofer 22 APU coupons. Figure 22 presents a schematic of the test setup for analysing the mechanical properties of the manufactured coatings on top of corrugated steel plates. These plates had a corrugated area of 34x34 mm^2, and a force of 50 N was applied on top of the assembly. See [38] for more details on sample preparation.

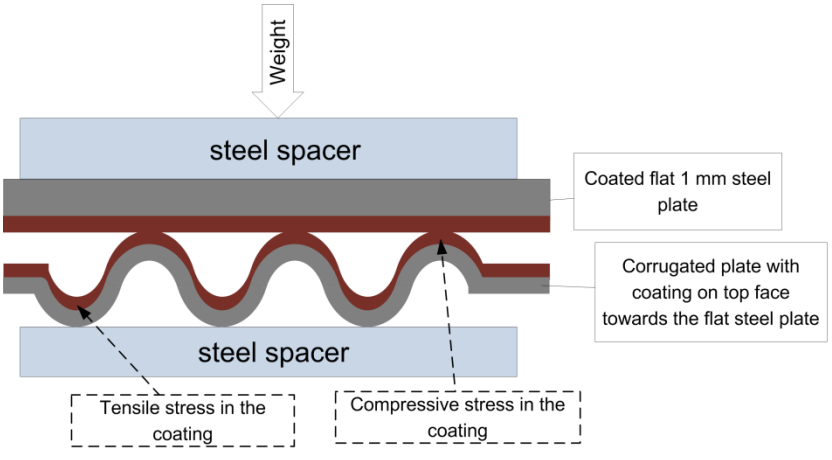

Figure 22. Protective coatings were deposited on corrugated steel coupons to analyse the effects of tensile and compressive stresses on the coating.

5.2.2 Area-specific resistance measurements

To evaluate the electrical performance of different chromium protective coatings, area-specific resistance (ASR) measurements were conducted on coated and uncoated steel plates. Two different coatings ($MnCo_2O_4$ and $MnCo_{1.8}Fe_{0.2}O_4$) were applied on flat steel plates and tested. Figure 23 shows the experimental setup of the ASR measurements. Plates were stacked into a tower, and $La_{0.85}Sr_{0.15}Mn_{1.1}O_3$ (LSM) spacers (IRD Fuel Cells A/S, Denmark) were inserted between samples to mimic the contact between the interconnect and cathode in the SOFC stack. Wires for voltage measurements were connected to the samples and current feed wires at the end of the tower. Current density in these measurements was 0.2 A/cm^2, which corresponds to the typical current density of an SOFC stack. A vertical load of 20 N was applied on the 20x20 mm^2 samples. The steady state measurements were conducted in dry air at 700 °C for 1000 h.

In order to avoid lateral current flow in the samples, the resistance of the samples needs to be significantly higher than that of the steel spacers. Resistivity of Crofer 22 H is about 1 µΩm, whereas resistivity of chromium oxides is of the order of 0.1…1 Ωm [29]. This difference of 5…6 orders of magnitude ensures that the current flow in the samples is perpendicular to the plane. Area specific resistances were calculated using

$$ASR = \frac{UA}{I}, \tag{9}$$

where U is voltage, A is sample area and I is current. Error estimate for the ASR can be calculated as

$$\Delta ASR = \frac{A}{I}\Delta U + \frac{UA}{I^2}\Delta I + \frac{U}{I}\Delta A = ASR\left(\frac{\Delta U}{U} + \frac{\Delta I}{I} + \frac{\Delta A}{A}\right) \tag{10}.$$

Majority of the error originates from the ΔA/A terms which denotes the placement error of samples on top of each other. The measurement accuracies were 5 µV, 0.5 mA and 0.5 cm^2. Therefore the total uncertainty of the ASR measurement is about 10%.

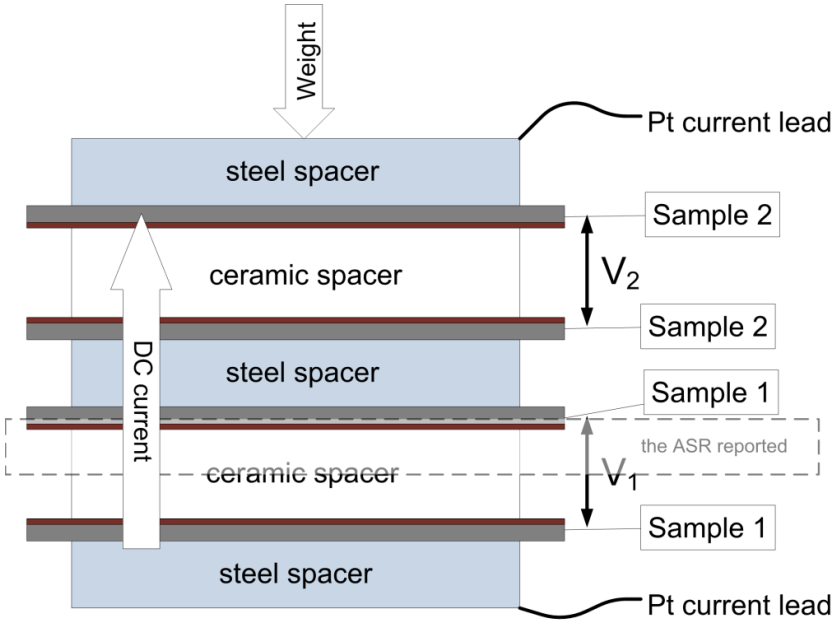

Figure 23. Setup for the ASR measurements.

5.2.3 Stack tests

To study corrosion phenomena in real SOFC stack operating conditions, two single cell stacks were manufactured. Table 6 provides information on the main components of the stacks used in these corrosion studies. The main purpose of stack one was to verify the effectiveness of the $MnCo_{1.8}Fe_{0.2}O_4$ spinel coating in suppressing chromium evaporation from the interconnect steels. The interconnect plates were manufactured from 1-mm-thick Crofer 22 APU steel and the gas channels were etched onto interconnects. A 20-µm-thick layer of $MnCo_{1.8}Fe_{0.2}O_4$ coating was sprayed with HVOF on the cathode side of interconnects. The stack was operated with hydrogen and air for 6000 h at 700 °C.

The main purpose of stack two was to study possible material interactions between sealing materials and interconnect steels. Seals for this stack were of a hybrid type consisting of compressible Thermiculite 866 core material [63] and glass interlayers. For more details on the sealing configuration, see [71]. The stack was operated for 1800 h at 700 °C with hydrogen and air. The effectiveness of the chromium barrier coating was also analysed.

Table 6. Main components of the two single cell SOFC stacks used in corrosion studies.

Stack	Cells	Inter-connects	Coatings	Coating method	Seals	Temp / °C	Duration / h
1	Anode supported Ni/YSZ/LSCF	Crofer 22 APU, d=1 mm	$MnCo_{1.8}Fe_{0.2}O_4$ (~20 µm)	HVOF	Thermiculite 866	700	6000
2	Anode supported Ni/YSZ/LSCF	Crofer 22 APU, d=0.2 mm	None	None	Thermiculite 866 + Schott GM31107 glass tapes	700	1800

5.3 Results

5.3.1 Mechanical properties of protective coatings

Protective coatings were first manufactured on top of flat and corrugated steel plates to analyse mechanical strength, adherence, and coverage of the layers. Figure 24 shows cross-sections of $MnCo_{1.8}Fe_{0.2}O_4$ coating on a flat Crofer 22 APU steel plate after 1000 h exposure in air at 700 °C. It can be noted that the coating is dense with only about 5% of closed porosity. The thickness of the chromium oxide layer on top of the steel is about 0.5 µm, which is a good result compared to a non-coated control sample, which showed an oxide layer of about 3 µm. Therefore, it can be concluded that the coating effectively reduces oxidation of the interconnect, thus prolonging its lifetime.

Figure 25 shows cross-sectional SEM images of the $MnCo_2O_4$-coated corrugated plate. It can be noticed that at both the top and the bottom of the groove, the coating is homogeneous and dense, with only about 5% of closed porosity. The image on the left (the top of the groove) shows that the coating has been able to withstand the compressive stress. In the right image (the bottom of the groove), small fractures can be noticed, suggesting that the tensile stress present in this location has caused fractures in the coating.

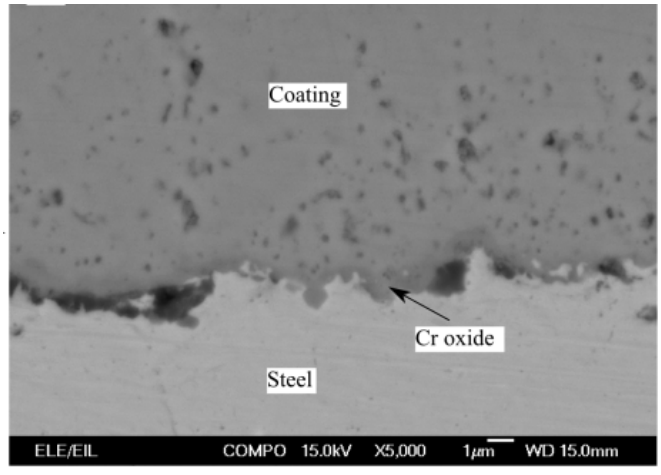

Figure 24. BSE SEM image $MnCo_{1.8}Fe_{0.2}O_4$ coating on Crofer 22 APU substrate exposed to air at 700 °C for 1000 h.

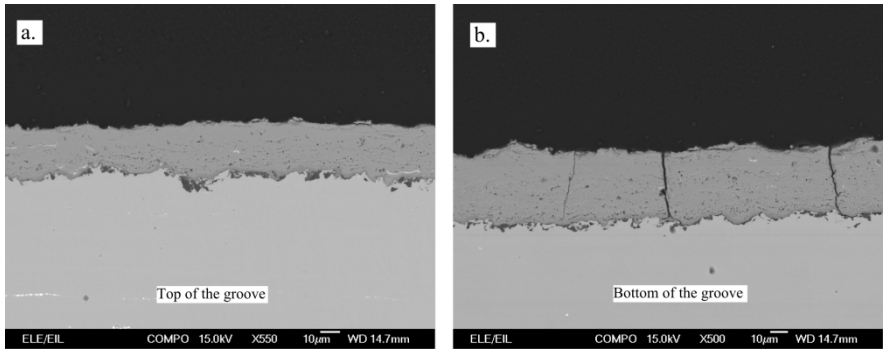

Figure 25. SEM images of $MnCo_2O_4$ coating deposited on top of corrugated Crofer 22 APU plates (Figure 22) after 1000 h exposure in air at 700 °C. Left: top of the groove (compressive stress); right: bottom of the groove (tensile stress).

5.3.2 Area-specific resistance measurements

Area-specific resistance measurements were carried out to evaluate ohmic losses associated with steel/cathode interfaces. Figure 26 shows ASRs of coated and uncoated Crofer 22 APU steel plates. It can be noted that both coatings show stable resistances of about 20 mOhmcm^2 throughout the 1000 h test. Resistance of the uncoated Crofer 22 APU plate declines during the test, starting from 100 mOhmcm^2, and shows signs of levelling at the end of the test, at about 50 mOhmcm^2. The decrease of ASR of the uncoated sample is related to the faster oxide layer growth compared to the coated samples. This growing oxide layer widens the actual contact area and therefore decreases the observed contact resistance.

The target for this work was to achieve less than 1% ohmic contact loss between the interconnect and cell. At 0.3 Acm^{-2} current density and 0.85 V cell voltage, this would correspond to an ASR of about 30 mΩcm^2. The coated steels showed ASRs of about 20 mOhmcm^2, which was well below this target.

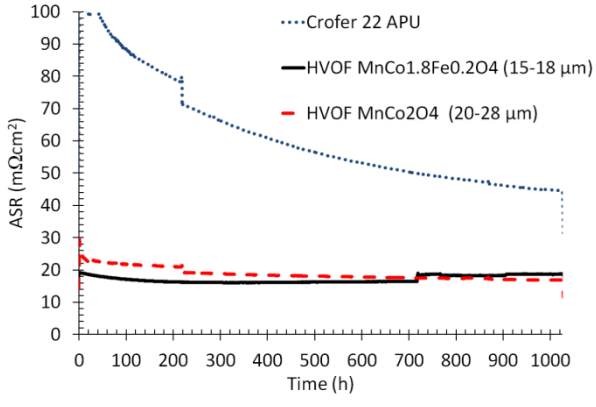

Figure 26. Area-specific resistance of coated and uncoated Crofer 22 APU plates.

5.3.3 Analyses of protective coatings after SOFC operation

The two stacks tested (Table 6) enabled a study of effectiveness of the $MnCo_{1.8}Fe_{0.2}O_4$ coating in preventing chromium evaporation. Figure 27 presents SEM images of the stack one cross section. Figure 27a shows that the coating has been uniformly deposited on the interconnect plate. What is noticeable is that the coating is also thick and dense at the sides of the rib, which are difficult areas for HVOF coating, as they are almost perpendicular to the spraying direction. After 6000 h of SOFC operation, the coating is still dense and the amount of porosity (~5%) is similar to the 1000 h ex-situ test (Figure 25). It seems that there have been no changes in the coating when compared to the 1000 h ex-situ test and the 6000 h SOFC operation tests, which is a good result indicating the stability of the coating. Figure 27b shows a cross-section at the location of the interconnect rib. EDS analyses of this area showed no signs of chromium in the cathode, suggesting that the coating has suppressed the chromium transport to the cathode. Figure 27d shows an EDS line scan of chromium in the middle of the gas channel (no contact with the interconnect). It can be noticed that there is a maximum of about 2% of chromium in the outer/middle part of the cathode furthest away from the electrolyte. To ascertain this result, 19 line scans from this area were measured. As a result, five of these scans showed chromium amounts over the detection limit (~0.3%). Since there was no chromium detected in the cathode area that was against the rib, it must be concluded that the chromium in the channel area has been most probably transported to this location in a gaseous phase. The origin for this chromium could be the uncoated end plates of the stack.

To compare the effectiveness of the chromium barrier coating against uncoated interconnect, the chromium content of the cathode was also analysed at two locations (Figure 28) of stack two. At the air channel location, EDS analysis showed a chromium concentration of 0…2% mostly at the outer surface of the cathode, which is in line with the findings of stack one. However, at the location where the cathode is in contact with the rib, there was as much as 18% of chromium near the contact area. This is a very significant amount compared to the coated stack, which showed no chromium at the cathode in this contact area.

These two stack tests have shown that the chromium evaporation-related corrosion and deactivation mechanisms were mitigated using protective $MnCo_{1.8}Fe_{0.2}O_4$ manufactured with HVOF. There was no noticeable change in the $MnCo_{1.8}Fe_{0.2}O_4$ coating when comparing the 1000 h ex-situ test and the 6000 h tests, suggesting it would be a good candidate in achieving a 10000 h operational lifetime.

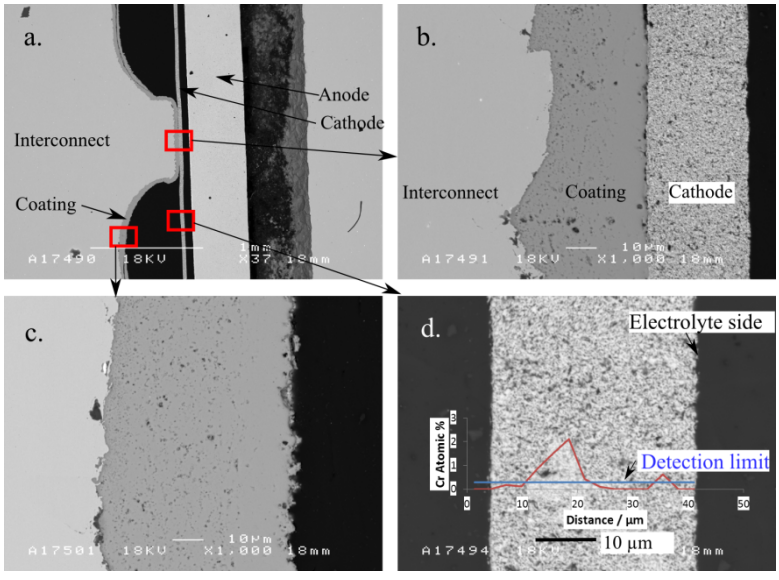

Figure 27. Cross-sectional SEM images of stack 1 with coated interconnects.

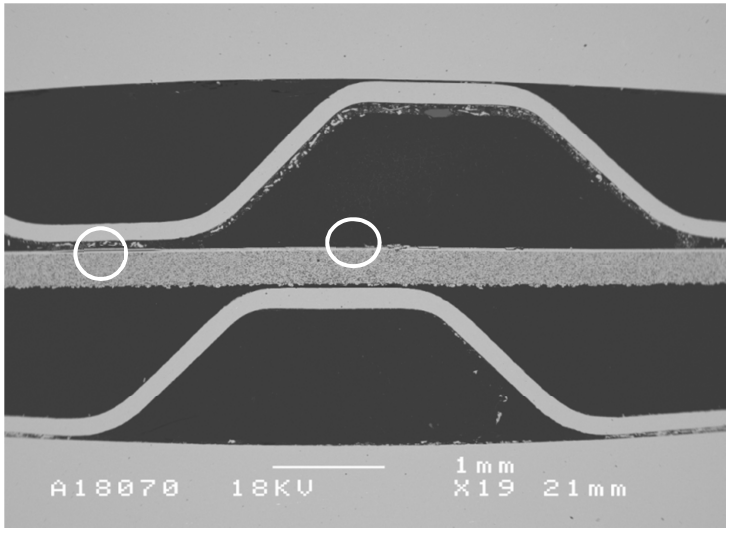

Figure 28. Cross-sectional SEM image of stack two. White circles indicate locations of the EDS analysis. Left: cathode against the interconnect rib; right: cathode at the gas channel.

5.3.4 Analysis of material interaction after SOFC operation

The main purpose of stack two (Table 6) was to study possible material interaction between sealing materials, interconnects, and the cell. Figure 29 shows a SEM image of the seal away from its outer edges, meaning it is only exposed to a gas atmosphere through leakage. The oxide layer thickness on the Crofer 22 APU interconnect is about 1 µm, which can be seen as a good value after 1800 h of SOFC operation. Figure 30a&b shows SEM images of the steel/glass/air triple interface at the upper and lower parts of the same seal. The upper part is free of corrosion, but in the lower location there is a corrosion layer of about 20 µm of thickness, spreading 200 µm from the triple interface. A similar corrosion layer was also found on the bottom of the gas manifold. The bottom of the manifold channel is the most difficult spot to clean before assembly. This suggests that this corrosion effect might have been caused by insufficient cleaning of the plates.

Figure 31 shows a SEM image of the glass/electrolyte interface. The adherence of the glass to the electrolyte is good, and no visible material interaction can be seen.

Figure 32 shows a SEM image of the steel/glass interface exposed to an anode atmosphere. The location is close to the anode outlet, so in addition to hydrogen there is also steam present, due to fuel cell reactions. No material interaction is detectable at this point. The cracks in the glass layer have been caused by the sample preparation.

Corrosion behaviour of interconnects in single and dual atmosphere exposure was also studied with this stack. Figure 33 shows SEM images of interconnects in a fuel/air atmosphere (left) and in an air/air atmosphere (right). In both atmospheres, oxide layer thicknesses are 1…2 µm, and the scales seem dense and well adhered to interconnects. In both exposure conditions, there is a limited amount of inward oxidation, with a depth of 5 µm. There are no signs of detrimental corrosion, which is a good result considering that the interconnects were not coated.

The hybrid seal developed in this work did not cause unwanted corrosion at the interfaces of sealing during 1800 h of testing. Therefore, it can be concluded that these material solutions have the potential to be used in SOFC stacks in long-term operation.

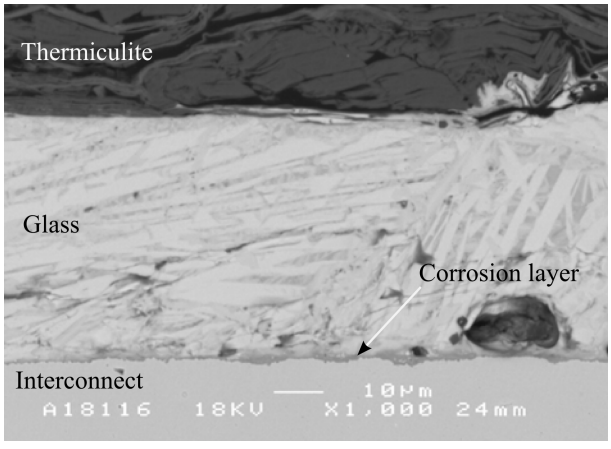

Figure 29. SEM-image taken in the middle of the seal, away from the outer faces.

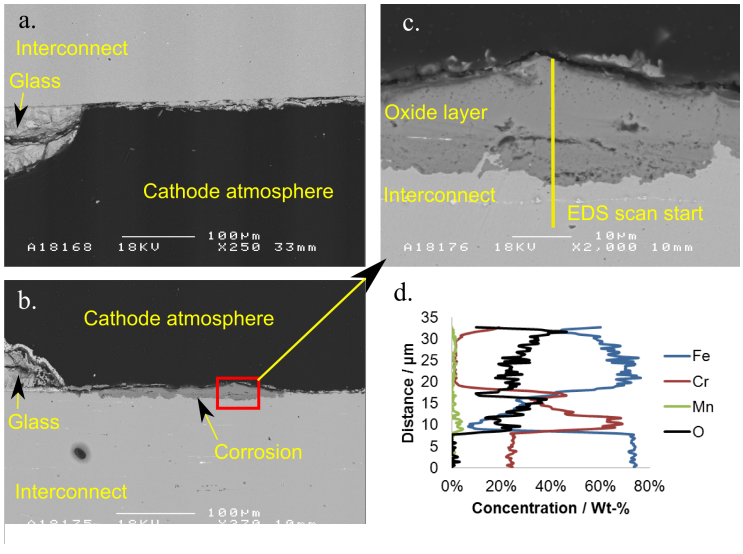

Figure 30. SEM cross-sectional images of steel/glass interfaces exposed to a cathode atmosphere.

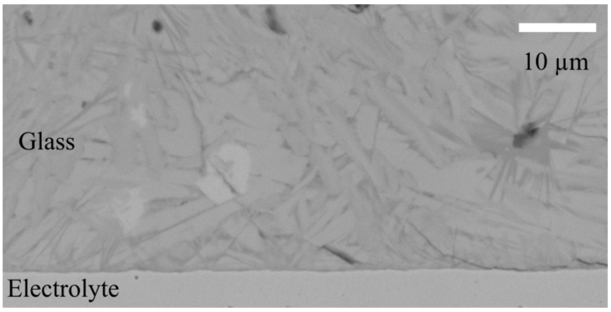

Figure 31. SEM image of the glass/electrolyte interface.

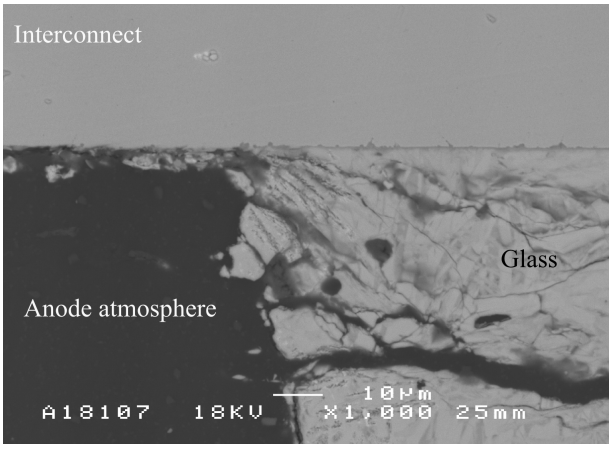

Figure 32. SEM image of the steel/glass interfaces exposed to an anode atmosphere.

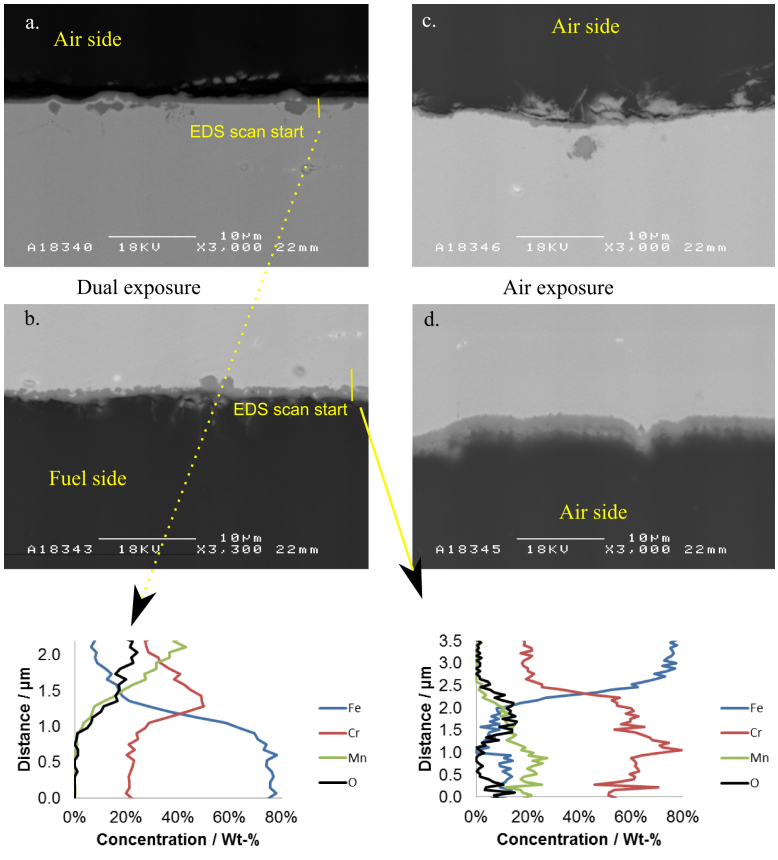

Figure 33. SEM images showing interconnects exposed to a dual atmosphere (left) and an air atmosphere (right).

6. Summary and conclusions

The aim of this thesis was to achieve a performance increase and cost reductions in SOFC stack technology. This goal was pursued by analysis and development of in-stack materials and their behaviour. The SOFC stack creates a challenging environment in which materials are subjected to high temperatures in a dual atmosphere. Therefore, a thorough understanding of the materials is needed to achieve the lifetime and performance increases to which the SOFC research community is committed.

This thesis contributes to the field first by drawing attention to the importance of the mechanical properties of sealing materials and their relation to stack sealing and electrical contact. The mechanical properties of several materials were analysed between room temperature and 700 °C. It is clear that the properties of SOFC sealing materials depend on temperature and their properties need to be evaluated over the given stress and temperature range before using them in-stack. The literature is very short on relevant data on the mechanical properties of these materials. Therefore, the data and guidelines set forth in this work contribute to the field.

To realise cost reductions in SOFC stack technology, it is tempting to reduce stack material usage. Therefore, aiming to lower the necessary compressive stress on the stack is needed to allow for less bulky components to be used. In this thesis, a hybrid sealing solution consisting of compressible core material and glass-based coating was developed. The coating effectively decreased the interfacial leakages and allowed for the material to be used at low compressive stress, down to 0.1 MPa, with leak rates as low as around 0.3 ml (m min)$^{-1}$ using 50/50 H_2/N_2. This is a reduction of about 60…90% compared to the uncoated core material. For example, Chou et al. have measured leak rates of the order of 0.5 ml (m min)$^{-1}$ using mica papers with glass interlayers at compressive stresses of 0.1 MPa [65]. The tests were carried out with 2.64% H_2 in humidified Ar, which, according to the results presented in this work, significantly reduces the observed leak rate compared to 50/50 H_2/N_2. Although different conditions make direct comparison difficult, it is clear that the results presented in this thesis compare favourably with the state-of-the-art SOFC sealing materials. The intellectual property

rights of the hybrid sealing solution presented in this thesis have been transferred to Flexitallic Ltd, which has further developed this technology and issued a patent application on it [72]. In October 2014, they launched a product called Thermiculite 866LS based on this work.

Understanding corrosion phenomena in SOFC stacks is crucial in increasing their lifetime. Compatibility of the developed hybrid seals with the adjacent stack components was analysed. Post-mortem analyses of the stack in which these seals were used showed no signs of seal-induced corrosion. To further increase the lifetime of stacks, a $MnCo_{1.8}Fe_{0.2}O_4$-based protective coating was developed. The coating showed very good stability over 6000 h of in-stack testing. The amount of chromium deposited on the cathode decreased significantly with the coating, compared to the non-coated stack. This development work forms a very good starting point in achieving stack lifetimes of over 10 000 h.

In total, it can be concluded that the targets set for this research work were well met. The materials and methods developed in this work help to realise stacks with lower leak rates and ohmic losses, resulting in higher electrical efficiency. This, together with increased stack lifetime, helps in bringing the price per produced energy unit down.

In the future, understanding of the mechanical properties of SOFC stack sealing materials should be further enhanced. With the methodology presented here, tests should be carried out to find out long-term properties, such as creep and stress retention of the materials. Thermal cycling tests using the hybrid seals should be carried out to find out the effects of coating parameters such as coating thickness and porosity on the seals resistance to thermal cycling. Stack tests or ex-situ tests in realistic conditions with durations of several thousands of hours should also be carried out to further study possible long-term material interactions between interconnects, seals, the coating, and the SOFC cell.

References

[1] W. Schönbein, "Prof. Schönbein's Discussion of M. Fechner's Views of the Theory of Galvanism, with reference, particularly, to a Circuit including Two Electrolytes, and to the relations of Inactive Iron", *London and Edinburgh Philosophical Magazine and Journal of Science*, vol. 10, pp. 161-171, 1938.

[2] K. Kordesch, "25 Years of Fuel Cell Development (1951-1976)", *Journal of the Electrochemical Society*, vol. 125, pp. 77C-88C, Mar. 1978.

[3] B. Pollet, I. Staffell, and J. Shang, "Current status of hybrid, battery and fuel cell electric vehicles: From electrochemistry to market prospects", *Electrichimica Acta*, vol. 84, pp. 235-249, 2012.

[4] FuelCellToday, "The Fuel Cell Industry Review 2013", 2013.

[5] I. Staffell and R. Green, "The cost of domestic fuel cell micro-CHP systems", *International Journal of Hydrogen Energy*, vol. 38, no. 2, pp. 1088-1102, 2013.

[6] K. Krulla et al., "Assessment of the Distributed Generation Market Potential for Solid Oxide Fuel Cells", U.S. Department of Energy, DOE/NETL- 342/093013 2013.

[7] D. Brengel, "Solid State Energy Conversion Alliance (SECA) SOFC Program Review", 2010.

[8] B. James, A. Spisak, and W. Colella, "Manufacturing Cost Analysis of Stationary Fuel Cell Systems", Strategic analysis Inc, 2012.

[9] W. Schafbauer, N. Menzler, and H. Buchkremer, "Tape Casting of Anode Supports for Solid Oxide Fuel Cells at Forschungszentrum Jülich", *International Journal of Applied Ceramic Technology*, vol. 11, no. 1, pp. 125-135, 2014.

[10] Elcogen. (2014, Dec.) Elcogen. [Online]. http://www.elcogen.com/en/sofc-single-cells/technical-data

[11] S. Angeli, G. Monteleone, A. Giaconia, and A. Lemonidou, "State-of-the-art catalysts for CH_4 steam reforming at low temperature", *International Journal of Hydrogen Energy*, vol. 39, pp. 1979-1997, 2014.

[12] SOFCMAN Energy Technology. (2015, Jan.) SOFCMAN Energy Technology. [Online]. http://www.sofc.com.cn

[13] (2014, Dec.) Kerafol. [Online]. http://www.kerafol.com/en/sofc/components-for-fuel-cell-technology/electrolyte-supported-cells-esc.html

[14] B. Borglum, "Solid Oxide Fuel Cell Development at Versa Power Systems" in *2012 Fuel Cell Seminar*, Nov. 2012. [Online]. http://www.fuelcellseminar.com/media/51287/sta42-3.pdf

[15] N. Menzler, F. Tietz, S. Uhlenbruck, H. Buchkremer, and D. Stöver, "Materials and manufacturing technologies for solid oxide fuel cells", *Journal of Material Science*, no. 45, pp. 3109-3135, 2010.

[16] "Fuel Cell Handbook," U.S. Department of Energy, Office of Fossil Energy, National Energy Technology Laboratory, Morgantown, 2004. [Online]. http://www.netl.doe.gov/File%20Library/research/coal/energy%20systems/fuel%20cells/FC Handbook7.pdf

[17] M. Rautanen, O. Himanen, J. Kiviaho, and J. Pennanen, "Method and arrangement for feeding reactants into a fuel cell stack and an electrolyzer stack", Application WO 2014068168 A1, Oct. 31, 2012.

[18] L. Blum et al., "Recent results in Jülich solid oxide fuel cell technology development", *Journal of Power Sources*, no. 241, pp. 477-485, 2013.

[19] B. Borglum, E. Tang, and M. Pastula, "The Status of SOFC Development at Versa Power Systems", *ECS Transactions*, vol. 25, no. 2, pp. 65-70, 2009.

[20] J. Fergus, "Lanthanum chromite-based materials for solid oxide fuel cell interconnects", *Solid State Ionics*, vol. 171, no. 1-2, pp. 1-15, 2004.

[21] T. Armstrong, J. Stevenson, L. Pederson, and P. Raney, "Dimensional Instability of Doped Lanthanum Chromite", *Journal of the Electrochemical Society*, vol. 143, no. 9, pp. 2919-2925, 1996.

[22] Z. Yang, K. Weil, D. Paxton, and J. Stevenson, "Selection and Evaluation of Heat-Resistant Alloys for SOFC Interconnect Applications", *Journal of The Electrochemical Society*, vol. 150, no. 9, pp. A1188-A1201, 2003.

[23] ThyssenKrupp. Crofer 22 H material datasheet, June 2008. [Online]. http://www.fcdic.com/ja/member/data/Crofer22H.pdf

[24] Outokumpu, "AISI 441 Datasheet," *2009*.

[25] Hitachi Metals America. (2014, Dec.) Fuel Cell Interconnector. [Online]. http://www.hitachimetals.com/product/specialtysteel/fuelcellseparator/

[26] M. Schuisky, "Pre-coated 441 strip steel for SOFC interconnects" in *Fuel Cell Seminar*, Orlando, 2011.

[27] Allegheny Technologies Incorporated. (2015, Jan.) E-Brite technical datasheet. [Online]. https://www.atimetals.com/Documents/ati_e-brite_tds_en_v1.pdf

[28] Plansee. (2014, Dec.) CFY: Chromium alloy for SOFC interconnects. [Online]. http://www.plansee.com/en/CFY-1484.htm

[29] Z. Yang, J. Stevenson, D. Paxton, P. Singh, and K. Weil, "Materials Properties Database for Selection of High-Temperature Alloys and Concepts of Alloy Design for SOFC Applications", Pacific Northwest National Laboratory, 2002. [Online]. http://www.pnl.gov/main/publications/external/technical_reports/PNNL-14116.pdf

[30] P. Huczkowski et al., "Oxidation limited life times of chromia forming ferritic steels", *Materials and Corrosion*, vol. 55, no. 11, pp. 825-830, 2004.

[31] J. Froitzheim, H. Ravash, E. Larsson, L. Johansson, and J. Svensson, "Investigation of Chromium Volatilization from FeCr Interconnects by a Denuder Technique", *Journal of The Electrochemical Society*, vol. 157, pp. B1295-B1300, 2010.

[32] E. Opila et al., "Theoretical and Experimental Investigation of the Thermochemistry of $CrO_2(OH)_2(g)$", *Journal of Physical Chemistry A*, vol. 111, pp. 1971-1980, 2007.

[33] O. Thomann, M. Pihlatie, J. Schuler, O. Himanen, and J. Kiviaho, "Method for Measuring Chromium Evaporation from SOFC Balance-of-Plant Components", *ECS Transactions*, vol. 35, pp. 2609-2616, 2011.

[34] J. Fergus, "Effect of cathode and electrolyte transport properties on chromium poisoning in solid oxide fuel cells", *International Journal of Hydrogen Energy*, vol. 32, pp. 3664-3671, 2007.

[35] A. Balland, P. Gannon, M. Deibert, S. Chevalier, G. Caboche, and S. Fontana, "Investigation of La_2O_3 and/or $(Co,Mn)_3O_4$ deposits on Crofer22APU for the SOFC interconnect application", *Surface Coating Technology*, vol. 203, no. 20-21, pp. 3291-3296, 2009.

[36] C. Chu, J. Wang, and S. Lee, "Effects of $La_{0.67}Sr_{0.33}MnO_3$ protective coating on SOFC interconnect by plasma-sputtering", *International Journal of Hydrogen Energy*, vol. 33, no. 10, pp. 2536-2546, 2008.

[37] Z. Yang, G. Xia, G. Maupin and J. Stevenson, "Evaluation of Perovskite Overlay Coatings on Ferritic Stainless Steels for SOFC Interconnect Applications", *Journal of The Electrochemical Society*, vol. 153, pp. A1852-A1858, 2006.

[38] O. Thomann et al., "Development and application of HVOF sprayed protective coatings for SOFC interconnects", *Journal of Thermal Spray Technology,* vol. 22, no. 5, pp. 631-639, 2013.

[39] F. Tietz, D. Sebold, H. Buchkremer, A. Ringuede, M. Cassir, A. Laresgoiti, I. Villarreal and X. Montero, "$MnCo_{1.9}Fe_{0.1}O_4$ spinel protection layer on commercial ferritic steels for interconnect applications in solid oxide fuel cells", *Journal of Power Sources*, vol. 184, no. 1, pp. 172-179, 2008.

[40] D. Lim, D. Lim, J. Oh, and I. Lyo, "Influence of Post Treatments on the Contact Resistance of Plasma-Sprayed $La_{0.8}Sr_{0.2}MnO_3$ Coating on SOFC Metallic Interconnector", *Surface Coating Technology*, vol. 200, no. 5-6, pp. 1248-1251, 2005.

[41] H. Zhai, W. Guan, Z. Li, C. Xu, and W. Wang, "Research on Performance of LSM Coating on Interconnect Materials for SOFCs", *Journal of the Korean Ceramic Society*, vol. 45, no. 12, pp. 777-781, 2008.

[42] M. Garcia-Vargas, M. Zahid, F. Tietz, and A. Aslanides, "Use of SOFC Metallic Interconnect Coated with Spinel Protective Layers Using the APS Technology", *ECS Transactions*, vol. 7, p. 2399, 2007.

[43] S. Fontana et al., "Metallic interconnects for SOFC: Characterisation of corrosion resistance and conductivity evaluation at operating temperature of differently coated alloys", *Journal of Power Sources*, vol. 171, pp. 652-662, 2007.

[44] S. Fontana, S. Chevalier, and G. Caboche, "Performance of reactive element oxide coating during long time exposure" *Materials and Corrosion*, vol. 62, pp. 650-658, 2011.

[45] T. Suntola and J. Antson, "Method for producing compound thin films", U.S. Patent No. 4058430, 1977.

[46] D. Gödeke, J. Besinger, Y. Pflügler, and B. Ruedinger, "New Glass Ceramic Sealants for SOFCs", vol. 25, no. 2, pp. 1483-1490, 2009.

[47] J. Suffner and C. Dobler, "Long Term Behavior of Viscous High-Temperature Sealing Glasses", *ECS Transactions*, vol. 57, pp. 2375-2383, 2013.

[48] VIOX. (2014, Dec.) Glass Options for SOFC Applications. [Online]. http://viox.thomasnet.com/viewitems/electronic-specialty-glass/glass-options-for-sofc-seal-applications-2?

[49] T. Ertugrul, S. Celik, and M. Mat, "Effect of binder burnout on the sealing performance of glass ceramics for solid oxide fuel cells", *Jounal of Power Sources*, no. 242, pp. 775-783, 2013.

[50] A. Shyam et al., "Microstructural evolution in two alkali multicomponent silicate glasses as a result of long-term exposure to solid oxide fuel cell environments", *J Mater Sci*, 2013.

[51] K. Weil, "The state-of-the-art in sealing technology for solid oxide fuel cells", *The Journal of The Minerals, Metals & Materials Society (TMS)*, vol. 58, no. 8, pp. 37-44, 2006.

[52] V. Kumar, A. Arora, O. Pandey, and K. Singh, "Studies on thermal and structural properties of glasses as sealants for solid oxide fuel cells", *International Journal of Hydrogen Energy*, vol. 33, pp. 434-438, 2008.

[53] L. Blum et al., "Investigation of solid oxide fuel cell sealing behaviour under stack relevant conditions at Forschungzentrum Jülich", *Journal of Power Sources*, vol. 196, no. 17, pp. 7175-7181, 2011.

[54] M. Peksen, A. Al-Masri, L. Blum, and D. Stolten, "3D transient thermomechanical behaviour of a full scale SOFC short stack", *International journal of hydrogen energy*, vol. 38, pp. 4099-4107, 2013.

[55] G. Wypych, *Handbook of Fillers – A Definitive User's Guide and Databook*, 2nd ed. Toronto, Canada: ChemTec Publishing, 2000.

[56] P. Ciullo, Ed., *Industrial Minerals and Their Uses – A Handbook and Formulary*. Noyes, Westwood, USA: William Andrew Publishing, 1996.

[57] Feodor Burgmann Dichtungswerke GmbH, *Sealing Technology*, vol. 6, 2000.

[58] Y. Chou, J. Stevenson, and L. Chick, "Ultra-low leak rate of hybrid compressive mica seals for", *Journal of Power Sources*, vol. 112, no. 1, pp. 130-136, 2002.

[59] Y. Chou, J. Stevenson, and L. Chick, "Novel compressive mica seals with metallic interlayers", *Journal of the American Ceramic Society*, vol. 86, no. 6, pp. 1003-1007, 2003.

[60] M. Rautanen, O. Himanen, V. Saarinen, and J. Kiviaho, "Compression Properties and Leakage Tests of Mica-Based Seals for SOFC applications", *Fuel Cells*, pp. 753-759, 2009.

[61] S. Simner and J. Stevenson, "Compressive mica seals for SOFC applications", *Journal of Power Sources*, vol. 102, no. 1-2, pp. 310-316, 2001.

[62] M. Bram et al., "Deformation behavior and leakage tests of alternate sealing materials for SOFC stacks", *Journal of Power Sources*, vol. 138, no. 1-2, pp. 111-119, 2004.

[63] J. Hoyes and S. Bond, "Gaskets for sealing solid oxide fuel cells", *Sealing Technology*, no. 8, pp. 11-14, 2007.

[64] J. Hoyes and M. Rautanen, "SOFC Sealing with Thermiculite 866 and Thermiculite 866 LS", *ECS Transactions*, vol. 57, no. 1, pp. 2365-2374, 2013.

[65] Y. Chou and J. Stevenson, "Long-term ageing and materials degradation of hybrid mica", *Journal of Power Sources*, vol. 191, no. 2, pp. 384-389, 2009.

[66] Y. Chou, J. Stevenson, and P. Singh, "Thermal cycle stability of a novel glass-mica composite", *Journal of Power Sources*, vol. 152, no. 1-2, pp. 168-174, 2005.

[67] M. Rautanen, V. Pulkkinen, J. Tallgren, O. Himanen, and J. Kiviaho, "Effects of the first heat up procedure on mechanical properties of solid oxide fuel cell sealing materials", *Journal of Power Sources*, vol. 284, pp. 511-516, 2015.

[68] V. Haanappel, V. Shemet, I. Vinke and W. Quadakkers, "A novel method to evaluate the suitability of glass sealant–alloy combinations under SOFC stack conditions", *Journal of Power Sources*, vol. 141, no. 1, pp. 102-107, 2005.

[69] M. Mahapatra and K. Lu, "Glass-based seals for solid oxide fuel and electrolyzer cells – A review", *Materials Science and Engineering*, vol. 67, no. 5-6, pp. 65-85, 2010.

[70] *ASTM D445-15 Standard Test Method for Kinematic Viscosity of Transparent and Opaque Liquids (and Calculation of Dynamic Viscosity)*.: ASTM International.

[71] M. Rautanen, O. Thomann, O. Himanen, J. Tallgren, and J. Kiviaho, "Glass coated compressible solid oxide fuel cell seals", *Journal of Power Sources*, vol. 247, pp. 243-248, 2014.

[72] M. Rautanen, J. Hoyes, O. Himanen, and J. Kiviaho, "Gasket for fuel cells", Application PCT/GB2014/050161 WO2014111735 A1, Jan. 21, 2013.

[73] N. Menzler et al., "Studies of Material Interaction After Long-Term Stack Operation", *Fuel Cells*, vol. 07, no. 05, pp. 356-363, 2007.

[74] W. Liu and E. Konysheva, "Conductivity of $SrCrO_4$ and its Influence on Deterioration of Electrochemical Performance of Cathodes in Solid Oxide Fuel Cells", *ECS Transactions*, vol. 59, pp. 327-332, 2014.

[75] N. Shaigan, W. Qu, D. Ivey and W. Chen, "A Review of Recent Progress in Coatings, Surface Modifications and Allou Developments for Solid Oxide Fuel Cell Ferritic Stainless Steel Interconnects", *Journal of Power Sources*, vol. 195, no. 6, pp. 1529-1542, 2010.

[76] Y. Larring and T. Norby, "Spinel and Perovskite Functional Layers Between Plansee Metallic Interconnect (Cr-5 Wt% Fe-1 Wt% Y_2O_3) and Ceramic $(La_{0.8}Sr_{0.15})_{0.91}MnO_3$ Cathode Materials for Solid Oxide Fuel Cells", *Journal of the Electrochemical Society*, vol. 147, no. 9, pp. 3251-3256, 2000.

[77] J. Puranen et al., "The Structure and Properties of Plasma Sprayed Iron Oxide Doped Manganese Cobalt Oxide Spinel Coatins for SOFC Metallic Interconnectors", *Journal of Thermal Spray Technology*, vol. 20, no. 1-2, pp. 154-159, 2011.

[78] J. Lagerbom et al., "$MnCo_2O_4$ Spinel Chromium Barrier Coatings for SOFC Interconnects by HVOF", in *9th Liege Conference on Materials for Advanced Power Engineering*, 2010, pp. 925-932.

PUBLICATION I

Compression properties and leakage tests of mica-based seals for SOFC stacks

Fuel Cells. Vol. 9 (2009) No: 5, 753–759.

DOI: 10.1002/fuce.200900029

Compression Properties and Leakage Tests of Mica-Based Seals for SOFC Stacks

M. Rautanen*, O. Himanen, V. Saarinen, and J. Kiviaho

VTT Technical Research Centre of Finland, Fuel Cells, P.O. Box 1000, Biologinkuja 5, Espoo, FI-02044 VTT, Finland

Received February 18, 2009; accepted April 15, 2009

Abstract

Sealing properties and compression properties of two mica-based materials, Thermiculite 866 and Statotherm HT were measured. Thermiculite 866 was tested in two forms: as-made and precompressed (consolidated). Sealing tests were carried out at 800 °C with simulated fuel cell anode gas. Seals were pressed to a constant thickness, which represents the conditions in fuel cell stacks. Both seals showed stable leak rates over test periods of roughly 400 h. Leak rates of Thermiculite 866 samples were found to be independent of the hydrogen overpressure within the measurement accuracy in the pressure range of 10–100 mbar(g). However, a Statotherm HT gasket tested with lower compression stress compared to Thermiculite 866 gaskets showed roughly linear dependency on the overpressure. Compression tests were carried out at room temperature and at 800 °C. Compression properties of both materials were found to strongly depend on temperature. Both materials experienced swelling when heated to 800 °C and were more ductile compared to room temperature.

Keywords: Leak Rate, Mica, Seal, SOFC, Statotherm HT, Thermiculite 866

1 Introduction

A solid oxide fuel cell (SOFC) is an electrochemical device in which reactants are converted into electricity and heat. Main components of fuel cell stacks are cells, interconnects and seals. Seals should be stable, both in reducing atmospheres with high water vapour contents and in oxidising atmospheres. Chemical stability with interconnects in operating temperature and during thermal cycles is also required. A sealing failure in SOFC stack causes gas leakage which decreases the overall performance and the lifetime of the stack. Leakages can cause cell degradation by a number of mechanisms, e.g. increased thermal gradients [1], local shortage of fuel, oxidation of the anode and increased chromium evaporation [2] due to higher water vapour content at the cathode.

Seals in SOFCs are often either glass or glass-ceramics. Glass-ceramic sealants are rigidly bonded and thus may offer excellent sealing characteristics. However, using glass ceramics requires that all the stack components need to have matching coefficients of thermal expansion (CTE) to avoid mechanical failures. Typically, glass-ceramics also require a specific heat treatment in which binder is evaporated and a stable phase is formed. Chemical reactions have also been reported between glass-ceramics and other stack components. These reactions can include cross-diffusion [3] and excessive surface and internal oxidation at steel-sealant interface [4] as well as increased chromium evaporation from interconnect steels [5].

In order to mitigate the drawbacks of glass-ceramic sealants, a number of compressive sealing materials mainly based on mica have been proposed. Mica is a group of silicate minerals having a general structure of $AB_{2-3}(Al,Si)Si_3O_{10}(OH)_2$ in which A is either K, Na, Ca or Ba and B is either Al, Fe, Mg or Li [6]. Micas can also contain other elements such as F^- replacing some of the OH^- ions [7]. A few studies have been undertaken to assess the high temperature sealing properties of phlogopite ($KMg_3(AlSi_3O_{10})(OH)_2$) and muscovite ($KAl_2(AlSi_3O_{10})(OH)_2$) type micas. In temperatures exceeding 600 °C, muscovite mica has been reported to lose its constitutional water whereas phlogopite mica experiences the loss of constitutional water around 950 °C. This behaviour causes swelling of the mica material, which however might not necessarily affect the sealing properties [8]. It

[*] *Corresponding author, markus.rautanen@vtt.fi*

has been found that to achieve good sealing properties, mica papers comprising of discrete mica platelets require high compression stresses in excess of 6 MPa [8, 9]. Therefore, a number of hybrid seals have been proposed. Good sealing properties have been observed with hybrid sealing structures such as mica with glass-ceramic contact layers [10, 11] and mica with a corrugated metallic profile [9]. Thermal cycle capability of mica-based seals has been demonstrated with minimum drop in open-circuit voltage during 1,000 thermal cycles [12]. Some experimental compressive seals have also been developed based on ceramics [13] and fibre papers infiltrated with ceramic powders [14].

Considering stack-design, it is important to know the compression properties of the sealing materials. Sufficient mechanical stress on the cell and on the seals is required to achieve good electrical contact between cells and interconnects as well as to achieve good sealing properties. Compression stresses in the stack are limited by the material properties of seals, interconnects and cells. All the publications found on compressible mica seals were carried out with the sealing material compressed with a constant force. However, in a planar SOFC stack, this is often hard to achieve since the cell needs to have a good electrical contact to the interconnect and thus it needs to carry at least some of the load. Therefore, the seals around the cells are actually pressed into a constant thickness rather than with a constant force. This is illustrated in Figure 1a in which an anode-supported cell is pressed between two interconnects. Sealing is required between the electrolyte and interconnect and between the interconnects. In both cases, the cell acts as a spacer keeping the seals at constant thickness.

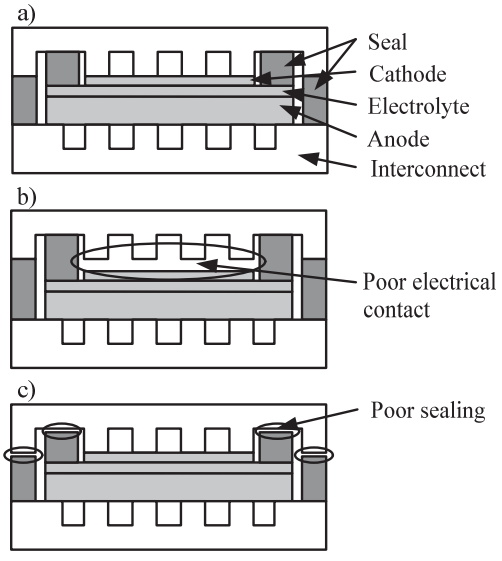

Fig. 1 (a) Simplified structure of a single repeating unit of a fuel cell stack based on an anode supported cell. (b) Poor electrical contact between cell and interconnect due to insufficient compressibility of the seals. Good sealing properties due to high surface stress on the seals. High mechanical stresses on interconnects. (c) Good electrical contact due to excess compressibility of the seals. Poor sealing properties due to low surface stress on the seals.

Figure 1b shows a case in which compression of the seals is insufficient. Thus, the seals experience most of the mechanical load on the stack and good sealing properties may be achieved. However, stresses on the interconnect are concentrated on a smaller area which can lead to mechanical failure. In this case, the cell experiences insufficient mechanical load, thus decreasing electrical contact. Figure 1c shows a case in which seals are either too thin or too compressible. This leads to insufficient compression stress on the seals and to poor sealing properties. However, electrical contact between cell and interconnect is maximised.

In this study, the long term sealing properties and compression properties of two types of commercial mica-based seals were studied. The sealing tests were carried out at 800 °C with seals compressed to a constant thickness. Compression properties of the materials were measured at room temperature and at 800 °C. Materials studied were Thermiculite 866 [15] and Statotherm HT [16].

2 Experimental

2.1 Materials

Thermiculite 866 (Flexitallic Ltd) [16] is a composite material consisting of chemically exfoliated vermiculite mica. Thermiculite 866 is available in two forms: as-made and consolidated, which were both tested. Consolidated form is a densified form of Thermiculite 866 and it is made by precompressing as-made material. Figure 2 illustrates SEM cross-sections of Thermiculite 866 samples. Images show horizontal vermiculite platelets (light-grey), steatite (grey) and voids (black). It can be noted that precompression diminishes the porosity of Thermiculite 866.

Statotherm HT (Burgmann industries) [4] is phlogopite mica with organic binder. Figure 3 illustrates the SEM cross-section of uncompressed Statotherm HT. Large voids between discreet mica platelets are seen.

2.2 Compression Properties

Compression tests were carried out with Instron 8801 fatigue system. Figure 4 shows a picture of the test setup. Round samples (12 mm diameter) were compressed between 13 mm diameter rods made of 253MA steel, and their thickness was measured with a strain-gauge. Tests were carried out at room temperature and at 800 °C. The high temperature tests were done by inductively heating the compression rods and measuring their temperature with thermocouples inserted into the compression rods.

2.3 Sealing Properties

Sealing properties were tested by compressing the seals to constant thickness and measuring the leak rates. Figure 5 shows the exploded view of the gasket holder setup. Gasket holder plates with circular groves for the seal-

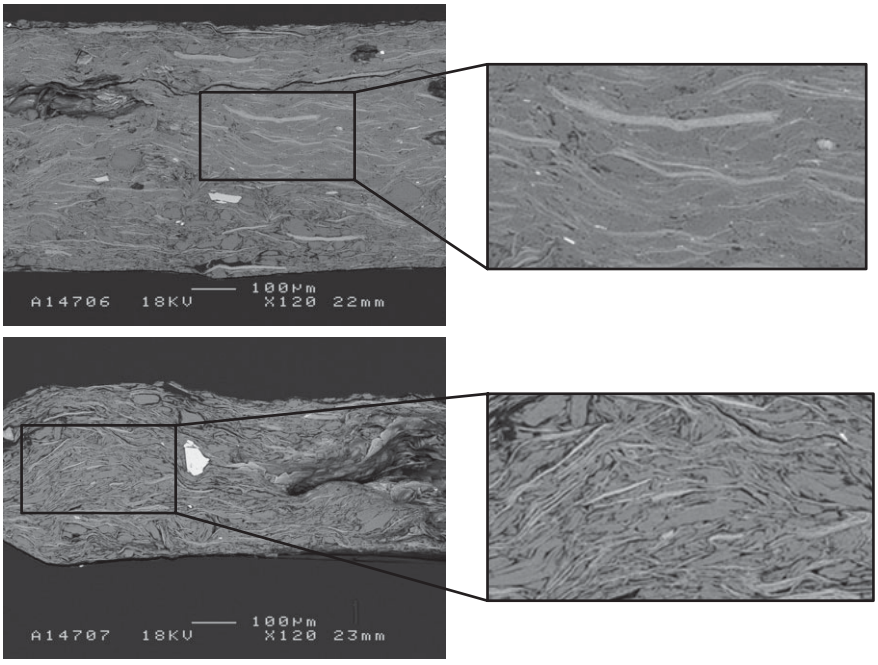

Fig. 2 SEM images of the consolidated (above) and as-made Thermiculite 866 cross-sections.

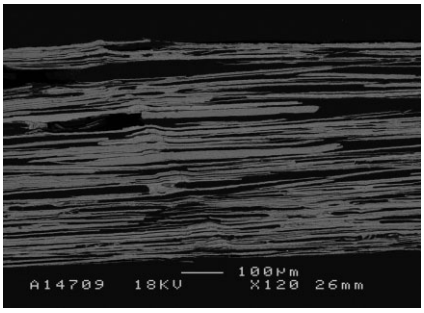

Fig. 3 SEM image of the uncompressed Statotherm HT cross-section.

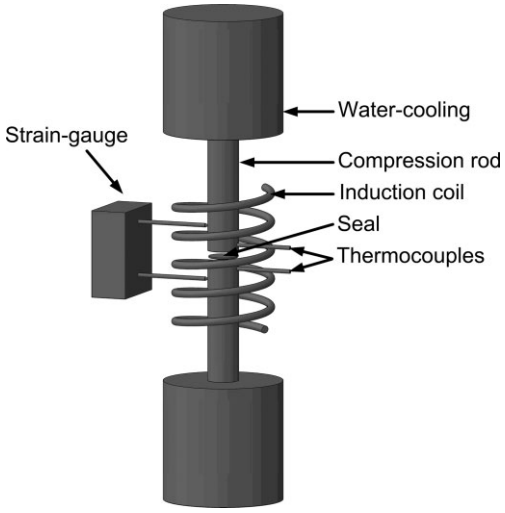

Fig. 4 Test setup for the compression tests.

ing gaskets were manufactured of 3 mm thick 253 MA steel. The groves were manufactured by etching. The surface roughness of the sealing surfaces was measured to be around R_a = 40 nm with Taylor Hobson Surtronic 3+ surface roughness analyser. Radial groves were etched into the plates to allow leaked gas to evacuate. Inner diameter of the gaskets was 72.5 mm and width 5 mm. A gasket holder plate with a gasket was then pressed between two 253 MA steel plates, and the structure was tightened with 253 MA bolts. Bolts were fastened tight enough so that the seals compressed to accommodate the grove. Gas was introduced through a 6 mm Inconel 600 pipe welded to the endplate and gas outlet was via a 3 mm pipe welded to the gasket holder plate.

Flow diagram of the sealing tests is illustrated in Figure 6. Hydrogen feed to

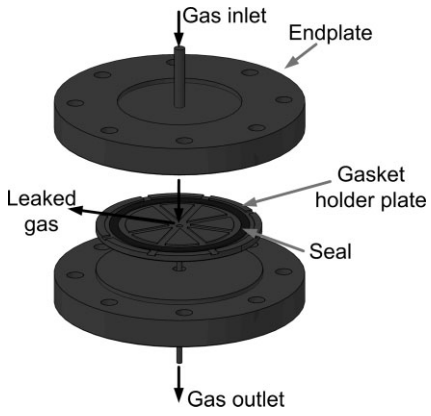

Fig. 5 Gasket holder setup.

the system is controlled with a Bronkhorst EL-FLOW-series mass flow controller. Inlet gas is fed through a humidifier (Fuel Cell Technologies) or through the by-pass line. The gas enters the furnace via a heated pipeline and exits the furnace through a pressure controller. Valves V2, V3 and V4 were used to change the inlet gas between dry and humidified hydrogen. Pressure upstream of the gasket was measured with pressure transducer and controlled by pressure controller V5. The pipeline between humidifier and the outlet was heated to avoid condensation. Inlet and outlet gas flows were measured with a Sensidyne Gillibrator II flow calibrator.

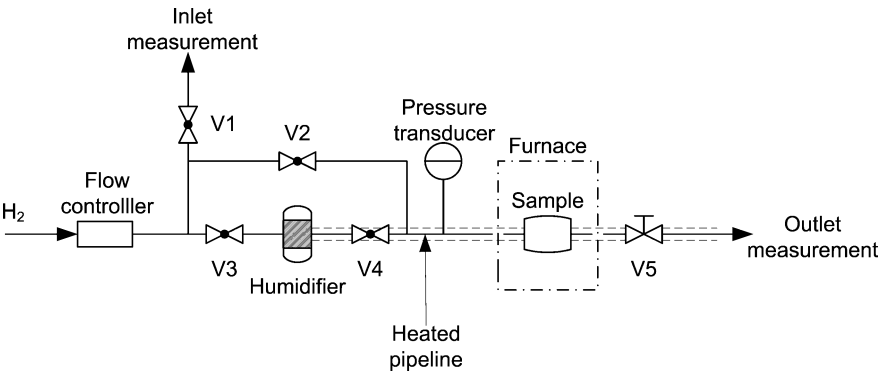

Fig. 6 Flow diagram of the leak measurements.

Sealing tests were carried out according to the following procedure.

(i) Heating up to 800 °C with 97% N_2 + 3% H_2.
(ii) Purging the pipelines with dry H_2 until water vapour content at the outlet dropped below 10 hPa.
(iii) Leak rate measurement with dry H_2.
(iv) Exposure with either 200 ml min^{-1} H_2 or 200 ml min^{-1} H_2 + 120 ml min^{-1} H_2O. Overpressure of the gas during the exposure was always 100 mbar.
(v) Cooling down to room temperature with 97% N_2 + 3% H_2.

Steps two to four were repeated periodically during the tests.

Table 1 summarises the tested gasket materials, test conditions and thicknesses of the compressed gaskets. Gasket holder grove depths for Thermiculite 866 samples were chosen so that the compressive stress on consolidated version would be lower (~4 MPa) than the compressive stress on the as-made version (~8 MPa). This was done because it was postulated that the smoother surface structure of the consolidated version would allow lower stresses. Since Statotherm HT consists of only discrete mica platelets with no additional filler, it was postulated that leak rates would be highly dependable on the compression stress. To test this hypothesis, two samples with different gasket holder plate grove depths, 290 and 230 µm, were tested.

Table 1 Samples used in the sealing tests.

Sample	Gas	Thickness of compressed gasket (µm)	Time (h)
Thermiculite 866, 0.5 mm, as-made	H_2	340	480
	H_2 + H_2O	340	480
Thermiculite 866, 0.5 mm, consolidated	H_2 + H_2O	460	360
	H_2 + H_2O	460	360
Statotherm HT, 0.4 mm	H_2 + H_2O	290	480
	H_2 + H_2O	230	480

3 Results and Discussion

3.1 Compression Properties

3.1.1 Thermiculite 866

Figure 7 shows thickness of consolidated Thermiculite 866 as a function of compression stress. It can be noted that at 800 °C, consolidated Thermiculite 866 compresses from 540 to 422 µm (118 µm/22%) between 1 and 8 MPa compared to compression from 497 to 464 µm (33 µm/6%) at room temperature. Figures 7–9 only show thicknesses of the seals above ~0.3 MPa because the ductile nature of the seals constricts measurement accuracy at lower compression stresses.

Figure 8 shows thickness of as-made Thermiculite 866 as a function of compression stress. It can be noted that at 800 °C, as-made Thermiculite 866 compresses from 444 to 346 µm (98 µm/22%) between 1 and 8 MPa compared to compression from 380 to 310 µm (70 µm/18%) at room temperature.

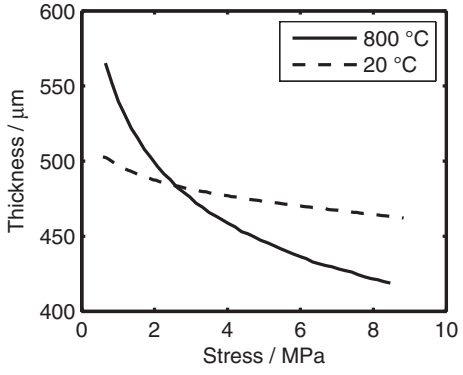

Fig. 7 Thickness of consolidated Thermiculite 866 as a function of compression stress.

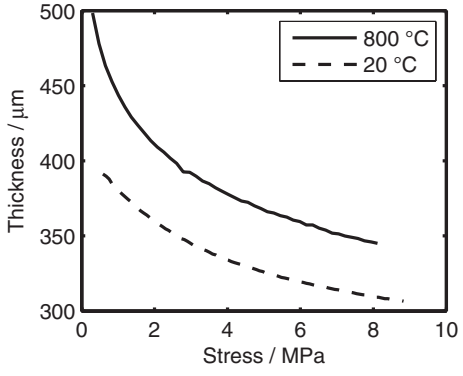

Fig. 8 Thickness of as-made Thermiculite 866 as a function of compression stress.

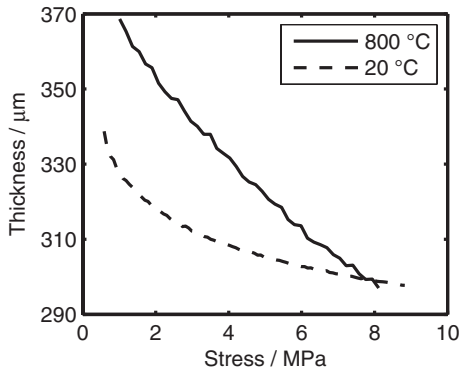

Fig. 9 Thickness of Statotherm HT as a function of compression stress.

Thermiculite 866 samples tested at elevated temperatures appeared to be thicker than those at room temperature. This might be accounted to the expansion of vermiculite mica at application of heat [6].

3.1.2 Statotherm HT

Figure 9 shows the thickness of Statotherm HT as a function of compression stress. It can be seen that at room temperature after the initial compression to 1 MPa the seal compresses from 328 to 299 µm (29 µm/8.8%) from 1 to 8 MPa. This behaviour accounts to the structure of Statotherm HT, consisting of phlogopite mica platelets. When stress is applied on the seal, the platelets are compressed together decreasing the porosity of the structure. At 800 °C, Statotherm HT also experienced swelling and became more ductile, compressing from 369 to 299 µm (70 µm/19%) from 1 to 8 MPa.

3.2 Sealing Properties

The leak rates of the samples were measured as a function of hydrogen pressure. Figure 10 shows leak rates of the samples at different pressure levels. The leak rate of Statotherm HT sample compressed to 290 µm seems to increase linearly with increasing pressure, which is in line with the leak rate model for micas developed by Sang et al. [17]. It is also notable that leak rate of Statotherm HT depends strongly on the compression stress. All other samples showed constant leak rates within the measurement accuracy. However, all the samples also showed significant leak rates, even at overpressures below 10 mbar(g).

Figure 11 shows the results of the leak rate tests at 100 mbar(g) H_2. As-made Thermiculite 866 samples show leak rates of 29 ml(m min)$^{-1}$ with humidified H_2 and 33 ml(m min)$^{-1}$ with dry H_2. Consolidated samples showed leak rates of 43 ml(m min)$^{-1}$ and 49 ml(m min)$^{-1}$. Statotherm HT sample pressed to 290 µm showed a leak rate of 90 ml(m min)$^{-1}$, and the sample pressed to 230 µm showed a leak rate of 22 ml(m min)$^{-1}$. Chou et al. [10] have measured leak rates of phlogopite mica to be around 200 ml(m min)$^{-1}$ (1 bar(g), air) at 800 °C and with compressive stress of 3.5 MPa. Simner and Stevenson [8] measured leak rates of 59 ml(m min)$^{-1}$ (103 mbar(g), He) for phlogopite samples compressed to 4.8 MPa load. These results are in good agreement with the results presented in this paper.

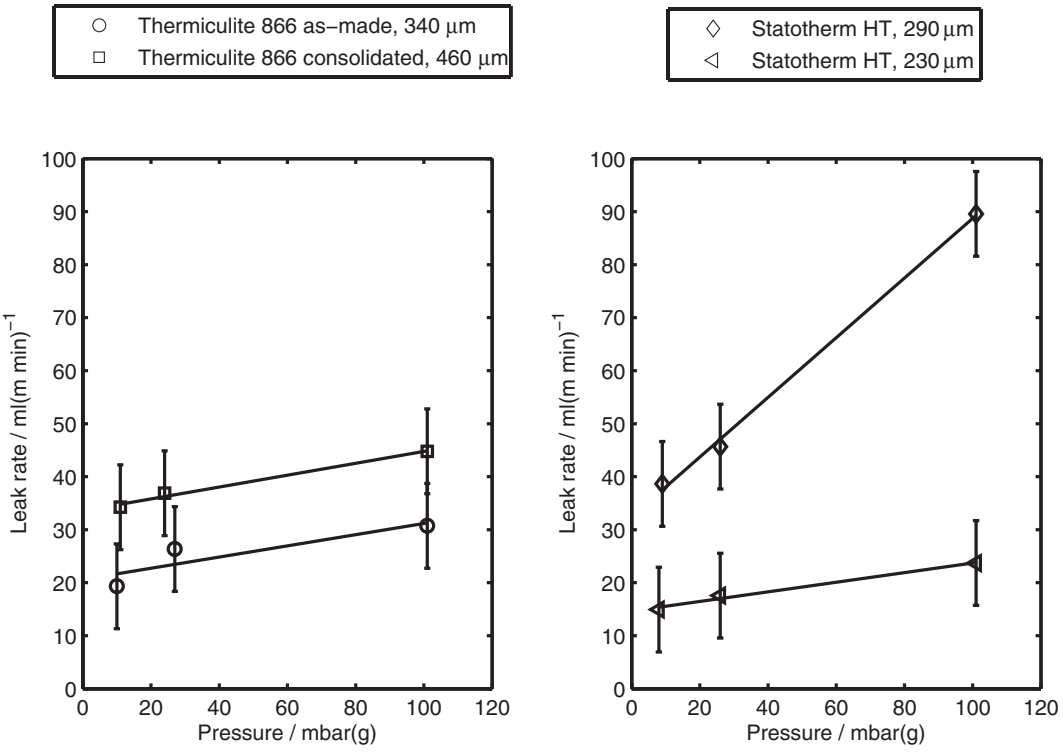

Fig. 10 Leak rates of the samples at different H_2 overpressures.

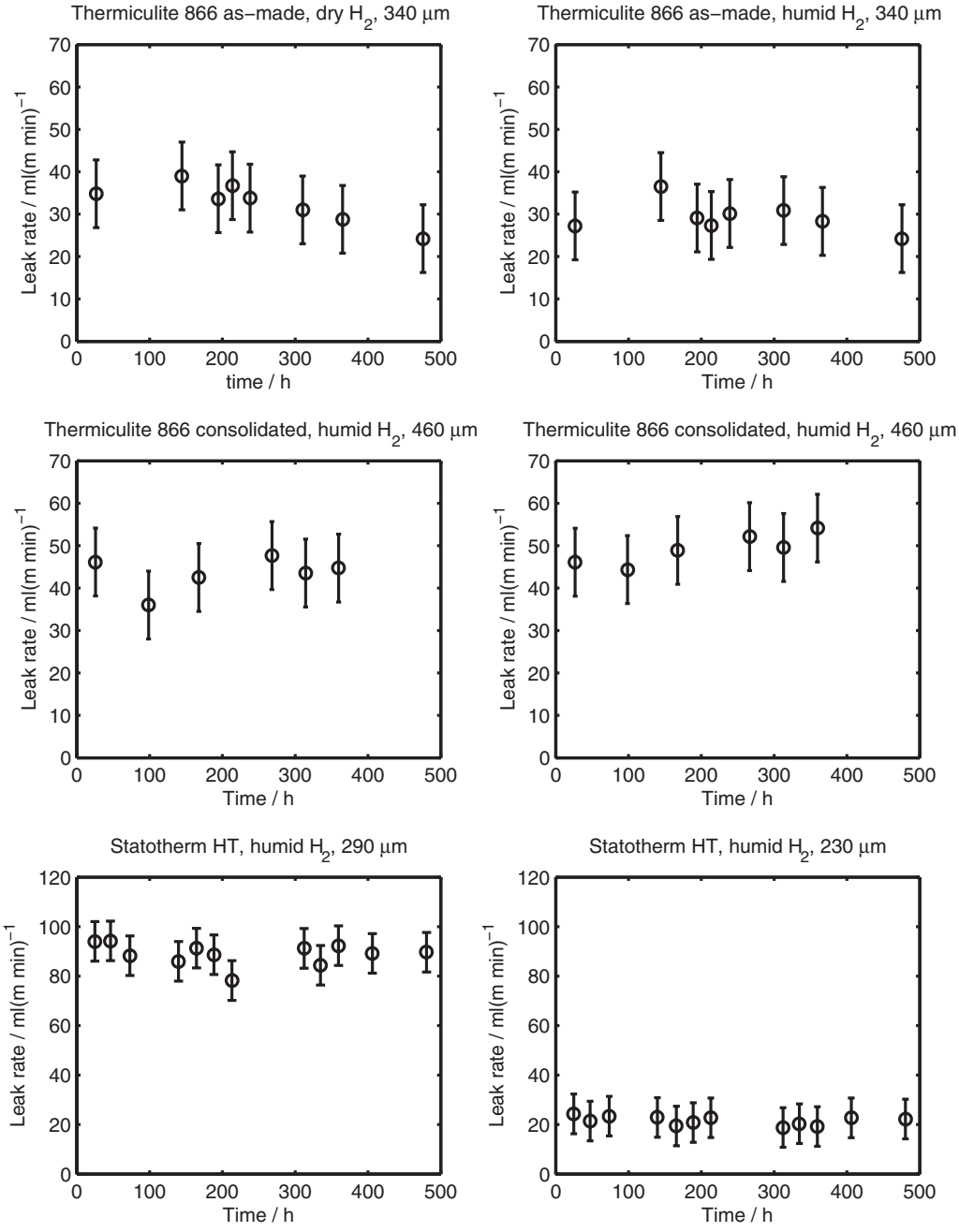

Fig. 11 Leak rates of the tested gaskets as a function of time.

Allowable leak rates of SOFC stacks vary greatly depending on design issues and materials used in the stack. For example let us consider a SOFC stack with 10 × 10 cm^2 cells (active area 9 × 9 cm^2) with sealing length of 1 m per single repeating unit. If the stack was used with 0.7 A cm^{-2} and 50% fuel utilisation, the fuel input would need to be 790 ml min^{-1} H_2. Therefore, Thermiculite 866 samples used in a stack, would lead to a stack leaking 4–6% of the input fuel flow. Statotherm HT samples would yield leak rates of 3 and 11%. If lower leakage levels in SOFC stacks are required, either lower pressure levels or higher compression stresses would need to be used. Another possibility is to minimise leakages through the contact interfaces of the seals. This has been discussed by Chou et al. [10], who measured leak rates of phlogopite mica with and without glass ceramic contact layers. In these measurements, samples without glass ceramic contact layers showed leak rates of the order of 100 times greater than those with glass ceramic contact layer.

4 Conclusion

Conclusion of the work presented here can be summarised into four items:

(i) Both Thermiculite 866 and Statotherm HT showed stable leak rates during the tests at 800 °C with simulated anode gas (62% H_2 + 38% H_2O, 100 mbar(g) overpressure).

(ii) Leak rates of as-made Thermiculite 866 samples were independent of the water vapour content in gas within the measurement accuracy.

(iii) Leak rate of Statotherm HT sample compressed to 290 µm was found to be roughly linear within the measurement range of 10 to 100 mbar(g). All other samples showed constant leak rates within the measurement accuracy.

(iv) Compression properties of both materials are very different at room temperature compared to 800 °C. Consolidated (precompressed) Thermiculite 866 and Statotherm HT showed similar compressibility (6.6 and 8.8%, respectively from 1 to 8 MPa) at room temperature, while as-made Thermiculite 866 compressed 18%. At 800 °C both Thermiculite types compressed 22% from 1 to 8 MPa. Also the Statotherm HT samples became more ductile at 800 °C compressing 19% from 1 to 8 MPa.

Further research needs to be done to assess the long term chemical stability of the sealing materials in SOFC operating conditions.

Acknowledgements

This work is a part of the Finnish National Fuel Cell Programme 2007–2013. The financial support from the National Technology Agency of Finland, VTT Technical Research Centre of Finland and the Finnish companies involved in the programme are gratefully acknowledged.

John Hoyes of Flexitallic Ltd. is acknowledged for providing the Thermiculite 866 samples. Ville Piirainen of Tampere University of Technology is acknowledged for conducting most of the compression tests.

References

[1] J. Fergus, *J. Power Sources* **2005**, *147*, 46.
[2] M. Stanislowski, E. Wessel, K. Hilpert, T. Markus, L. Singheiser, *J. Electrochem. Soc.* **2007**, *154*, 295.
[3] Z. Yang, K. Meinhardt, J. Stevenson, *J. Electrochem. Soc.* **2003**, *150*, A1095.
[4] P. Batfalsky, V. A. C. Haanappel, J. Malzbender, N. H. Menzler, V. Shemet, I. C. Vinke, R. W. Steinbrech, *J. Power Sources* **2006**, *155*, 128.
[5] K. Ogasawara, H. Kameda, Y. Matsuzaki, T. Sakurai, T. Uehara, A. Toji, N. Sakai, K. Yamaji, T. Horita, H. Yokokawac, *J. Electrochem. Soc.* **2007**, *154*, B657.
[6] G. Wypych, *Handbook of Fillers – A Definitive User's Guide and Databook*, 2nd Edn., ChemTec Publishing, Toronto, Canada **2000**.
[7] P. A. Ciullo, Ed., *Industrial Minerals and Their Uses – A Handbook and Formulary*, William Andrew Publishing, Noyes, Westwood, USA **1996**.
[8] S. Simner, J. W. Stevenson, *J. Power Sources* **2001**, *102*, 310.
[9] M. Bram, S. Reckers, P. Drinovac, J. Mönch, R. W. Steinbrech, H. P. Buchkremer, D. Stöver, *J. Power Sources* **2004**, *138*, 111.
[10] Y. Chou, J. W. Stevenson, L. A. Chick, *J. Power Sources* **2002**, *112*, 130.
[11] Y. Chou, J. W. Stevenson, J. Hardy, P. Singh, *J. Power Sources* **2006**, *157*, 260.
[12] Y. Chou, J. W. Stevenson, *J. Power Sources* **2005**, *140*, 340.
[13] S. Sang, W. Li, J. Pu, L. Jian, *J. Power Sources* **2008**, *177*, 77.
[14] S. Le, K. Sun, N. Zhang, Y. Shao, M. An, Q. Fu, X. Zhu, *J. Power Sources* **2007**, *168*, 447.
[15] J. Hoyes, S. Bond, *Sealing Technol.* **2007**, 11.
[16] Feodor Burgmann Dichtungswerke GmbH & Co, *Sealing Technol.* **2000**, 6.
[17] S. Sang, J. Pu, S. Jiang, L. Jian, *J. Power Sources* **2008**, *182*, 141.

PUBLICATION II

Effects of the first heat up procedure on mechanical properties of solid oxide fuel cell sealing materials

Journal of Power Sources. Elsevier. Vol. 284 (2015), 511–516.

Journal of Power Sources 284 (2015) 511–516

Contents lists available at ScienceDirect

Journal of Power Sources

journal homepage: www.elsevier.com/locate/jpowsour

Effects of the first heat up procedure on mechanical properties of solid oxide fuel cell sealing materials

Markus Rautanen*, Valtteri Pulkkinen, Johan Tallgren, Olli Himanen, Jari Kiviaho

VTT Technical Research Centre of Finland, Fuel Cells, P.O. Box 1000, Biologinkuja 5, Espoo FI-02044 VTT, Finland

HIGHLIGHTS

- Mechanical properties of glass, compressible, and hybrid SOFC seals were studied.
- Compressibility of the materials is presented at different temperatures.
- The effect of first heat up on mechanical properties of the materials is presented.
- Design guidelines are given for stack assembly and first heat up.

ARTICLE INFO

Article history:
Received 29 November 2014
Received in revised form
20 February 2015
Accepted 3 March 2015
Available online 5 March 2015

Keywords:
SOFC
Seal
Stack
Hybrid
Compression
Stress

ABSTRACT

SOFC stack seals need to be correctly dimensioned to achieve a gas tight stack with low electrical contact resistances. Mechanical properties of SOFC stack sealing materials are presented for three assembly and first heat up procedures: applying full compressive stress at room temperature before first heat up (1), applying no compressive stress before first heat up and applying the full compressive stress at operating temperature (2), applying partial compressive stress at room temperature and full compressive stress at operating temperature after first heat up (3). The behaviour of the glass seal (Schott GM31107) is not affected significantly by compressive force during heat up. Compressibility of both compressible sealing material (Thermiculite CL87) and hybrid sealing material (Thermiculite CL87LS) was found to be about 40% (between 0.1 and 0.9 MPa) at room temperature but only about 4% (between 0.1 and 0.9 MPa) at 700 °C. Therefore it is beneficial to carry out as much of the compression as possible at room temperature before first heat up. This allows for maximum amount of deformability in the sealing materials resulting in the highest ability to compensate for stack manufacturing and assembly tolerances, which is needed to realize a gas tight stack with low electrical contact resistances.

1. Introduction

One of the key challenges in solid oxide fuel cell stack development is achieving a robust mechanical design. SOFC stack consists usually of steel interconnect plates, cells and seals. The only component of these that can offer a significant amount of deformability is the seal, which needs to compensate for manufacturing and assembly tolerances of other components in a stack. Understanding mechanical properties of sealing materials is important as improper seal design can lead to poor electrical contact, gas leakages and cause additional mechanical stresses to the stack [1–4]. A stack designer needs to know the mechanical properties of the seals not only at room temperature or at operating temperature but throughout the whole operating region. Of special interest are the mechanical properties of materials during the first heat up, in which the stack is sealed, reduced and tested before shipping to customer.

The two most common groups of sealing materials used in SOFC stacks are glass seals and compressible seals from the mineral group called mica [5]. At least for the first group, mechanical properties depend not only of temperature but of heat treatment history due to phase changes such as crystallization of amorphous glass phases. Compressible seals from the mica group are usually used in a form of mica paper or other highly anisotropic forms [6]. Therefore sufficient experimental data of the chosen set of materials is a necessity for the stack designer. Literature data of the mechanical properties of SOFC sealing materials is usually not

* Corresponding author.
E-mail address: markus.rautanen@vtt.fi (M. Rautanen).

http://dx.doi.org/10.1016/j.jpowsour.2015.03.012
0378-7753/

sufficient to provide enough input for designing a stack. Properties of various glasses are often measured with hot stage microscopy, see e.g. Ref. [7]. While this is a simple and reliable method in determining mechanical changes in glass samples, it is very removed from the actual conditions inside a stack: there is no compressive force applied on the sample and there is only one (bottom) surface for the glass to wet, making the situation unrealistic. In the case of compressible sealing materials, literature data on the mechanical properties is rather focused on the mineralogical properties of mica-materials [6,8] and data related to designing SOFC stacks is scarce [9,10].

This article presents mechanical properties of three sealing materials: a compressible seal, glass seal and hybrid seal. The focus is on the first mechanical compression of stack after assembly and on the first heat up procedure. Three possible procedures for applying the compression to the stack were investigated:

1. applying full compressive stress at room temperature before first heat up,
2. applying no compressive stress before first heat up and applying the full compressive stress at operating temperature (700 °C) and
3. applying partial compressive stress at room temperature and full compressive stress at operating temperature (700 °C) after first heat up.

Compressibility data of these cases is presented and its significance to stack design and manufacturing process is discussed. Results and discussion are presented from SOFC point of view but it is equally applicable to solid oxide electrolysis (SOEC) stacks.

2. Experimental

2.1. Materials

Three sealing materials were chosen for this study: glass (Schott GM31107), compressible sealing material (Thermiculite CL87, Flexitallic Ltd) and hybrid sealing material (Thermiculite CL87LS, Flexitallic Ltd). The first material is a traditional glass sealing material manufactured by Schott. Viscosity of the glass at it's softening temperature of 649 °C is $10^{6.6}$ Pa and at 750 °C 10^5 Pa [7]. Based on previous studies, the glass has good bonding properties at 700 °C with both Crofer 22H steel and Thermiculite 866 sealing material [11]. The glass powder is cast into a tape of 250 μm green thickness.

The second material is a compressible sealing material based on chemically exfoliated vermiculite and steatite. This material is an offspring of the Thermiculite 866 range [12].

The third material is based on the same compressible core but includes a coating of Schott GM31107 glass and organic binders diminishing interfacial leaks and thus allows it to be used at very low compressive stress levels (<1 MPa). For more details on this material, see Refs. [9,13]. The amount of glass in the coating was 5 mg cm^{-2}. The density of the core material of Thermiculite CL87 and CL87LS was 0.85 g cm^{-3} and weight per unit area was 36 mg cm^{-2}. Before testing, the materials were stored in a constant temperature and humidity room (T = 22 °C, RH = 42%) as humidity might affect the compressibility of Thermiculite materials.

2.2. Test setup

A double push-rod mechanical dilatometer was used to measure material thicknesses in this study. Fig. 1 presents the basic principle of the device. A sample is inserted between the measurement rod and weight is clamped on the top of both rods. The thickness of the sample is read of a dial gauge mounted at the top of the push-rods.

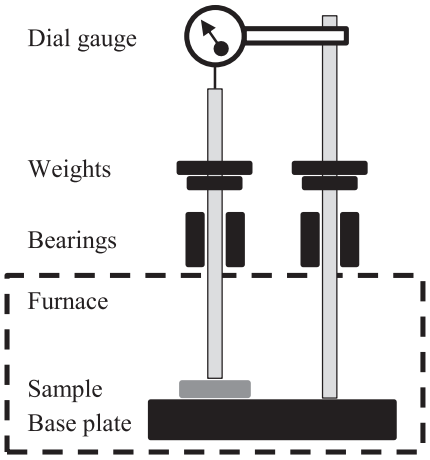

Fig. 1. Schematic of the used measurement setup.

The lower part of the assembly can be inserted in a dedicated furnace to control the temperature of the sample. The double push-rod design allows for the compensation of thermal expansion in the push-rods and therefore allowing for high accuracy. To test the accuracy of the measurement setup, calibration measurements were done at room temperature with 500 μm, 750 μm and 1000 μm precision strip steel plates. Results indicated a constant systematic error of 6 μm. The known, systematic error was reduced from actual measurements with seal materials. Accuracy of the device at elevated temperatures was studied with zero point deviation measurements where no sample material was present. The average zero point error was 0.5 μm and random uncertainty 0.9 μm (considered to be 2σ). Furthermore the accuracy of the device was studied by measuring thermal expansion of Crofer 22H plate and comparing the results against thermal expansion data provided by the manufacturer [14]. Fig. 2 shows the measured and calculated thicknesses of the Crofer 22H plate. Initial thickness of the plate was 1020 μm and the end value at 800 °C was 1029 μm. The measured values are in good agreement with the data provided by the manufacturer: average difference is 1.2 μm and random uncertainty 2.6 μm (2σ of residuals). Based on the above analysis, accuracy of the device is considered to better than ±10 μm at operating range of 0–700 °C.

2.3. Test cases

To simulate first compression and heat up treatments of stacks, three different procedures were tested for all materials:

1. applying full compressive stress (1 MPa) at room temperature before first heat up,
2. applying no compressive stress before first heat up and applying the full compressive stress (1 MPa) at operating temperature (700 °C) and
3. applying partial compressive stress (0.44 MPa) at room temperature and full compressive stress (1 MPa) at operating temperature (700 °C) after first heat up.

Applying full compressive force at room temperature (case 1) could be done during assembly process of a stack. However, applying virtually no compression at room temperature before first heat up might be necessary with initially thick green glass tapes if e.g. mechanical structure of the stack is such that it will deform under compressive stress. In such a case full compression can only be applied at operating temperature (case 2). A compromise

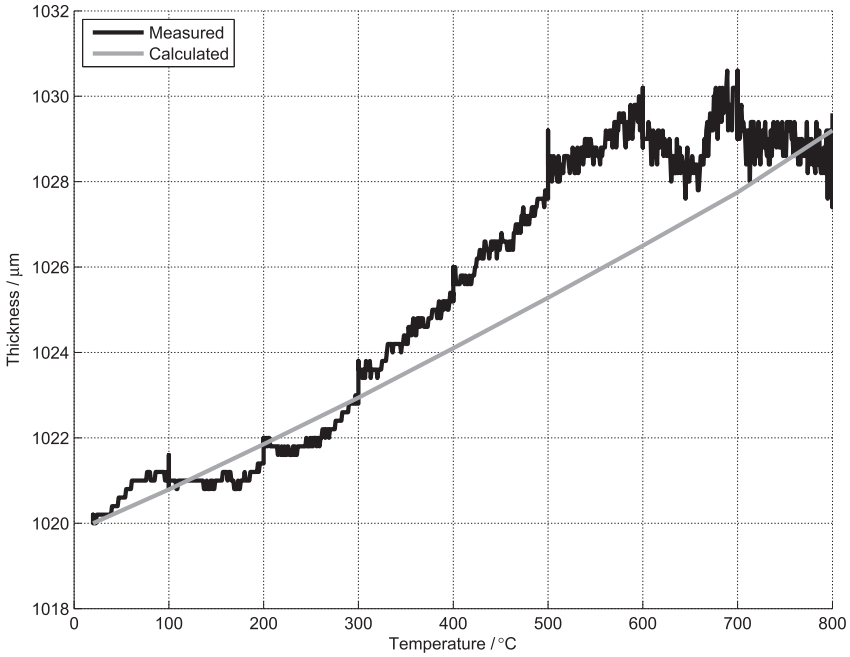

Fig. 2. Measured thickness of Crofer 22H plate (1020 µm initial thickness) as a function of temperature together with calculated thickness based on manufacturers datasheet.

between these two is the case 3 where partial compressive stress (0.44 MPa) is applied at room temperature and final compressive stress (1 MPa) at operating temperature.

3. Results and discussion

3.1. Glass seal

The three procedures for compression and first heat up were tested. Fig. 3 shows Schott GM31107 glass sealing material thickness as a function of temperature and time. The grey curve corresponds to heating under 0.44 MPa of compressive stress and the black curve to heating under no compressive stress. Heating rate was 60 °C/h and the shown temperature corresponds to furnace temperature. This means that the temperature of the sample lags behind the shown furnace temperature during heating, meaning it should be only considered as indicative until reaching steady state. It is noticed that there is only very little thickness change until about 570 °C. Above that temperature two distinct changes are noticed, the first at 570–615 °C and the second at 660–700 °C. Based on hot stage microscopy data [7], the first of these changes relates to binder burn out and sintering and the second change to softening and wetting of the surfaces. The final thickness of the glass was about 12 µm at 0.44 MPa. Further compression to 1.0 MPa

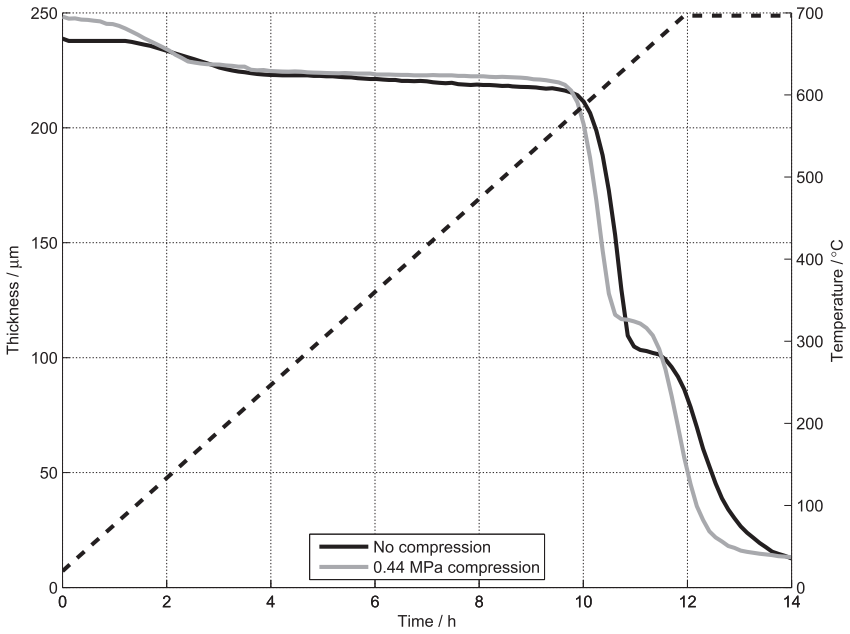

Fig. 3. Glass seal heated up at 0.44 MPa compressive stress.

at 700 °C did not reduce this thickness. The difference throughout the heating using 0.44 MPa of compressive stress and no stress at all is minimal.

Based on these results, behaviour of the Schott GM31107 glass does not depend greatly on compression procedure during first heat up. However, if a significant amount of compression is applied at room temperature where the glass tape is very thick compared to its final thickness, the stress distribution within a stack structure should be analysed to be sure that stresses are within acceptable limits.

3.2. Thermiculite CL87

Fig. 4 shows the effect of temperature on the compressibility of the seal. It can be noted that heating the material significantly reduces the compressibility: already at 200 °C the compressibility is the same as at 700 °C. If the compressive stress is applied at room temperature before first heat up, Thermiculite CL87 compresses about 42% between 0.1 and 0.9 MPa. If full compression to 1.0 MPa is applied after first heat up, the compressibility between 0.1 and 0.9 MPa is limited to 4%. The compressibility (slope of the thickness vs. stress curves) at 700 °C remains the same for both cases and is not affected by the pre-compression at room temperature. Most probably the loss of compression is related to drying of the sealing material and therefore it is likely that any heating above room temperature results in partial loss of compressibility. Based on these results the best practise would be to apply at least part of the compression already at room temperature. Fig. 5 shows the compressibility curves of Thermiculite CL87 in the three different heat up cases. It can be noticed that compressibility is very significantly affected by the application method of compressive stress.

These results indicate that with Thermiculite CL87 the preferred method of stack assembly should be to apply a major part of the compression already at room temperature as compression at operating temperature requires roughly ten times more stress to induce similar deformation in the sealing material. Applying compression at room temperature gives the sealing material the best chance to compensate for manufacturing and assembly tolerances leading to a gas tight stack with low electrical contact resistance.

3.3. Thermiculite CL87LS

Fig. 6 shows compressibility of Thermiculite CL87LS at different temperatures. It is noticeable that the initial thickness of the material (below 0.4 MPa) is higher at low temperatures than at operating temperature. This is due to the binder burn out, shrinkage and sintering of the coating layer which naturally only occurs during heating. The low-stress difference between measurements conducted at room temperature and at operating temperature is associated with the final thickness of the glass layer.

Fig. 7 shows compressibility curves of Thermiculite CL87LS corresponding to the three test cases. It can be noted that the general behaviour follows that of Thermiculite CL87 which is expected as the core material is the same. However, Thermiculite CL87LS is slightly thicker because of the coating. The thickness of the material is also reduced during heat up as binders evaporate from the coating and glass particles sinter. This is especially noticeable by looking at the sample that has been pre-compressed to 0.44 MPa at room temperature (grey dashed line). After pre-compression the same sample was heated to operating temperature and compressed 1.0 MPa (black dashed line). The thickness during heating has been reduced by around 10% (580 μm–520 μm).

These results indicate that also with Thermiculite CL87LS the preferred method should be to apply as much compression as possible already at room temperature to ensure maximum amount of deformability of the seal.

4. Conclusions

Compressibility of SOFC stack sealing materials was evaluated for three assembly and first heat up procedures. The behaviour of the glass seal (Schott GM31107) was not affected significantly by compressive force during heat up. The end thickness of the 250 μm

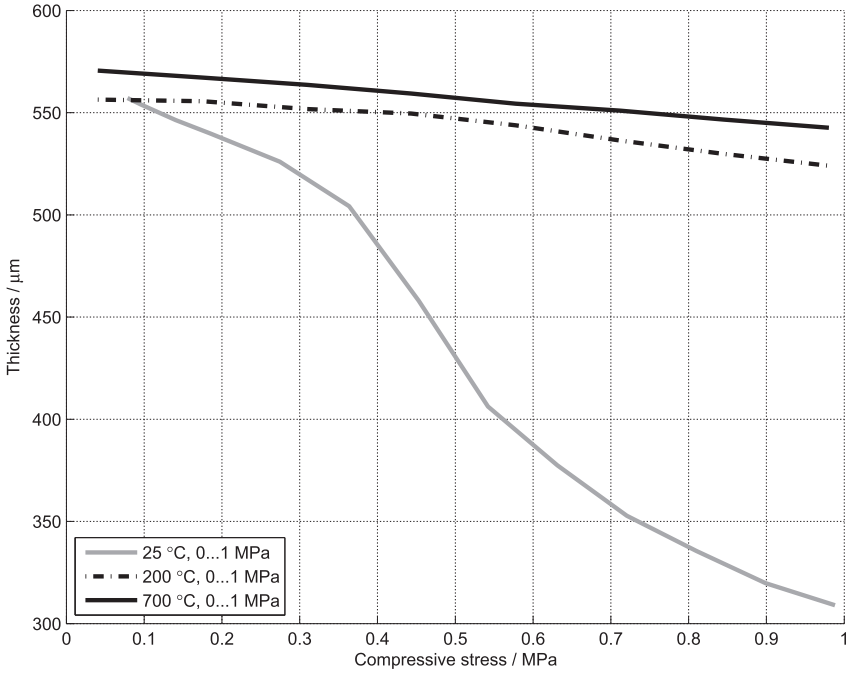

Fig. 4. Compressibility curves of CL87 at different temperatures.

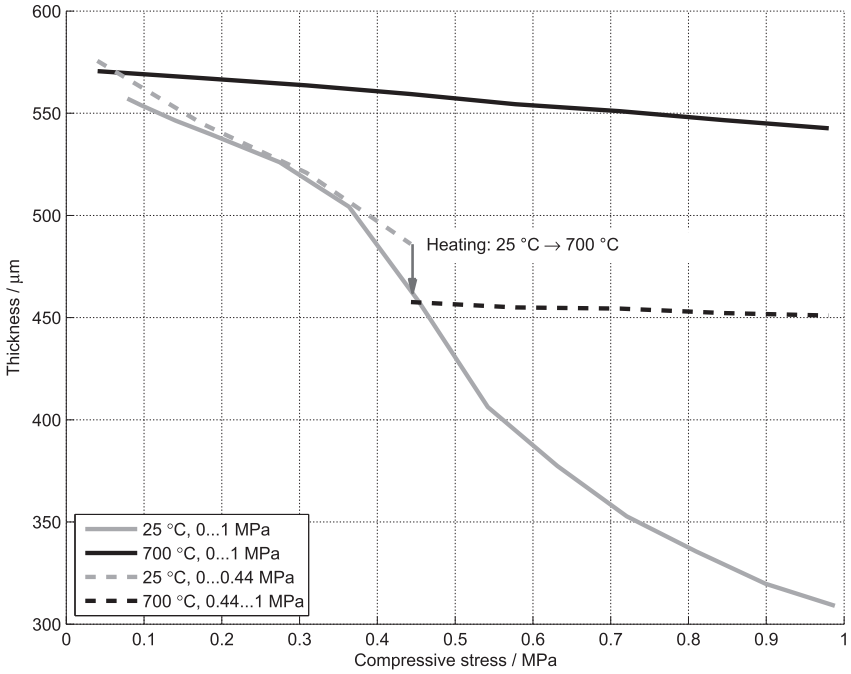

Fig. 5. Thermiculite CL 87 compressibility curves. Grey lines indicate compression at room temperature and black lines at operating temperature (700 °C). The grey dashed line represents pre-compression at room temperature and black dashed line the same sample after heat up.

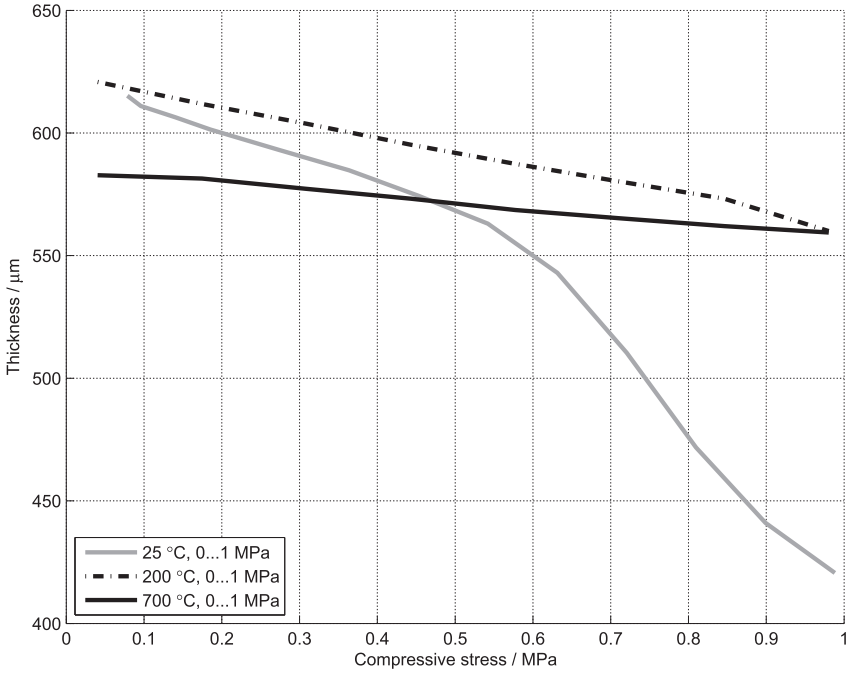

Fig. 6. Compressibility curves of CL87LS at different temperatures.

(green thickness) tape at 700 °C was about 12 µm independent of compressive stress (0–1 MPa). Compressibility of both Thermiculite CL87 and CL87LS materials was found to be around 40% between 0.1 and 0.9 MPa at room temperature, meaning these materials are well able to compensate for manufacturing or assembly tolerances in a stack. However, a significant amount of compressibility is lost when the material is heated: at 700 °C the compressibility is only around 4% between 0.1 and 0.9 MPa. Therefore it is very beneficial to carry out as much of the first compression as possible at room temperature before first heat up. This would allow for maximum amount of deformability in the sealing materials resulting in the highest ability to compensate for stack manufacturing and assembly tolerances leading to a gas tight stack with low electrical contact resistances. The provided methodology, data and guidelines should allow for a stack designer to optimize the mechanical design, first compression during assembly and first heat up procedure of the stack.

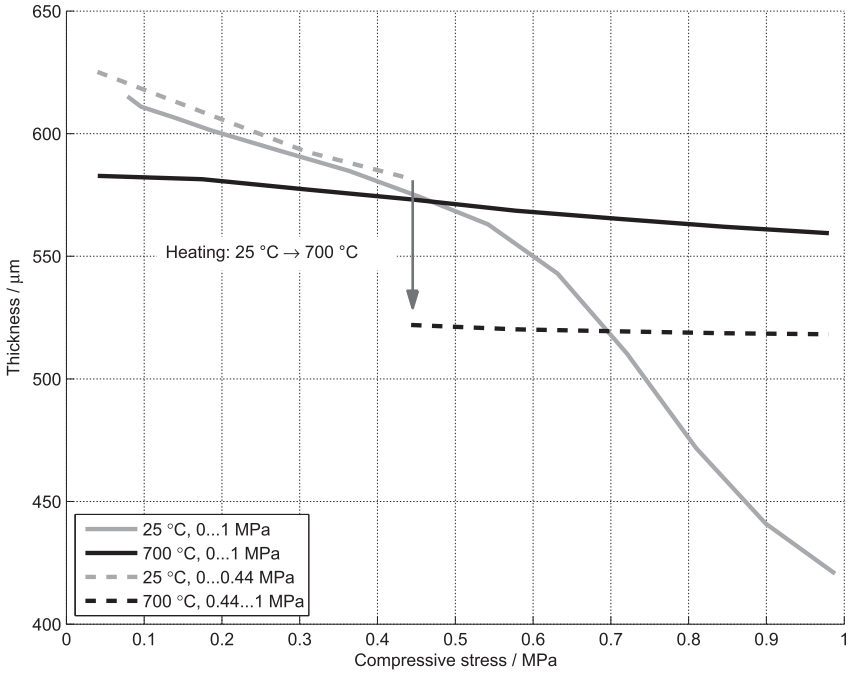

Fig. 7. Compressibility curves for Thermiculite CL 87LS. Grey lines indicate compression at room temperature and black lines at operating temperature (700 °C). The grey dashed line represents pre-compression at room temperature and black dashed line the same sample after heat up.

Acknowledgements

This research was supported by the Fuel Cells and Hydrogen Joint Undertaking under grant 621227 (NELLHI). Olivier Thomann, Kari Koskela and Juha Järvinen of VTT Technical Research Centre of Finland are acknowledged for useful discussions regarding this work.

References

[1] S. Gross, D. Federmann, J. Remmel, M. Pap, Reinforced composite sealants for solid oxide fuel cell applications, J. Power Sources 196 (2011) 7338–7342.
[2] L. Blum, S. Gross, J. Malzbender, U. Pabst, M. Peksen, R. Peter, I. Vinke, Investigation of solid oxide fuel cell sealing behaviour under stack relevant conditions at Forschungzentrum Jülich, J. Power Sources 196 (17) (2011) 7175–7181.
[3] A. Nakajo, F. Mueller, J. Brouwer, J. Van herle, D. Favrat, Mechanical reliability and durability of SOFC stacks. Part II: modelling of mechanical failures during ageing and cycling, Int. J. Hydrog. Energy 37 (11) (2012) 9269–9286.
[4] C.-K. Lin, L.-H. Huang, L.-K. Chiang, Y.-P. Chyou, Effects of clamping load on the thermal stress distribution in a planar SOFC with compressive sealing, ECS Trans. 25 (2) (2009) 349–358.
[5] J.W. Fergus, Sealants for solid oxide fuel cells, J. Power Sources 147 (1–2) (2005) 46–57.
[6] S. Habelitz, G. Carl, C. Rüssel, S. Thiel, U. Gerth, J.-D. Schnapp, A. Jordanov, H. Knake, Mechanical properties of oriented mica glass ceramic, J. Non-Cryst. Solids 220 (1997) 291–298.
[7] D. Gödeke, J. Besinger, Y. Pflügler, B. Ruedinger, New Glass Ceramic Sealants for SOFCs, ECS Trans. 25 (2) (2009) 1483–1490.
[8] S.P. Simner, J.W. Stevenson, Compressive mica seals for SOFC applications, J. Power Sources 102 (1–2) (2001) 310–316.
[9] J. Hoyes, M. Rautanen, SOFC sealing with Thermiculite 866 and Thermiculite 866 LS, ECS Trans. 57 (1) (2013) 2365–2374.
[10] M. Rautanen, O. Himanen, V. Saarinen, J. Kiviaho, Compression properties and leakage tests of mica-based seals for SOFC applications, Fuel Cells (2009) 753–759.
[11] M. Rautanen, O. Thomann, O. Himanen, J. Tallgren, J. Kiviaho, Glass coated compressible solid oxide fuel cell seals, J. Power Sources 247 (2014) 243–248.
[12] J. Hoyes, S. Bond, Gaskets for sealing solid oxide fuel cells, Seal. Technol. 2007 (8) (2007) 11–14.
[13] Flexitallic, "Thermiculite 866/866LS," Flexitallic Ltd, [Online]. Available: http://www.flexitallicsofc.com/downloads/Flexitallic_SOFC_thermiculite_866.pdf. [Accessed 28 01 2015].
[14] ThyssenKrupp. [Online]. Available: http://www.fcdic.com/ja/member/data/Crofer22H.pdf.

PUBLICATION III

SOFC sealing with Thermiculite 866 and Thermiculite 866 LS

ECS Transactions. Electrochemical Society. Vol. 57 (2013)
No: 1, 2365–2374.

ECS Transactions, 57 (1) 2365-2374 (2013)
10.1149/05701.2365ecst ©The Electrochemical Society

SOFC Sealing with Thermiculite 866 and Thermiculite 866 LS

J R Hoyes[a] and M Rautanen[b]

[a] Flexitallic Ltd, Hunsworth Lane , Cleckheaton, West Yorkshire , BD19 4LN, UK
[b] VTT, PO Box 1000, Biologinkuja 5, Espoo, Fl-02044 VTT , Finland

This paper outlines the structure and properties of a unique compression sealing material that is entirely free of any organic component which has been giving excellent sealing in SOFC service for a number of years. The paper also discusses a new material that combines the advantages of a compression seal with that of a glass seal to provide a compression sealing material needing as little as 0.1 MPa surface stress in order to achieve excellent levels of tightness.

Introduction

Flexitallic has been a manufacturer of industrial sealing materials since before 1871 and has an enviable record of innovation of sealing materials and gaskets. The well known spiral wound gasket, used in a huge range on industrial sealing applications around the world, was invented by Flexitallic in 1913, USP 1,089,134.

Recently, innovation by the sealing industry in terms of types of sealing materials has blossomed as the industry has developed materials to replace the traditional ones based upon asbestos fibre. Asbestos fibre was used in a very high proportion of all the sealing materials available and was, in particular, the basis of the materials having the highest application temperature which was about 550 °C.

Flexitallic has been to the fore of this surge of innovation to replace asbestos based sealing materials with one new form of sealing material, Thermiculite, being of particular relevance to the sealing of solid oxide fuel cells. The Thermiculite technology developed and patented by Flexitallic, for instance USP 2004/0214032, is capable of excellent service at up to 1000 °C and was initially conceived after it became obvious that the then most promising material for high temperature sealing, exfoliated graphite, suffered disastrous service failures due to oxidation at temperatures as low as 350 °C.

More recently, once it became obvious that there was a need for a compression gasket suitable for SOFC sealing, the Thermiculite range of sealing materials was extended to include Thermiculite 866 which has since been proven around the world to provide reliable SOFC sealing. The structure, capability and service experience of Thermiculite 866 is outlined in this paper and the benefits that it can provide to the groups around the world who are developing SOFC stacks are indicated.

As a result of the experience gained with Thermiculite 866 and the development of a production plant for its large scale manufacture, further members of the Thermiculite range targeted at SOFC sealing have been, or are being, developed either in collaboration with SOFC development teams or in accordance with their requirements. The first of

these new materials, Thermiculite 866 LS, developed in collaboration with VTT is also discussed.

Thermiculite Technology

This technology is based upon the use of vermiculite, a naturally occurring mineral of the phyllosilicate grouping. The members of this group of minerals are all plate silicates and are noted for their high temperature capability and chemical resistance. Two other members of the group are china clay and mica.

The mica family of minerals within the phyllosilicate group consists of a number of well known mineral species such as muscovite and biotite, both of which are widely used in industry because of their thermal and electrical resistance. Together with another member of the group, phlogopite, biotite forms a series of minerals which can be naturally modified over eons of time by hydrothermal action into a mineral known as vermiculite. This mineral, available in large, easily mined, deposits around the world is also used widely in industry because of its temperature capability and its thermal insulating properties.

A key feature of vermiculite is that the individual crystal sheets which stack together to form the plates can be separated from each other, exfoliated, by practical means, a feature that is unique to vermiculite. The simplest way of achieving this exfoliation, although incompletely, is by the application of heat to the plates as mined. This causes the plates to open up into “books” to produce the familiar and widely used material that is the basis of a wide range of industrial products ranging from thermal insulation to garden compost. This material is known as thermally exfoliated vermiculite.

This type of exfoliation is not practical with other members of the mica group. Micas such as muscovite, biotite and phlogopite can be milled to produce a fine powder but that process only produces particles of low aspect ratio having increasingly smaller dimensions. Exfoliation of these micas by the application in the same way that vermiculite can be transformed into “books” is not possible.

For vermiculite far more efficient method of exfoliation than by heat is by chemical means as by this route the plates can be opened up into individual sheets of thickness measured in nanometres. This material, known as chemically exfoliated vermiculite, CEV, together with diluent fillers and elastomer forms the basis of the Thermiculite grades 815, 835 and 715 intended for general industrial sealing. These are all are providing excellent service in a diverse range of industrial applications around the world.

The individual sheets of the CEV are very flexible and can be used to form very thin films of vermiculite. This film forming capability, as a result of the sheets adhering one to another, is very useful forms the basis of the use of Thermiculite in SOFC applications.

Thermiculite 866

Thermiculite 866 consists of only CEV and steatite, another phyllosilicate mineral also known as talc; there is no other component and no organic binder. The sheets of the

CEV act as a binder to hold the whole together to form a flexible sheet that is robust enough to be cut into complex shapes.

A compression sealing material is dependent upon an external load being applied to it so that a seal is created. In order to maintain the seal, the material has to ensure that the load is maintained under service conditions for a long as is required.

To be successful a sealing material has to have certain features which can be summarised as:

Conformability --- the material has to be soft enough to be able to conform to the irregularities of the surfaces being sealed so that a seal is created.

Stress retention --- the material has to resist the tendency for its thickness to reduce under load or as a result of the application of heat or as the result of the burn off of any components at the service temperature. If the thickness reduces then if the stress imposed upon it via the elastic stack tie bars will reduce.

Sealing --- the structure of the material has to be such that the medium being sealed cannot penetrate through it or between it and the surfaces being sealed at any temperature up to the service temperature.

Thermiculite 866 and Thermiculite 866 LS meet all of these objectives.

The Structure of Thermiculite 866

Figure 1A illustrates the structure of Thermiculite 866. This shows why the sealing is so good as the highly aligned sheets of the CEV interspersed with the steatite create a very tortuous path along which any gas molecules would have to travel in order to escape.

In contrast, Figure 1B shows the structure of a traditional mica sheet material. This shows the thick & blocky nature of the mica, relative to the CEV of Figure 1A. These materials rely upon the inclusion of an elastomer in the material to bind it together. If too much elastomer is added, to ensure good ambient temperature sealing, then the creep characteristics will be poor. At elevated temperature the binder will burn off creating a higher leakage rate than at ambient temperature.

The Properties of Thermiculite 866

Thermiculite 866 is available in a thickness range of 0.3 to 1.0 mm at a density of 1.9 gm / cm^3. The standard thicknesses available are 0.3 mm, 0.5 mm, 0.7 mm and 1.0 mm, with intermediate thicknesses being available as required. The material is made at a width of 450 mm and is supplied in sheets of any length up to 1000 mm with 450 mm by 350 mm being a standard sheet size.

The conformability or compression characteristics as a function of both the applied stress and material thickness are given in Figure 2. This shows that there is sufficient conformability in the material to compensate for the irregularities in the surfaces.

The stress retention capability of a sealing material is dependent upon two key aspects of the material :

1 Whether or not the material creeps under load thus reducing the thickness and therefore allowing a reduction of extension of the stack tie bars with the load on the gasket reducing as a consequence. If this happens then the level of sealing achieved will reduce.

2 Whether or not the thickness of the material under load reduces due to the burn off of any component of the material.

In both cases Thermiculite 866 has minimal tendencies to allow stress loss due to thickness reduction. Figure 3 shows that the creep resistance of Thermiculite 866, which contains no organic content to burn off, is superb even at 20 MPa at both ambient temperature and also elevated temperature. This means that the stress retention in a stack of Thermiculite 866 will be outstanding.

A comparison of the performance of Thermiculite 866 and a mica sheet sealing material is given in Figure 4. It can be seen, even at ambient temperature where the elastomer in the mica sheet would still be present, that the superiority of Thermiculite 866 is very significant. It will be appreciated that at SOFC temperatures after burn off of the elastomer, the difference will be even more significant.

The sealing capability of Thermiculite 866 increases as the stress imposed upon the gasket increases. For a given loading from the tie bars of an SOFC stack the stress on the gasket can be maximised by reducing the gasket area as far as is possible. Sometimes this can be achieved by design changes but otherwise the area can only be reduced by changing the dimensions of the gasket. Figures 5A and 5B illustrate how the sealing of Thermiculite 866 varies as a function of the landwidth of the gasket, the landwidth being the difference between the inner & outer dimensions of the gasket along the radial direction from the centre of the gasket, the stress on the gasket and the pressure being contained. The landwidth should not be reduced below about 4 mm as cut gaskets with landwidths below this value become less robust and the sealing achieved for a given stress reduces as the landwidth reduces.

The combination of the excellent creep resistance, minimal burn off at service temperature and inherent sealing capability mean that Thermiculite 866 provides excellent sealing performance in SOFC service. This is illustrated by Figure 6A and Figure 6B where sealing data collected by a customer during actual stack testing are shown. It can be seen that the level of sealing achieved was well below the required level and that thermal cycling down to 100 °C did not reduce the level of seal achieved.

Apart from creating and maintaining a seal to the required level of sealing, Thermiculite 866 also provides electrical isolation. The electrical insulating resistance of Thermiculite 866, as determined by IE 167 [BS 2782 : Part 2 :1992], is given below in Table I.

TABLE I.

Thickness	As Received [MΩ]	After 50˚C for 24 hours [MΩ]
0.5 mm	0.33	7.5
0.7 mm	0.50	7.5

Thermiculite 866 as a Precision Component of the Stack

As well as its sealing and isolation benefits, Thermiculite 866 can act as an engineering component in the stack because the robustness of its manufacturing process makes it possible to ensure that under the assembly load the thickness of the gasket is held within tight tolerances. Similarly, the level of conformability of Thermiculite 866 under the assembly load can be controlled so that the manufacturing tolerances of other components can be accommodated thus avoiding the cost of better tolerance control of those components.

Gaskets are generally expected to just seal two rigid and, at least approximately, parallel surfaces. The thickness of the gasket is generally not critically important. This may be the case in SOFC applications but we have learnt that there are distinct advantages to the SOFC stack designer if the thickness as a function of applied stress can be controlled to limits much tighter than those current for traditional industrial sealing or the conformability at the stress required to achieve the required level of sealing can be tightly controlled.

The manufacturing process for Thermiculite 866 is similar to the traditional tape casting processes and was developed to provide very tight control of the weight per unit area of the product across and along the sheet and between production runs. The simplicity of the Thermiculite 866 formulation, just two components, and the use of computer controlled dispensing, mixing and casting systems, ensure that the dough from which the product is made is highly consistent. Given control of the weight per unit area and of the ratio of the two ingredients, it is possible to supply Thermiculite 866 such that under the specified stress the thickness is controlled to +/- 0.02 mm.

Gasket Cutting

Thermiculite 866 can be easily cut with a knife or scissors and cut gaskets are robust provided that the landwidth is not reduced significantly below about 4 mm. Gasket cutting by the use of laser or water jet methods is not recommended . Where quantities of gaskets or gaskets with complex shapes are required then they should be cut by those organisations that specialise in the supply of cut gaskets to their users. These can be found in every city in the industrial world. Flexitallic offers a gasket cutting service to assist its customers. A confidentiality agreement can be signed where required so that

confidential gasket shape information can be supplied with security in order to allow the production of the necessary gasket cutting tooling.

Thermiculite 866 LS

Lowering the stress that has to be imposed upon a compression gasket to achieve the required level of sealing has significant advantages for the SOFC stack designer. As the loading required on the gasket falls so the cost of the raw materials of the stack falls. Similarly, components made of brittle materials that could not survive the higher loads can be successfully utilized.

There are two types of leakages from a compression seal; they are interfacial, the leakage between the surface to be sealed and the gasket, and permeation, the leakage through the core of the gasket. The relative magnitude of the two types of leakage depends upon many factors, not least the pressure and nature of the gas to be sealed. Figure 7 shows how the sealing of Thermiculite 866 is influenced by material thickness when the surfaces to be sealed are either smooth or spirally grooved. The difference, for a given thickness, between the results from the two types of surface finish gives an indication of the magnitude of the interfacial leakage component and the intercepts give an indication of the magnitude of the permeation leakage component. In parallel, Figure 8 gives an indication of how the pressure of the gas being contained influences the sealing performance of Thermiculite 866.

One user of Thermiculite 866 for a number of years has been the VTT Technical Research Centre of Finland, one of the leading research institutes in fuel cell research in the Nordic countries. The focus of the SOFC research at VTT is to develop new technology and to provide information for industrial enterprises in order to support development work on SOFC based power plants. VTT also supports the development of stacks, the development of balance of plant components, and the application of SOFC power plants. A further purpose is to increase the understanding of the fundamentals of SOFC science and systems.

As the result of collaboration over the supply of tailored forms of Thermiculite 866 to VTT to assist their SOFC development work, a very positive relationship developed between Flexitallic and VTT. One important requirement from VTT was for an SOFC sealing material with a sealing stress requirement well below that of Thermiculite 866. In order to cover the reduction of both types of leakage without duplication of effort the necessary work was be shared between VTT & Flexitallic. VTT concentrated on the reduction of the interfacial leakage component of compression gasket materials whilst Flexitallic concentrated on the reduction of the permeation component of the leakage because the latter was formulation dependent and the former was not.

VTT were highly successful in their work. The interfacial leakage reduction method developed by VTT is based upon the application to each surface of the gasket of a glass powder having a melting point lower than the service temperature so that under service conditions the glass becomes a highly viscous paste which blocks off the leakage paths. This work has resulted in excellent sealing at stresses below 0.5 MPa.

Figure 9 compares the sealing achieved at stresses of both 0.1 and 0.4 MPa for standard Thermiculite 866 and Thermiculite 866 plus the glass containing coating known as Thermiculite 866 LS, The dramatic gain in sealing can be clearly seen Figure 10 shows the surface of Thermiculite 866 LS with the glass particles being clearly visible.

Figures 11 shows the effect of time and thermal cycling on the sealing of Thermiculite 866 and Thermiculite 866 LS at a temperature of 700 °C . The gasket stress during these tests was 0.1 MPa and during the overall test period of over 600 hours, using 4% H_2 in N_2, a series of five thermal cycles down to 150°C were carried out between the 300 to 530 hour periods of the test. The sealing performance of the coated material was throughout the tests very significantly lower than the standard Thermiculite 866 and it was constant. The sealing performance of the plain Thermiculite 866 increased somewhat during the tests, an effect that has been reported by a number of users. The thermal cycles had no significant impact on the performance of either type of gasket indicating that the thin glass coating provides excellent performance without the cracking and excessive leakage associated with the use of conventional wholly glass seals.

In parallel with this work by VTT, Flexitallic has been investigating formulation changes aimed at creating a material with lower permeation than Thermiculite 866 which simultaneously has a higher level of conformability. This work, as yet not completed, is progressing well as can be seen in Figure 12 where the thickness dependency of the leakage from the development material can be seen to be minimal.

Conversion Factor for Helium Leakage Rates

At STP 1 mg /m/s of He = 3.306 ml/cm/min He = 0.361 ml/mm/min He.

Acknowledgments

The work of all the laboratory staff at both Flexitallic and VTT without which these products and this paper would not have been possible, is gratefully acknowledged. Also, our thanks are due to the Thermiculite customer who allowed us to include in this paper some of the stack sealing data that they had generated.

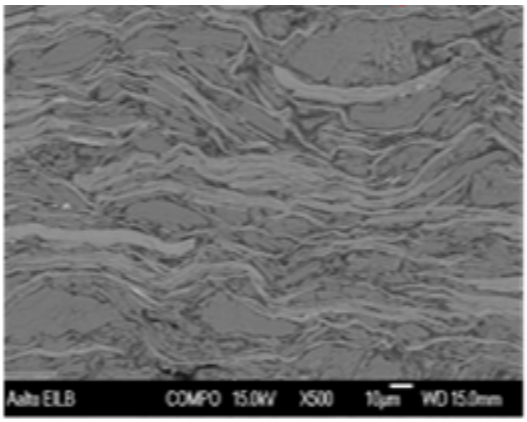

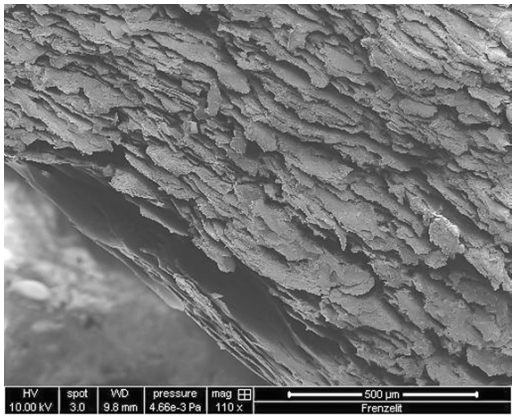

Figure 1A Thermiculite 866

Figure 1B Traditional Mica Sheet

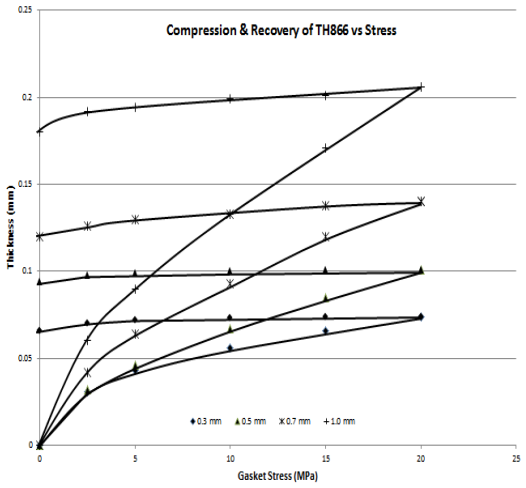

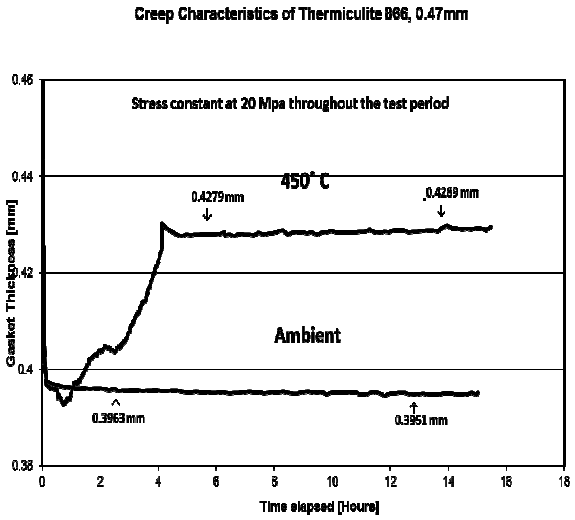

Figure 2 Compression

Figure 3 Creep Resistance

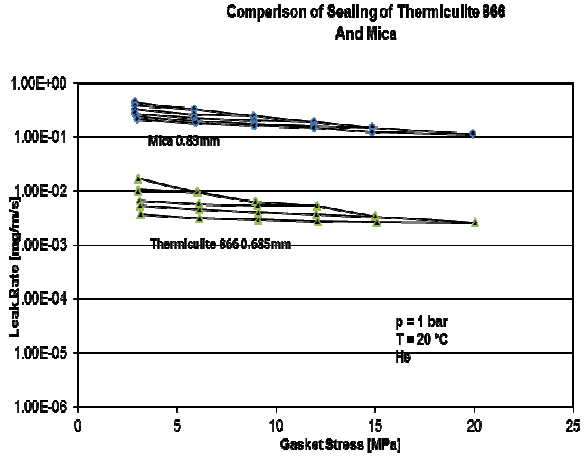

Figure 4 Comparison of sealing Characteristics of Mica and Thermiculite 866

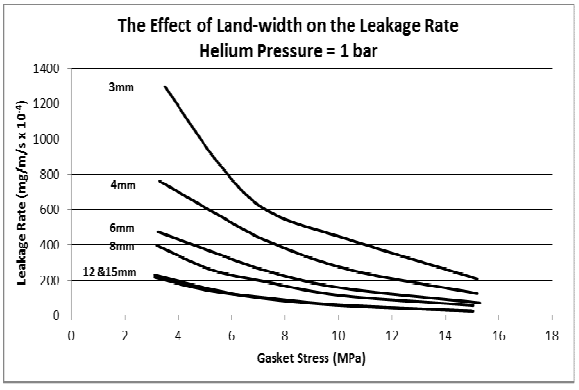

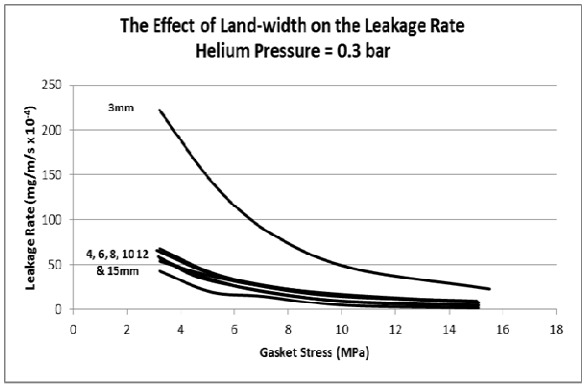

Figures 5A and 5B Effect of Landwidth on Sealing of Thermiculite 866

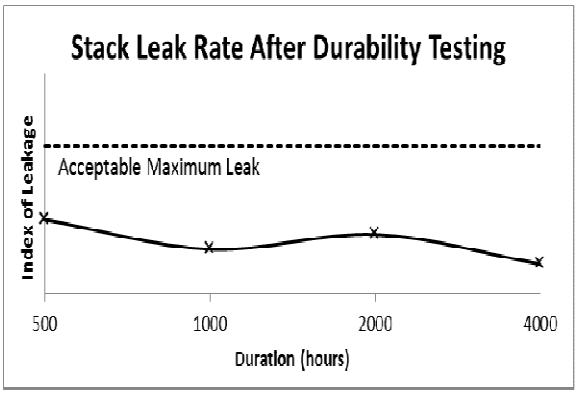

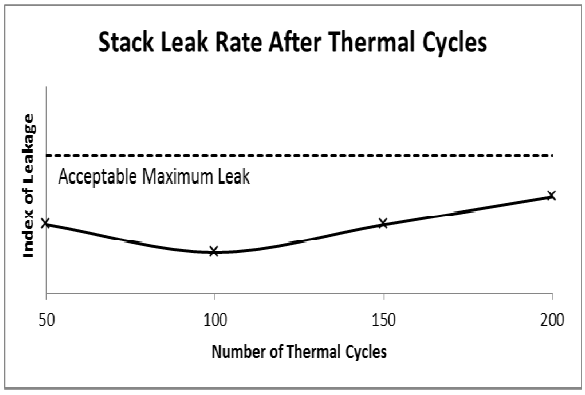

Figures 6A and 6B Thermiculite 866 Stability of Service in SOFC Stack Service

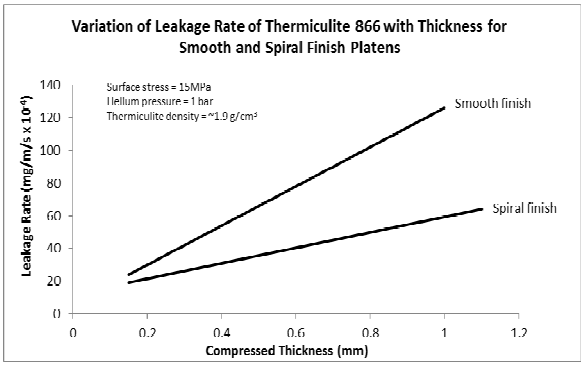

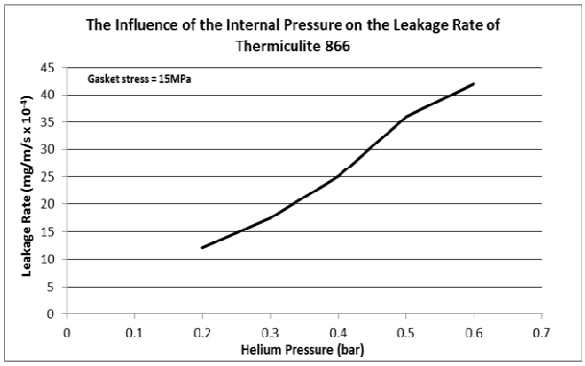

Figures 7 and 8 Influence of Surface Finish and Pressure on the Sealing Performance of Thermiculite 866

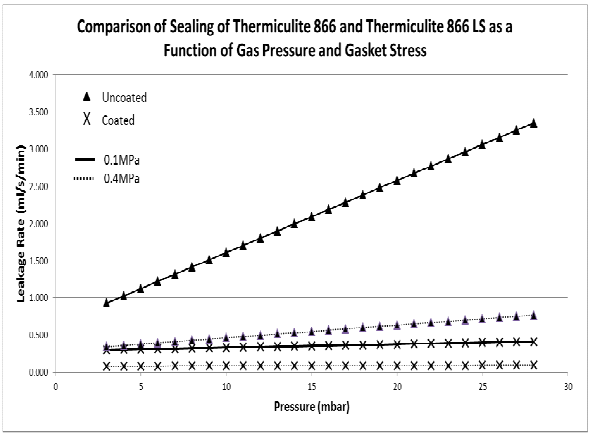

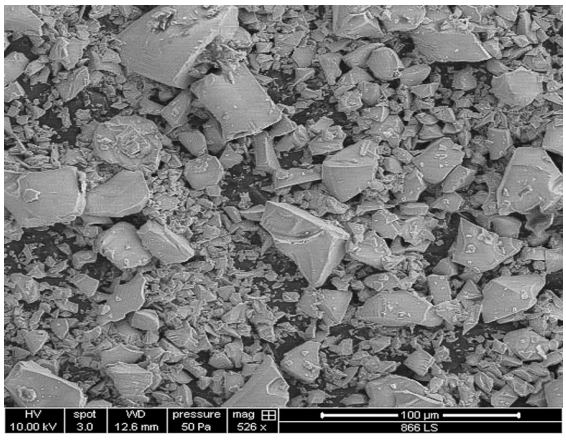

Figure 9 Thermiculite 866 LS Sealing

Figure 10 The Coating on Thermiculite

866 LS

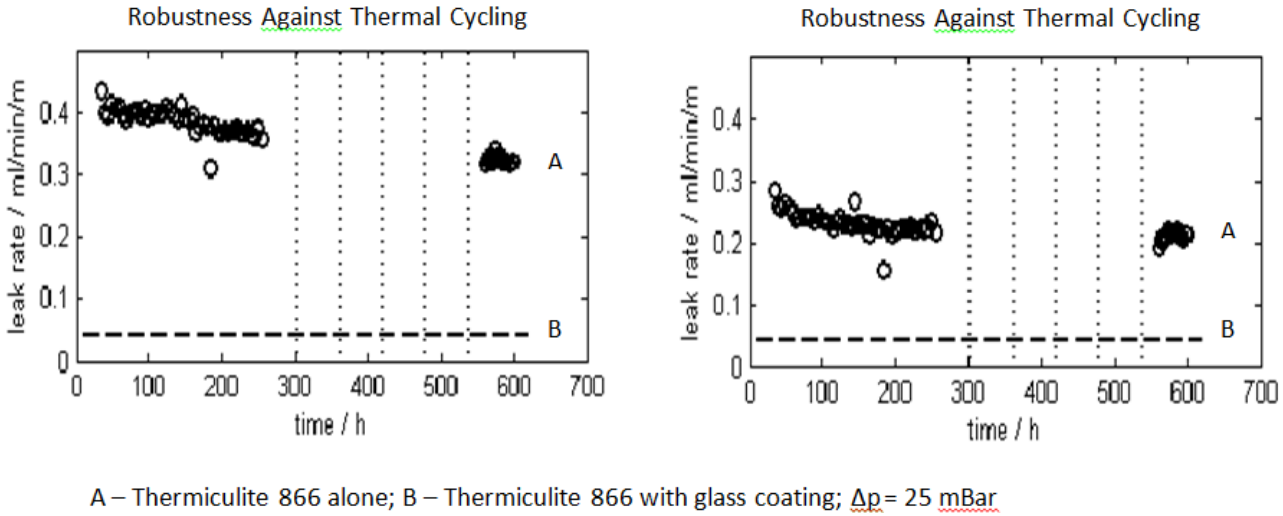

A – Thermiculite 866 alone; B – Thermiculite 866 with glass coating; Δp = 25 mBar

Figure 11 The Robustness and Sealing Performance of Thermiculite 866 and Thermiculite 866 LS

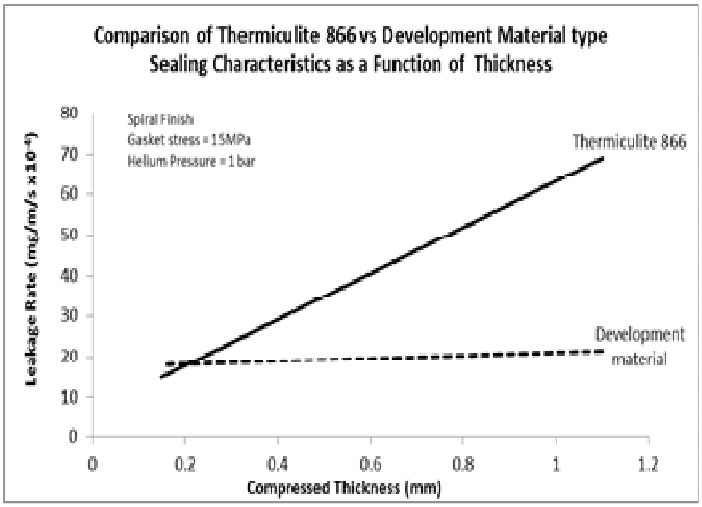

Figure 12 Progress on the Development of Further Materials

PUBLICATION IV

Glass coated compressible solid oxide fuel cell seals

Journal of Power Sources. Elsevier. Vol. 247 (2014), 243–248.

Journal of Power Sources 247 (2014) 243–248

Contents lists available at ScienceDirect

Journal of Power Sources

journal homepage: www.elsevier.com/locate/jpowsour

Glass coated compressible solid oxide fuel cell seals

M. Rautanen*, O. Thomann, O. Himanen, J. Tallgren, J. Kiviaho

VTT Technical Research Centre of Finland, Fuel Cells, P.O. Box 1000, Biologinkuja 5, Espoo, FI-02044 VTT, Finland

HIGHLIGHTS

- A novel sealing material for solid oxide fuel cell stacks: conformable Thermiculite 866 core with thin glass coating.
- A method to coat thin glass layers using an organic carrier.
- Leak test results of glass coated seals.
- Stack test results using glass coated seals.

ARTICLE INFO

Article history:
Received 8 May 2013
Received in revised form
23 July 2013
Accepted 21 August 2013
Available online 31 August 2013

Keywords:
SOFC
Seal
Thermiculite 866
Glass
Leak
Stack

ABSTRACT

With the growing footprint of solid oxide fuel cell stacks, there is a need to extend the operating range of compressible gaskets towards lower stress levels. This article describes a method to manufacture SOFC seals by coating a compressible sealing material (Thermiculite 866) with glass to obtain good sealing performance even at compression stresses as low as 0.1 MPa. Glass layer can be coated using an organic carrier consisting of terpineol, ethanol and ethyl cellulose. The coated seals can be heat treated by simply ramping the temperature up to operating temperature at 60 Kh^{-1} and therefore no extra steps, which are typical to glass seals, are required. Coated seals were manufactured using this route and evaluated both ex-situ and in a real stack. Leak rates of 0.1–0.3 ml $(m\ min)^{-1}$ were measured at 2–25 mbar overpressure using 50/50 H_2/N_2. A 30-cell stack was manufactured and tested using coated seals. At nominal operating conditions of 0.25 A cm^{-2} and 650 °C average cathode temperature, 46% fuel utilization and 20% air utilization the stack had a total hydrogen cross leak of 60 ml min^{-1} corresponding to 0.7% of the inlet hydrogen flow rate.

1. Introduction

Traditionally solid oxide fuel cell (SOFC) stack seals have been either bonding seals (glass/glass-ceramic or brazes) or non-bonding (compressible) seals [1,2]. Bonding seals wet adjacent surfaces forming a very gas tight structure with little interfacial leakages. The usual drawback is that the bonding seals are susceptible to thermo-mechanical stresses especially in thermal cycling. Properties of glasses or glass-ceramics, such as coefficient of thermal expansion (CTE), viscosity and porosity, often change over time. During long term operation these changes can create additional thermo-mechanical stresses leading to seal failure [3,4]. Non-bonding compressible seals are more resistant to thermo-mechanical stresses as they are not rigidly bonded to adjacent components. However, their leak rates are usually higher and dominated by the interfacial leak paths, especially at low compression stresses [5,6]. Compressible seals also require much higher compressive stresses compared to bonding seals, usually at least 2 MPa [7–9]. For example, in the results presented by Thomann et al. [10], with a cell footprint of 100 cm^2, the applied load on the stack was 2000 kg corresponding to roughly 4 MPa on the seals. If this stack was scaled up, the need for the applied load would naturally increase further complicating the mechanical design of the compression system.

Compressive stress is needed in SOFC stacks to ensure adequate sealing performance and to establish a good electrical contact between cells and interconnects. A general trend in SOFC stacks is towards larger cells and therefore towards larger stack footprints creating a need for higher compression on stacks, particularly the ones using compressible seals. This leads to heavier and more complicated compression systems. Compression rods usually need to go through the stack module heat insulation creating additional heat losses. Less compression would enable the use of thinner, less robust stack components. Therefore minimizing compressive stress required on the stack seals while maintaining the easy handling and assembly of the compressible seals would be beneficial.

* Corresponding author. Tel.: +358 405387552; fax: +358 207227048.
E-mail address: markus.rautanen@vtt.fi (M. Rautanen).

0378-7753/$ – see front matter © 2013 Elsevier B.V. All rights reserved.
http://dx.doi.org/10.1016/j.jpowsour.2013.08.085

In recent years, there has been some activity to develop composite seals combining properties from both compressible seals and glass-ceramic seals. The idea is to have a seal which would inherit its mechanical properties from the compressible core but, as opposed to standard compressive seals, would have very low interfacial leak rates because of the compliant surface coating. This would enable the compressible core to deform as a function of thermo-mechanical stresses without causing failure of the seal. Chou et al. have been experimenting with the hybrid sealing concept using different micas as substrates and glass or silver foil to seal the interfacial leak paths [5,6,11–15].

The hybrid seal developed at VTT Technical Research Centre of Finland is a composite structure consisting of compressible Thermiculite 866 [16] core coated with glass using an organic carrier. This method enables easy stack manufacturing as the seal can be coated beforehand and then cut and handled exactly in the same way as traditional compressible gaskets. The organic carrier is burned out in the first heat up and the remaining glass forms a thin conformable interlayer between the seal core and adjacent stack parts. The seal core is able to deform when subjected to stress and therefore can compensate e.g. differences in thermal expansion coefficients of adjacent components. A major advantage of the conformable core is also its ability to compensate for manufacturing tolerances of the adjacent components. Thermiculite 866 core is also less permeable compared to commonly used mica papers since voids between the platelets are filled with a fine grade of steatite. This paper presents a manufacturing method for the coated seals, ex-situ leakage test results and stack test results from a stack utilizing the sealing materials presented in this article.

2. Experimental

2.1. Seal manufacturing

Materials for the hybrid seals were chosen to target stack operation at around 700 °C. The chosen core material was Thermiculite 866 (Flexitallic Ltd) [16]. The glass layer was chosen to be relatively thin (<20 μm) so that the glass itself could be quite low in viscosity. The glass chosen for this study was a commercial glass material having a softening temperature of 650 °C.

Coating of the Thermiculite 866 seals was conducted using a mixture of glass powder and organic carrier. The organic carrier consisted of terpineol (mixture of isomers, Merck), ethanol (ETAX B, Altia) and ethyl cellulose (Fisher Scientific). Ethyl cellulose was mixed with terpineol and ethanol at 35 °C with a magnetic stirrer for 24 h. After that, glass powder was added and the mixture was stirred for 1 h. Table 1 presents typical compositions of the organic carriers and glass to organic ratios used in this study. When coating with brush/spatula/roller, a thicker coating paste proved easy to use and good coverage was achieved easily with a single layer. When using wet spraying, the carrier was diluted with more ethanol to achieve a lower viscosity of around 10–30 cSt which was suitable for the spray gun (U-POL Maximum HVLP mini with 1.0 mm nozzle). Several layers were sprayed from a distance of 10–20 cm.

Table 1
Typical composition of organic carrier and glass to organic ratio with different coating methods.

Coating method	Terpineol/w%	Ethanol/w%	Ethyl cellulose/w%	Glass to organic ratio/w/w
Brush/spatula/roller	81	15	4	2:1
Wet spraying	24	75	1	1:2

After applying the coating, the coated Thermiculite 866 sheets were dried at 75 °C for 2 h and then cut to the required shape. All the seals were heated from room temperature up to 700 °C using 60 Kh^{-1} ramp rate.

2.2. Ex-situ leak tests

Ex-situ leak tests were conducted on ring-shaped seals having 40 mm outer diameter and 5 mm width. The seal was placed on top of 20 mm thick Crofer 22 H (Thyssenkrupp VDM) plate. A 1 mm thick Crofer 22 H plate was placed on top of it and weight plates on top of the 1 mm plate. Gas was fed to the middle of the seal through the thick bottom plate. Fig. 1 presents the experimental setup for ex-situ leak rate measurements. Mass flow controllers fed a chosen gas mixture to the sample line and exhaust line. Sample pressure was controlled with a pressure controller which vents a sufficient flow of gas to the exhaust to keep the upstream pressure at a set level. During heat up, air was fed to the samples to ensure a complete organic burn off.

After heat up, samples were exposed to a 25 mbar overpressure using 50/50 mix of H_2/N_2 at 700 °C. Periodical leak rate measurements were conducted by shutting off the valve V 1 and measuring the pressure decay. A vessel of a known volume was connected to the sample enabling leak rate as a function of pressure to be calculated from the pressure decay curve. Based on the ideal gas assumption, the leak rate is proportional to the slope of the pressure decay curve and therefore the leak rate can be written

$$\dot{Q} = V\frac{T_{\mathrm{ntp}}}{Tp_{\mathrm{ntp}}}\frac{\mathrm{d}p}{\mathrm{d}t},$$

where V is the combined volume of the vessel and the sample, T is the average temperature of the gas in the volume and T_{ntp} and p_{ntp} are normal temperature and pressure. To calculate the leak rate one needs to evaluate dp/dt over the measurement data. If one wants to calculate leak rate at a specific pressure from the data which is a set of points taken at regular intervals, one could approximate dp/dt by

$$\frac{\mathrm{d}p}{\mathrm{d}t} \cong \frac{p_i - p_{i-1}}{t_i - t_{i-1}}.$$

If the sampling rate has been sufficient, the difference $p_i - p_{i-1}$ is bound to be small. As the uncertainty of dp/dt is proportional the uncertainty of the pressure measurement

$$\varepsilon\left(\frac{\mathrm{d}p}{\mathrm{d}t}\right) \propto 2\varepsilon(p),$$

this approach would yield very inaccurate results. To overcome this, a third degree polynomial was fitted to the $p(t)$ − data using least squares method thus minimizing the random uncertainty of the $p(t)$ measurement. Goodness of the fits were analyzed by calculating relative standard deviation of residuals and in case those were over

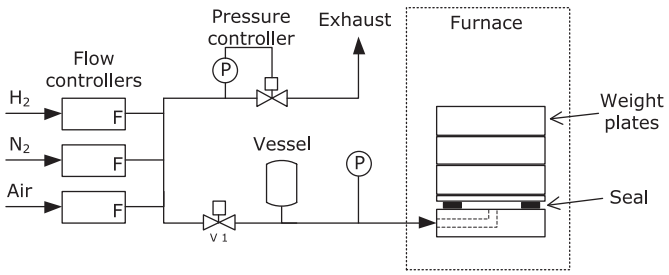

Fig. 1. Measurement setup for the ex-situ leak rate test. Four samples were tested simultaneously, although in here only one is shown for clarity.

Fig. 2. The 30-cell stack before testing.

1.0% fits were discarded. The fitted polynomial was then differentiated to obtain leak rate as a function of pressure. As the accuracy of the pressure transducer is very good (±0.5 mbar) it can be concluded that the accuracy of the pressure measurement has negligible effect on the results. The accuracy of the gas temperature measurement was ±15 °C corresponding to a leak rate uncertainty of 5%.

Quantifying leak rate using the pressure decay methodology described above offers the advantage of relatively simple measurement which can be easily automated. The disadvantage of the method is that by using it one only measures leak rate indirectly by measuring the pressure inside the volume, which is dependent on the flow rates of species through the seal boundary. By using other gas than air, there is always a concentration difference over the seal and therefore also a flux of species from outside to inside by diffusion, which has an effect on the observed flow rate.

2.3. Stack test

In addition to the ex-situ tests, a 30-cell stack was manufactured and tested together with Elcogen. The stack utilized Elcogen ASC-10B cells and ferritic steel interconnects. The seals were made of coated Thermiculite 866 except for the seal against the electrolyte which was made of glass, as it needed to be thinner than the thinnest coated seal that was achievable at the time the work was carried out. Fig. 2 shows the 30-cell stack in a furnace before testing. The compression on the stack was provided through a pipe seen at the upper end of the picture. Pipe coils seen at the bottom of the furnace acted as pre-heaters for air and fuel. On the right side of the picture current collectors attaching to the end plates are seen. Pipelines to measure stack pressures are seen to exit the furnace to the left. The stack was heated up using air flow at both anode and cathode. After reaching the operating temperature, nitrogen was fed to the anode side and afterwards reduction was carried out with hydrogen in nitrogen mixture. During stack polarization, hydrogen and air flows were increased while increasing current and nitrogen flow was kept constant at 8.5 NLPM.

Cross leakages were quantified by measuring steam and oxygen content from cathode and anode outlets. Steam was measured with Vaisala Humicap HMT-337 relative humidity meter (±1% RH) and oxygen with Sick TRANSIC100LP (±0.2% − units O_2). Zero level of the oxygen probe was calibrated with nitrogen and the accuracy was determined to be 0.05% − units below 1% O_2. Oxygen cross leak was calculated before reduction as

$$\dot{Q}_{O_2}^{\text{cross}} = X_{O_2}^{A,\text{out}} \dot{Q}_{N_2}^{A,\text{in}}$$

The hydrogen cross leak after reduction was calculated as

$$\dot{Q}_{H_2}^{\text{cross}} = \left(X_{H_2O}^{C,\text{out}} - X_{H_2O}^{C,\text{in}}\right)\left(\dot{Q}_{\text{air}}^{C,\text{in}} - n_{\text{cells}}\frac{I}{4F}\frac{RT_{\text{ntp}}}{p_{\text{ntp}}}\right),$$

where terms denoted with X are measured oxygen and steam volumetric fractions, n_{cells} is the number of cells in the stack (30), I is the current drawn from the stack and F is the Faradic constant. These calculations are based on the assumption that the leak rates between ambient and anode/cathode and the nitrogen cross leak are small compared to total flow rates.

3. Results and discussion

3.1. Seal manufacturing

Samples for the SEM analysis were cut out of coated Thermiculite 866 sheets and placed between two 1 mm Crofer 22 H sheets. The samples underwent a heat treatment described in Section 2.1 with a 50 h dwell at 700 °C. Fig. 3 shows SEM cross sections of the prepared samples. The horizontal platelets in the Thermiculite 866 are exfoliated vermiculite and the filler between them is steatite. The figure shows the advantage of this material over conventional mica papers as the inherent voids in the flaky mica structure are filled with steatite and therefore the gas tightness is improved. The compressibility of this material is also superior to conventional mica papers [9]. Thin glass layers of 2–10 μm are seen at the interfaces of Thermiculite 866 and Crofer 22 H plates. It can be noted that the glass has accommodated very well to the surface roughness of the Thermiculite 866 and even penetrated into its

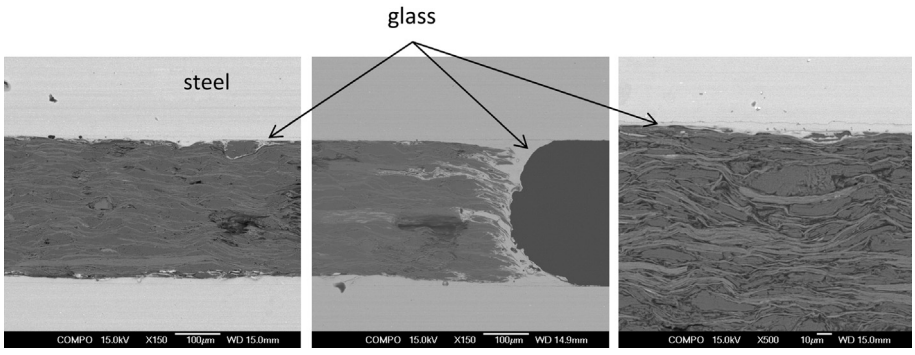

Fig. 3. SEM cross sections of the coated seals. From left to right: middle section of the seal, end of the seal and close up of the steel/glass/Thermiculite 866 interface.

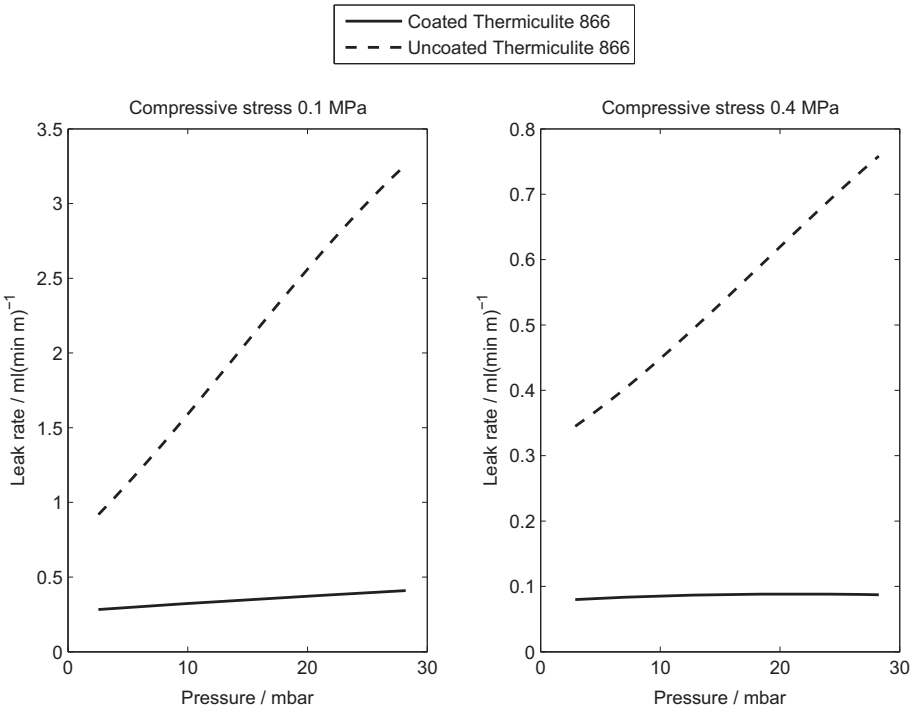

Fig. 4. Leak rates of coated and uncoated Thermiculite 866 at compressive stress of 0.1 MPa (left) and 0.4 MPa (right) with 50/50H_2/N_2. Note the different scales of the vertical axes.

pores. The low initial viscosity of the glass layer provides good conformability to the Thermiculite 866 core and to any surface imperfections on the adjacent components.

3.2. Ex-situ leak tests

Fig. 4 presents leak rates of the samples as a function of pressure at 0.1 MPa and 0.4 MPa compressive stress. From this figure it can be noticed that the surface coating decreases the leak rate of Thermiculite 866, especially at low compression stress levels. The coated Thermiculite 866 seals show leak rates of 0.1–0.3 ml (m min)$^{-1}$, which is a reduction of 60–90% compared to uncoated samples which showed leak rates of 0.3–3 ml (m min)$^{-1}$. Chou et al. have measured leak rates below 1 ml (m min)$^{-1}$ using mica papers with glass interlayers at compressive stresses of 0.04–0.7 MPa and less than 0.1 ml (m min)$^{-1}$ using glass sealing [5,12,15,17]. The tests have been carried out either with helium or 2.64% H_2 in humidified Ar. Although different conditions make direct comparison difficult, it is clear that the results presented in this paper are at a comparable level to the hybrid seals developed by Chou et al.

Fig. 5 presents leak rates of coated and uncoated Thermiculite 866 with different gas compositions and overpressures. The leak rate of the uncoated sample clearly depends on both overpressure and the hydrogen concentration but the leak rate of the coated sample only depends on the hydrogen concentration. As the driving potentials, overpressure and concentration gradients, are same for both measurements, it can be concluded that the coating effectively

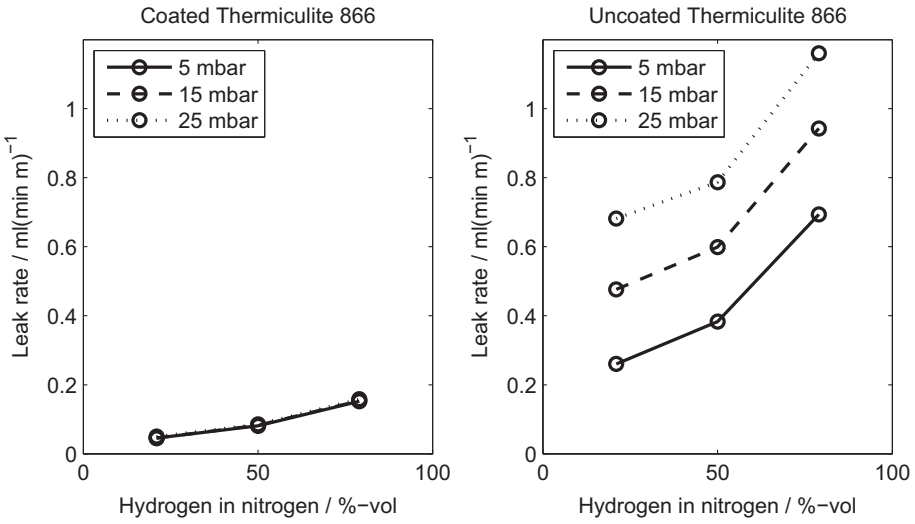

Fig. 5. Leak rates of coated (left) and uncoated (right) Thermiculite 866 at different overpressures as a function of hydrogen concentration. Compressive stress is 0.4 MPa.

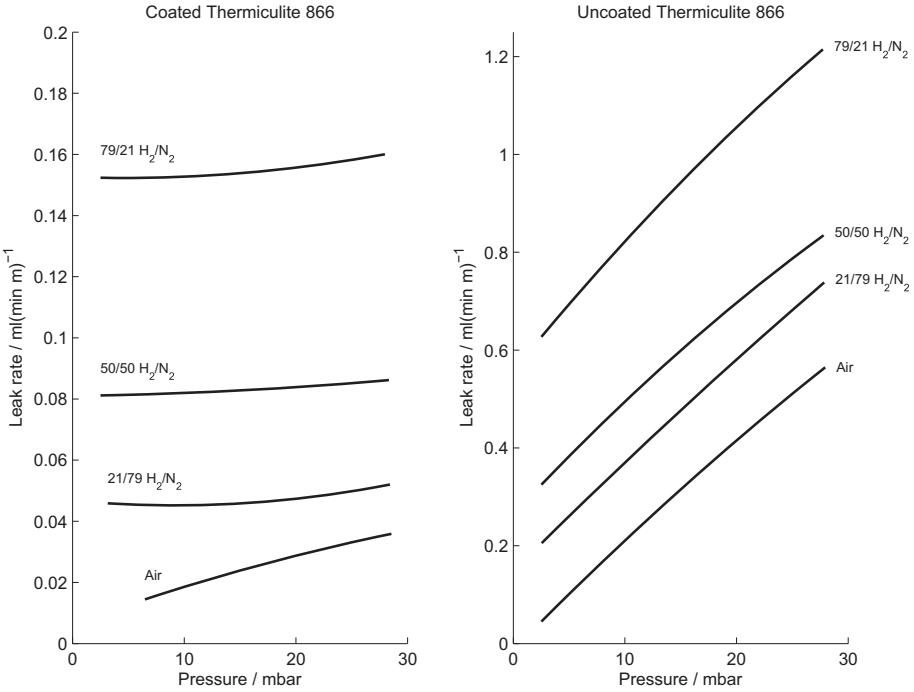

Fig. 6. Leak rates of coated (left) and uncoated (right) Thermiculite 866 as a function of overpressure with 0.4 MPa compression stress with different gas compositions.

blocks the direct leak paths and the remaining leak rate is due to diffusion rather than advection. This is further shown by looking at the curves measured with air (Fig. 6). Extrapolating the curves one obtains a zero leak rate at zero pressure difference when other gas compositions yield a non-zero leak rate also at zero pressure difference. The negligible dependency of the overpressure on the diffusive leak rate can understood by considering Fick's law of diffusion written for a component A using total concentration c_{TOT} total pressure p_{TOT} and the molar fraction x_A:

$$J_A = -D_{AB}\nabla c_A = -C_{TOT}D_{AB}\nabla x_A = -\frac{p_{TOT}}{RT}D_{AB}\nabla x_A.$$

From this equation one can notice that varying the absolute overpressure p_{TOT} in a range of ~1000–1030 mbar induces very little effect on the concentration driven leak rate. Although the real situation is more complex, the concentration dependency of the leak rates should be carefully considered as different research groups use very different gas compositions and overpressures for leak tests, such as 3% H_2 in nitrogen or argon, 100% H_2 or 100% He.

3.3. Stack test

Hydrogen cross leak was measured with purge gas and at nominal operating conditions (Table 2). Table 3 shows stack flows, measured values and the calculated cross leaks at different operating conditions. The air inlet humidity was constant 0.08%. Before reduction, the O_2 cross leak was 8 ml min^{-1}. After reduction the H_2 leak rate using purge gas was 10 ml min^{-1} and 60 ml min^{-1} at nominal operating conditions. Fig. 7 shows the hydrogen cross leak as a function of average hydrogen concentration between anode inlet and outlet during the test. The concentration dependency of the leak rate can be clearly noticed as in the ex-situ tests. During nominal operating conditions the overpressure at cathode was higher than the pressure at anode and therefore the measured hydrogen leak is against the pressure gradient which suggests that the remaining leak rate is due to diffusion rather than advection through the direct flow paths. However, as the measured quantity in stack test is hydrogen leak rather than total leak, even if the leak was totally advective of nature, the hydrogen leak rate would increase as a function of hydrogen concentration in the gas which makes it difficult to draw the final conclusions. At nominal operating conditions of 0.25 A cm^{-2} current density, 46% fuel utilization and 20% air utilization the stack had a total hydrogen cross leak of 60 ml min^{-1}. The hydrogen cross leak value at nominal operating conditions corresponds to a loss of 0.7% of the inlet hydrogen flow, which can be considered a very promising result for the first test using coated Thermiculite 866 seals in a real SOFC stack.

Table 2
Nominal operating conditions.

Cells	30 pcs Elcogen ASC-10B
Flow configuration	Co-flow
Active area	81 cm^2
Cathode inlet temperature	590 °C
Cathode outlet temperature	700 °C
Current density	0.25 A cm^{-2}
Air utilization	22%
Fuel utilization	46%
Pressure difference over anode	3 mbar
Cathode inlet pressure	13 mbar
Cathode outlet pressure	Ambient

Table 3
Summary of the measurements and calculated cross leak rates at different operating conditions. The cathode inlet humidity was constant 0.08%.

	Flow rate/ml min^{-1}			Measured quantity	Calculated cross leak/ml min^{-1}
	H_2	N_2	Air		
Before reduction	0	4500	4500	0.18% O_2 (anode out)	8 ± 2 (O_2)
Purge gas	500	8500	8500	0.20% H_2O (cathode out)	10 ± 2 (H_2)
Nominal	9000	8500	50,000	0.20% H_2O (cathode out)	60 ± 12 (H_2)

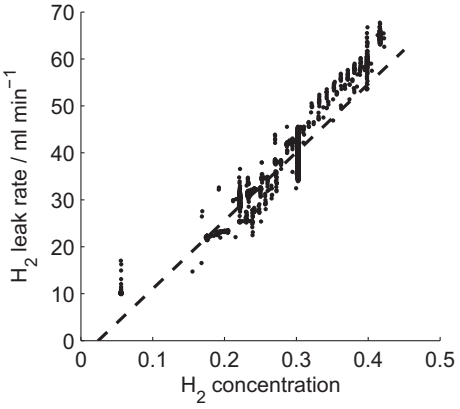

Fig. 7. Hydrogen cross leak as a function of average hydrogen concentration between anode inlet and outlet.

4. Conclusions

A coating method to deposit thin glass layers on compressible sealing materials was developed. Thermiculite 866 seals were coated with glass powder in organic carrier and were subsequently heat treated. The glass coating was conformable filling the surface imperfections of the Themiculite 866 core and the adjacent components effectively blocking interfacial leak paths. The coated Thermiculite 866 seals showed leak rates of 0.1–0.3 ml (m min)$^{-1}$, which is a reduction of 60–90% compared to uncoated samples which showed leak rates of 0.3–3 ml (m min)$^{-1}$. Leak rates of the coated seals as a function of overpressure were measured to be almost constant but very much dependent on the hydrogen concentration indicating that the coating effectively blocked the interfacial leak paths. The effect of gas composition to the leak rate should be considered carefully when comparing leak test results between different literature sources, as it can vary greatly.

A 30-cell stack was manufactured and tested to verify the feasibility of the coated seals in stack conditions. At nominal operating conditions of 0.25 A cm^{-2}, 46% fuel utilization and 20% air utilization the stack had a total hydrogen cross leak of 60 ml min^{-1} corresponding to 0.7% of the inlet hydrogen flow rate which can be considered a very promising result for the first stack test using these seals.

Acknowledgements

Finnish Funding Agency for Technology and Innovation in Finland (TEKES) and Elcogen Oy are acknowledged for financial support. Kai Nurminen and Kari Koskela of VTT Technical Research Centre of Finland and Jorma Stick of SataHitsaus are acknowledged for helping out with the experimental part of the work.

References

[1] J.W. Fergus, J. Power Sources 147 (2005) 46–57.
[2] P. Lessing, J. Mater. Sci. 42 (2007) 3465–3476.
[3] K. Weil, J. Miner. Metals Mater. Soc. (2006) 37–44.
[4] A. Shyam, R. Trejo, D. McGlurg, A. Ladoucceur, M. Kirkham, X. Song, J. Howe, E. Lara-Curzio, J. Mater. Sci. 48 (2013) 5880–5898.
[5] Y.S. Chou, J.W. Stevenson, L.A. Chick, J. Power Sources 112 (2002) 130–136.
[6] Y.S. Chou, J.W. Stevenson, L.A. Chick, J. Am. Ceram. Soc. 86 (2003) 1003–1007.
[7] M. Bram, S. Reckers, P. Drinovac, J. Mönch, R.W. Steinbrech, H.P. Buchkremer, D. Stöver, J. Power Sources 138 (2004) 111–119.
[8] S.P. Simner, J.W. Stevenson, J. Power Sources 102 (2001) 310–316.
[9] M. Rautanen, O. Himanen, V. Saarinen, J. Kiviaho, Fuel Cells (2009) 753–759.
[10] O. Thomann, M. Pihlatie, M. Rautanen, O. Himanen, J. Lagerbom, T. Varis, T. Suhonen, J. Kiviaho, J. Therm. Spray Technol. 22 (2013) 631–639.
[11] Y.S. Chou, J.W. Stevenson, J. Power Sources 191 (2009) 384–389.
[12] Y.S. Chou, J.W. Stevenson, Ceram. Trans. 161 (2005) 69–78.
[13] Y.S. Chou, J.W. Stevenson, J. Power Sources 157 (2006) 260–270.
[14] Y.S. Chou, J.W. Stevenson, J. Power Sources 135 (2004) 72–78.
[15] Y.S. Chou, J.W. Stevenson, P. Singh, J. Power Sources 152 (2005) 168–174.
[16] J. Hoyes, S. Bond, Sealing Technol. (2007) 11–14.
[17] Y.S. Chou, E.C. Thomsen, R.T. Williams, J.-P. Choi, N.L. Canfield, J.F. Bonnett, J.W. Stevenson, A. Shyam, E. Lara-Curzio, J. Power Sources 196 (2011) 2709–2716.

PUBLICATION V

Development and application of HVOF sprayed spinel protective coating for SOFC interconnects

Journal of Thermal Spray Technology. ASM; Springer.
Vol. 22 (2013) No: 5, 631–639.

JTTEE5 22:631–639
DOI: 10.1007/s11666-012-9880-9
1059-9630/$19.00 © ASM International

Development and Application of HVOF Sprayed Spinel Protective Coating for SOFC Interconnects

O. Thomann, M. Pihlatie, M. Rautanen, O. Himanen, J. Lagerbom, M. Mäkinen, T. Varis, T. Suhonen, and J. Kiviaho

(Submitted September 27, 2012; in revised form December 7, 2012)

Protective coatings are needed for metallic interconnects used in solid oxide fuel cell (SOFC) stacks to prevent excessive high-temperature oxidation and evaporation of chromium species. These phenomena affect the lifetime of the stacks by increasing the area-specific resistance (ASR) and poisoning of the cathode. Protective $MnCo_2O_4$ and $MnCo_{1.8}Fe_{0.2}O_4$ coatings were applied on ferritic steel interconnect material (Crofer 22 APU) by high velocity oxy fuel spraying. The substrate-coating systems were tested in long-term exposure tests to investigate their high-temperature oxidation behavior. Additionally, the ASRs were measured at 700 °C for 1000 h. Finally, a real coated interconnect was used in a SOFC single-cell stack for 6000 h. Post-mortem analysis was carried out with scanning electron microscopy. The deposited coatings reduced significantly the oxidation of the metal, exhibited low and stable ASR and reduced effectively the migration of chromium.

Keywords ASR, HVOF spraying, interconnect, protective coating, SOFC, spinel, stack testing

1. Introduction

Interconnects are required in solid oxide fuel cell (SOFC) stacks to staple together an array of cells in series. Interconnects collect electrons from an anode to the cathode of the neighboring cell, and are the physical barrier between the humid reducing atmosphere on one side and the oxidizing atmosphere on the other. Since SOFCs operate typically at 600-800 °C, the requirement for high-temperature corrosion resistance is high. Additionally, interconnects are designed to ensure homogenous distribution of fuel and oxidant to their respective electrodes. Therefore, their requirements are: (i) high electrical conductivity (i.e., the area-specific resistance (ASR) should be below 100 mΩ cm^2, Ref 1), (ii) high corrosion resistance, (iii) coefficient of thermal expansion (CTE) matching those of the other components of the cell (around $10.5 \times 10^{-6}\ K^{-1}$ for yttria-stabilized zirconia electrolyte), (iv) adequate mechanical properties at elevated temperature. At the same time, it is of paramount importance that the material used and the manufacturing methods are low cost as the high cost of SOFC systems is currently impeding their market entry (Ref 1-3).

Special metallic interconnect alloys such as Crofer 22 APU (ThyssenKrupp VDM), E-Brite (Allegheny Ludlum), or ZMG (Hitachi) are widely used in SOFC stacks as they are cheap compared to ceramic interconnects. State-of-the-art ferritic stainless steel interconnect alloys typically contain 20-25 wt.% Cr to meet the requirements concerning the CTE matching, sufficient oxidation resistance and low cost (Ref 4). At operating conditions, a double oxidation layer is formed consisting of a Cr-oxide layer at the surface of the metal and a Cr-Mn spinel as top layer (Ref 5). These oxide layers prevent the metal from excessive oxidation. However, Cr-oxide growth is associated with an increase in the ASR of the interconnect and is detrimental for the electrical efficiency. The corrosion behavior of the interconnect depends on various factors such as the pre-treatment, alloy composition, operating temperature, gas composition, thickness, and shape. However, it is possible to reduce the corrosion of the interconnect by the application of protective coating (Ref 6).

Another issue with uncoated metallic interconnect is the so-called Cr-poisoning of the cathode. It is by now well established that state-of-the-art SOFC cathodes are poisoned by the volatile Cr-species evaporated from the interconnects and other stainless steel components such as system balance-of-plant components (Ref 5, 7-13). Cr reacts at the cathode current collection to form $SrCrO_4$, increasing the ohmic resistance and additionally Cr-Mn spinel formation can impair the electrochemical activity of the cathode (Ref 12). Alloys specifically designed for interconnect applications exhibit up to 75% reduction of Cr evaporation rate compared to general purpose stainless steels (Ref 5). However, further Cr evaporation rate

O. Thomann, M. Pihlatie, M. Rautanen, O. Himanen, J. Lagerbom, M. Mäkinen, T. Varis, T. Suhonen, and **J. Kiviaho**, VTT Technical Research Centre of Finland, P.O. Box 1000, Espoo 02044 VTT, Finland. Contact e-mail: olivier.thomann@vtt.fi.

reduction is needed to achieve viable stack lifetime for market entry (Ref 14). Therefore, protective coatings are seen as a solution to address the issue of Cr release and the Cr-oxide scale growth of metallic interconnects.

The protective coating requirements are: (i) full density or at least closed porosity, (ii) low diffusivity of Cr and oxygen through the coating, (iii) low ohmic resistance to maximize electrical efficiency, (iv) chemical, physical, and structural compatibility with the adjacent components, e.g., the CTE of the coating and of the substrate must match closely (Ref 1).

A wide variety of protective coatings compositions and manufacturing routes have been reported in the literature and they have recently been the subject of a large review (Ref 6). $(Mn,Co)_3O_4$ spinel coatings have received attention due to their good performance compared to other types of coatings (Ref 15). $(Mn,Co)_3O_4$ spinel coatings have been prepared by slurry spraying (Ref 16, 17), radio-frequency sputtering (Ref 17), magnetron sputtering (Ref 18, 19), plasma spraying (Ref 20), atomic layer deposition (Ref 21), pulsed laser deposition (Ref 22), electrodeposition (Ref 23), and filtered arc (Ref 24). Additionally, $MnCo_{2-x}Fe_xO_4$ has also been tried for its better electrical conductivity (Ref 25, 26). To the authors' knowledge, $(Mn,Co)_3O_4$ and $MnCo_{2-x}Fe_xO_4$ spinel coatings prepared by HVOF spraying for interconnect application have not been previously reported in scientific journals.

Coatings produced on interconnect plates by thermal spraying have been previously reported in the literature. Lim et al. (Ref 27) reported applying $La_{0.8}Sr_{0.2}MnO_3$ (LSM) coating by plasma spraying. The coating was 70-90 μm thick and the ASR was about 20 mΩ cm^2 at 800 °C after 160 h. Zhai et al. (Ref 28) also reported applying LSM coating on interconnects by plasma spraying. The ASR was measured for 2 h and was ca. 30 mΩ cm^2. Vargas et al. (Ref 29) reported using atmospheric plasma spraying to produce $MnCo_2O_4$ coating. The coating was ca. 70 μm thick and the ASR was 50 mΩ cm^2 at 800 °C after 560 h. Cr retention capability was qualitatively evaluated to be sufficient by EDS analysis. Unfortunately, Cr retention is not systematically evaluated in papers reporting protective coatings. It can be evaluated qualitatively by EDS analysis of the coating or quantitatively by the transpiration method (Ref 10, 14, 30). Coatings produced by thermal spraying typically suffer from an as-sprayed lamellar microstructure, and there is a risk of cracking of the coating due to thermal or structural stress (Ref 5, 6). To remedy these issues, optimized powders and spraying parameters can improve the coating quality and ease the risk of fragmentation. In addition to interconnect protective coatings, some stack developers make use of a cathode contact layer of, e.g., $La(Ni,Fe)O_3$ between the protective coating and the cathode of the cell, to establish a good electrical contact (Ref 31).

The development of corrosion-resistant ferritic steels has allowed to use metal plates thinner than 1 mm as interconnect plates. Reducing the thickness of the interconnect allows to use low-cost manufacturing methods such as stamping, cutting, pressing, punching, and hydroforming among others. Additionally, thinner interconnects have a potential for faster start-up by reducing the thermal mass of the stack. But reducing the thickness of the interconnect might increase the corrosion rate because of selective depletion of an alloyed element. A thin plate is more prone to deformation and thus increases the risk of crack formation through the coating.

This article deals with experimental investigations of $MnCo_2O_4$ and $MnCo_{1.8}Fe_{0.2}O_4$ spinel coatings on Crofer 22 APU steel. The aim of the article is to present the results from protective coating development; in the first place the powder manufacturing and optimized coating HVOF method is described. Then, high-temperature oxidation behavior and the ASR of coated steel samples in contact with cathode material are investigated. In order to assess the mechanical behavior of the coating on thin corrugated interconnects, 0.2 mm thin coated corrugated plates were exposed at 700 °C under mechanical load for long-term testing. Furthermore, single-cell stack using the developed coating solution has been run for 6000 h to validate the coating solution in a relevant SOFC environment. The results of the post-mortem analysis of the stack are also presented.

2. Experimental

2.1 Powder Manufacturing

The powders used to produce the spinel coatings were either acquired commercially or manufactured in-house at VTT. The $MnCo_2O_4$ powder was commercial and prepared by the fused and crushed method. $MnCo_{1.8}Fe_{0.2}O_4$ powder was manufactured in-house by solid carbonate synthesis and suitable granule size for thermal spraying was obtained by spray drying. The particle shape of the powder is typically less regular for fused and crushed powders than for spray dried powders. The powder was prepared by weighing appropriate amounts of $MnCO_2$, $CoCO_2$, and Fe_2O_3 powders together and milling for 20 h in a drum ball mill (in-house built). After milling, the mixture was calcinated at 1000 °C for 6 h to form the spinel structure. Calcination was done prior to spray drying to avoid granule breakdown due to the large volume change associated to the phase change from the carbonate to oxide. The calcinated powder was sieved to below 63 μm. The powder was then ground and dispersed in water with dispersant Dispex A40 by BASF with a Hosokava Alpine AG bead mill (Hydro Mill 90 AHM). The bead milling was continued until average particle size of 1 μm was reached. Polyvinyl alcohol (PVA 22000 by VWR) was used as a bonding agent and was added to the slurry by a dispergator mixer. The PVA addition was carried out just before spray drying to avoid PVA chain shortening during bead milling. The suspension was spray dried with a Niro pilot p6.3 spray dryer. After spray drying parameter optimization, a high rotational speed (20,000 rpm) of centrifugal nozzle was used to obtain fine granule size. The spray dryer includes a cyclone separator and the cyclone fraction was not used further because of its small average particle size and irregular particle shape.

The chamber fraction of the powder was held at 500 °C for 2 h to pyrolyze the PVA without fracturing the agglomerates. Then, sintering occurred at 1150 °C for 6 h. After sintering the powder was sieved with 32 μm sieve. The cyclone fraction was pyrolyzed to remove the PVA and added to the sieved fraction over 32 μm for crushing and recycling to the bead milling stage. The powder fraction below 32 μm was used for HVOF spraying. The powder morphology was studied with Scanning Electron Microscope (SEM, JEOL JSM-636OLV). The crystal structures of the powders and coatings were determined by x-ray diffraction (XRD) using Mo Kα radiation with Philips X'pert diffractometer.

2.2 HVOF Spraying

Commercial Crofer 22 APU steel (ThyssenKrupp) of 0.2 mm thickness was used as substrate material for test coupons. The HVOF coatings were made using a Praxair HV2000 spray gun, fitted with a 22 mm combustion chamber. Nitrogen was used as powder carrier gas (20 slpm), hydrogen as fuel and oxygen as oxidant. For all the reported coatings but one, a hydrogen flow of 700 slpm and an oxygen flow of 350 slpm were used. The $MnCo_2O_4$ coating reported in Fig. 7 was deposited with a hydrogen flow of 687 slpm and an oxygen flow of 315 slpm. The spray gun was moved by an X-Y manipulator. Prior to deposition, the substrates were grit blasted using a −36 mesh alumina grit, brushed and ultrasonically cleaned in acetone. Grit blasting was conducted on both sides to keep the thin metal sheet substrates straight. For the same reason, the coating was applied on both sides. The targeted coating thickness was 20-30 μm, which is unusually thin for thermal spraying. More details on the HVOF coating process can be obtained from Ref 32.

2.3 Exposure Tests

Exposure tests were conducted using laser cut 10 × 10-15 × 0.2 mm samples. The samples were placed standing in a furnace in alumina sample holders so that no contact between samples occurred. The samples were coated on both sides and only the edges of the samples were uncoated. The tests were conducted in air for 1000 h at 700 °C. A continuous gas flow was implemented with the incoming air bubbled through a water bottle; the resulting humidity of the air was thus ~3%. Cross-sectional samples were prepared for SEM observation.

2.4 ASR Measurements

The ASR measurements were done for two coatings ($MnCo_{1.8}Fe_{0.2}O_4$ and $MnCo_2O_4$) applied on two flat 26 × 26 × 0.2 mm steel plates separated by an initially green ceramic layer mimicking a cathode. Additionally, an uncoated steel plate was also tested as a reference. Green 20 × 20 × 1 mm $La_{0.85}Sr_{0.15}Mn_{1.1}O_3$ (LSM) spacers (IRD Fuel Cells A/S, Denmark) were used as separation material between coated steel plates. The purpose of the LSM spacers is to serve as a contact surface with a material similar to a real SOFC cathode. The investigated contact resistance interface was therefore coated against LSM. For the experiments, several samples were stacked up and held together by a vertical load of 20 N. A sketch of the test arrangement is shown in Fig. 1. All samples were connected in a single DC current loop, the current was 0.8 A and the current density was 0.2 A/cm^2. Pt leads of 1 mm were mechanically attached to 1 mm thick steel plates at the bottom and top of the test sample stack. The voltage across each tested material couple was measured by thin (0.3-0.5 mm) Pt threads. To separate each tested substrate-coating system, 1 mm thick steel plates were used as separator disks. The binder was burned out from the green LSM spacers during a slow heat-up at 15 °C/min with a constant flow of air at 0.3 slpm, then the spacers were sintered at the beginning of the experiment for 12 h at 850 °C in contact with the coated steel to form the interface. The steady-state measurements were conducted in compressed filtered dry air at 700 °C during 1000 h. The data were logged using Agilent data logger and multiplexer. The post-mortem analysis was done using JEOL JSM-6335F field emission SEM equipped with a backscattered electron (BSE) detector and an Oxford Link Pentafet EDS analysator.

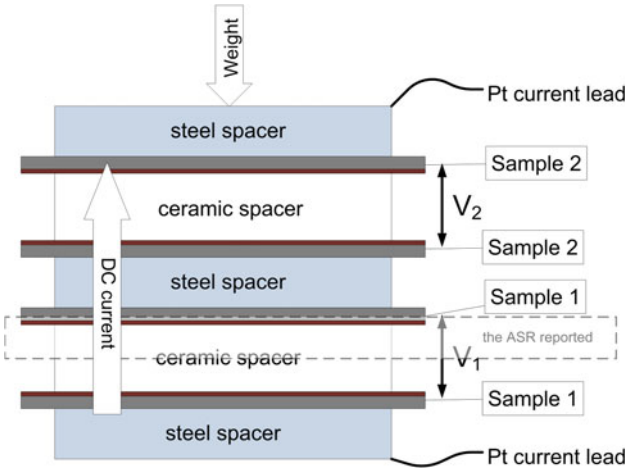

Fig. 1 The ASR measurement arrangement for coated Crofer 22 APU plates with LSM spacers. The protective coatings were applied on the Crofer 22 APU steel surfaces facing the ceramic spacers

2.5 Mechanical Behavior of the Coating in Corrugated Geometry

The coated corrugated samples were tested to examine the effect of mechanical loading and substrate deformation on the HVOF coatings. The corrugated plates were supplied by ECN/ETE (Petten, The Netherlands) and were made by stamping 34 × 4.3 mm corrugations of approximately 1 mm depth into a 0.2 mm plate of Crofer 22 APU (corrugated area: 34 × 34 mm). The HVOF coatings were applied on the corrugated plate and the flat steel plate surfaces and the coatings were placed facing each other.

The mechanical loading was applied by a vertical load of 50 N, causing compressive and tensile stresses at different

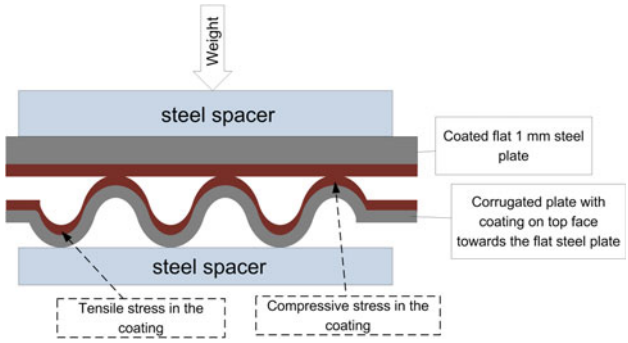

Fig. 2 The arrangement used to investigate the mechanical behavior of the coating on corrugated plates

locations of the coatings as illustrated in Fig. 2. Stationary ambient air was used in the large volume chamber furnace (lid breathable) which secured the sufficient amount of oxygen.

2.6 Stack Testing and Post-mortem Analysis

The $MnCo_{1.8}Fe_{0.2}O_4$ coating was tested in a single-cell stack that was operated for 6000 h at 700 °C. The metallic interconnects were made of 1 mm Crofer 22 APU plates and the gas channels were etched into the plates. Protective coating ($MnCo_{1.8}Fe_{0.2}O_4$) was sprayed on the cathode interconnect with approximately 20 μm as-sprayed thickness. The coated interconnect was not heat-treated and no contact coating was used. Compressible Thermiculite 866 made by Flexitallic Ltd (Cleckheaton, UK) was used as gasket (Ref 33). An anode-supported cell with a $(La,Sr)(Co,Fe)O_3$ (LSCF) cathode was used. Dry H_2 and dry air were used as fuel and oxidant, respectively. Current density was 0.3 A/cm^2.

The goals of the post-mortem analysis were to evaluate the coating, the oxide layers present on the cathode interconnect and possible Cr presence in the cathode. After testing, the single-cell stack was mounted in epoxy and cross sections were extracted from the middle area of the cell footprint. Post-mortem analysis was carried out using SEM observation and energy-dispersive x-ray spectroscopy (EDS) on JSM-6400 Scanning Microscope from JEOL equipped with a Prism 2000 detector and Spirit 1.06.02 Analyzer software from Princeton Gamma-Tech (PGT).

3. Results and Discussion

3.1 Powder and Coating Manufacturing

The applied synthesis route using carbonates was found practical in this case because of the simplicity of grinding and therefore thorough mixing of the raw materials. Additionally, the reactivity of the carbonates during calcination was found adequate. If larger amounts of powder would be done industrially, other means of mixing and perhaps other raw materials should be considered to avoid

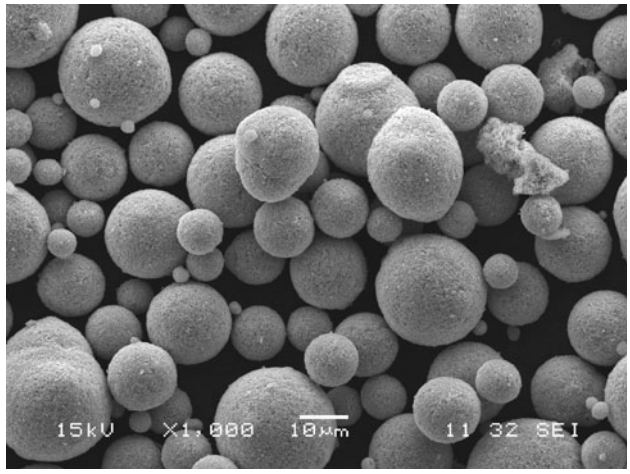

Fig. 3 Secondary electron SEM picture of spray dried $MnCo_{1.8}Fe_{0.2}O_4$ powder

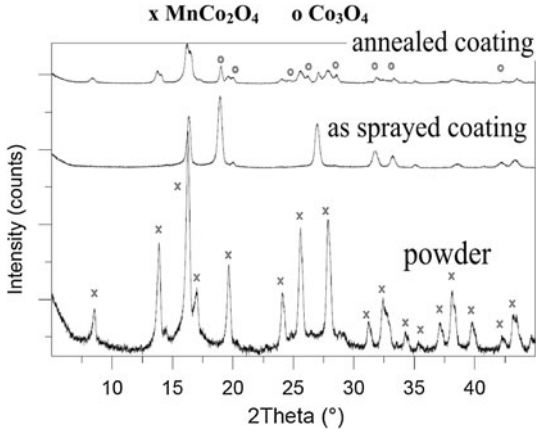

Fig. 4 XRD curves of $MnCo_{1.8}Fe_{0.2}O_4$ powder, coating in as-sprayed state and coating annealed for 2 h at 850 °C. All peaks in the as-sprayed coating correspond to simple cubic phase. The unmarked peaks in annealed coating correspond to the spinel phase $Mn_{1.5}Co_{1.5}O_4$ and $MnCo_2O_4$

the ball milling stage. For instance, chemical synthesis route using dissolved raw materials would ensure homogeneity of the end product.

The $MnCo_{1.8}Fe_{0.2}O_4$ powder prepared by spray drying had typical spherical particle shape which ensures good and constant powder feed rate during spraying. SEM pictures of the powders are presented in the Fig. 3. Only small amount of fine satellites can be seen on larger particles surface. This amount was not considered to cause any problems for HVOF spraying; dusting and feed issues were minimal. Using regular shape powder increases the deposition efficiency and decreases the amount of defects in the coating.

Illustrated in Fig. 4, the XRD pattern of $MnCo_{1.8}Fe_{0.2}O_4$ powder sintered at 1150 °C corresponds to the $MnCo_2O_4$ spinel structure. The XRD pattern of the coating in its as-sprayed state shows that the phase structure is changed during the coating process to simple cubic

structure corresponding for example to the structure of CoO and MnO (space group *Fm*-3*m*). This structure is a metastable state formed because of rapid cooling of the spray droplets during thermal spraying. The XRD curve of the coating after 2 h of annealing at 850 °C shows that the coating crystal structure transforms mainly to the spinel structures $Mn_{1.5}Co_{1.5}O_4$, Co_3O_4, and $MnCo_2O_4$. Exposure for longer time to the actual SOFC environment will fully transform the crystal structure to $MnCo_2O_4$ (Ref 32).

3.2 Exposure Tests

Figure 5 shows a typical microstructure of a $MnCo_2O_4$ as-sprayed protective coating made by HVOF; the coating shows typical lamellar structure and adequate density. Some alumina particles can be observed in the steel-coating interface from the grit blasting procedure. Oxidized steel with a HVOF $MnCo_{1.8}Fe_{0.2}O_4$ coating of 15-18 μm thickness is shown in Fig. 6 after exposure to air for 1000 h at 700 °C; the microstructure is shown in Fig. 6(a) and (b) and elemental profile from an EDS line scan is shown in Fig. 6(c). The Cr oxide layer formed between the steel and the coating during the exposure is about 0.5 μm. During high-temperature exposure, the coating sinters and loses its lamellar structure. Some closed porosity remains visible still after 1000 h of exposure with a decreasing porosity toward the surface. There is little or no Cr gradient in the coating (Fig. 6c), which means that the diffusion of Cr is effectively hindered. As a reference on oxidation, a non-coated Crofer 22 APU sample exposed to the same oxidizing conditions showed in microscopy an oxide layer of 2.5-3 μm of thickness, which is five times higher than for the coated sample. Therefore, the coating solution effectively reduces the oxidation of the steel interconnect.

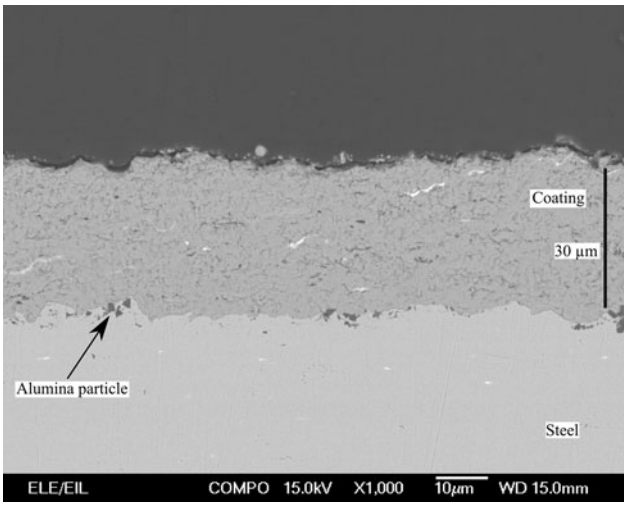

Fig. 5 A BSE SEM image of an as-sprayed HVOF $MnCo_2O_4$ coating on Crofer 22 APU substrate

3.3 ASR Measurements

The ASR measurements against time for coated and uncoated Crofer 22 APU steel are illustrated in Fig. 7. The reported ASR represents half of the ASR measured for one repeating unit in the sample stack shown in Fig. 1. The different components contributing to the ASR value consist of the steel substrate, the Cr oxide scale developing on the steel substrate surface, the protective coating, the contact resistance of the interface between the coating and the ceramic cathode material and the resistance of the ceramic cathode material (i.e., the resistance of 500 μm of LSM cathode material). The reason for the step change in the ASR taking place at 220 h is not completely understood, but is probably related to a structural instability. The change taking place at 720 h of the test in the $MnCo_{1.8}Fe_{0.2}O_4$ sample which was tested in a second test run is due to a small unintentional change in the test temperature (10 °C) due to a power shutdown. For the three samples, the test temperature was between 690 and 710 °C during the long-term test.

The ASRs of the $MnCo_{1.8}Fe_{0.2}O_4$ (15-18 μm thick) and the $MnCo_2O_4$ (20-28 μm thick) coatings are initially 20-30 mΩ cm^2 and decrease slightly to about 20 mΩ cm^2 during the first few hundred hours and then remain stable over the tested period. These results show that the coating solution is adequate to prevent degradation of the electric properties of the interconnect during SOFC operation. Comparisons of ASR values between different studies are delicate because the experimental parameters such as ASR measurement temperature, aging time, and type of spacer used are inconsistent throughout the literature. However, these ASR results are in line with results reported for similar types of coatings (Ref 6) or using a similar test arrangement (Ref 17, 34). The improvements of the ASRs during the first few hundred hours of test are attributed to the sintering of the initially lamellar coating.

The ASR of the bare Crofer 22 APU in contact with LSM is initially about 100 mΩ cm^2 and decreases throughout the tested period to reach 45 mΩ cm^2 after 1000 h of test. The observed decrease of ASR over time is mainly due to improvement in the electrical contact between steel and LSM. Both coatings show initially much lower ASRs compared to the bare Crofer 22 APU. The main source of the difference between the bare Crofer 22 APU and the coated samples is believed to originate from a lower contact resistance of the coated samples.

3.4 Mechanical Behavior of the Coating on Corrugated Geometry

The effect of the corrugated geometry on the mechanical behavior of HVOF $MnCo_2O_4$ coatings was investigated with SEM by looking at different locations of the corrugated geometry. The coating at the top of the corrugation ridges experiences a compressive force when the mechanical loading is applied. The load tends to straighten the corrugation by causing permanent plastic deformation (creep). Consequently, the coating at the bottom of the corrugation groove experiences a tensile

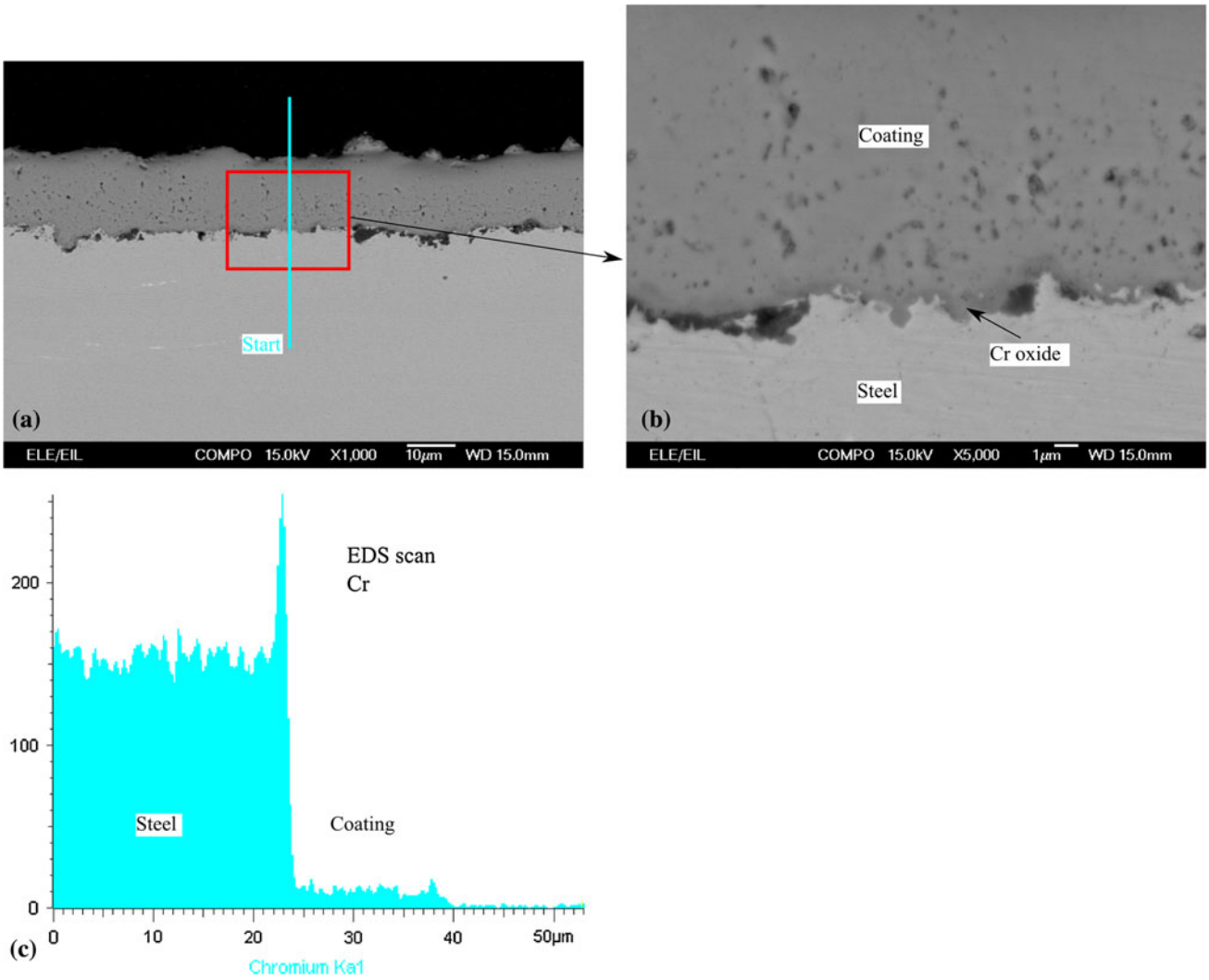

Fig. 6 (a) and (b) BSE SEM images of a HVOF $MnCo_{1.8}Fe_{0.2}O_4$ coating on Crofer 22 APU substrate exposed to air at 700 °C for 1000 h at different magnifications. (c) Measured Cr EDS profile

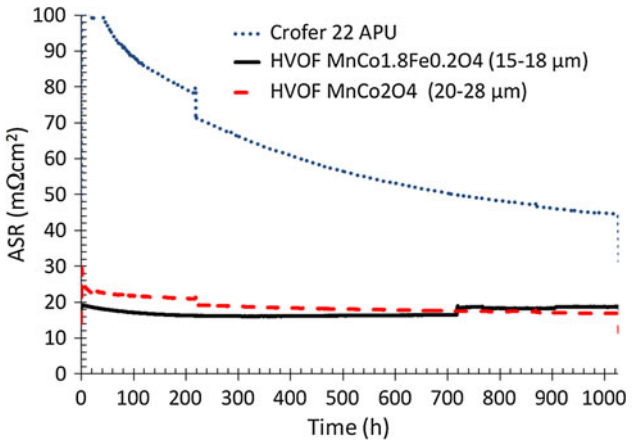

Fig. 7 Measured ASR in a 4-point DC measurement of Crofer 22 APU, coated and uncoated, all in contact with a LSM spacer. The coatings are $MnCo_{1.8}Fe_{0.2}O_4$ and $MnCo_2O_4$

stress. After a 1000 h exposure test at 700 °C, the HVOF coating at the top of the corrugation was largely intact as depicted in the SEM micrograph in Fig. 8(a). Conversely, several through-coating cracks were observed at the bottom of the groove due to tensile stress combined with the intrinsic brittleness of $MnCo_2O_4$ material and coating structure, Fig. 8(b). The stress needed for the fracture of the coating will depend closely on the distribution of flaws in the scale as well as the stress field, but it seems evident that the stresses had in this case been relaxed by through-coating cracks in the HVOF coating. Therefore, while the basic protective function of the HVOF coatings are well fulfilled, they may not be optimal for stack designs having metallic interconnects made of thin corrugated steel plates because of their propensity for cracking under tensile stress due to mechanical load. Although the steel interface at the bottom of the cracks do not show any accelerated corrosion in the present case, such effects or Cr release through the cracks could possibly take place in long-term operation. However, crack formations could possibly be

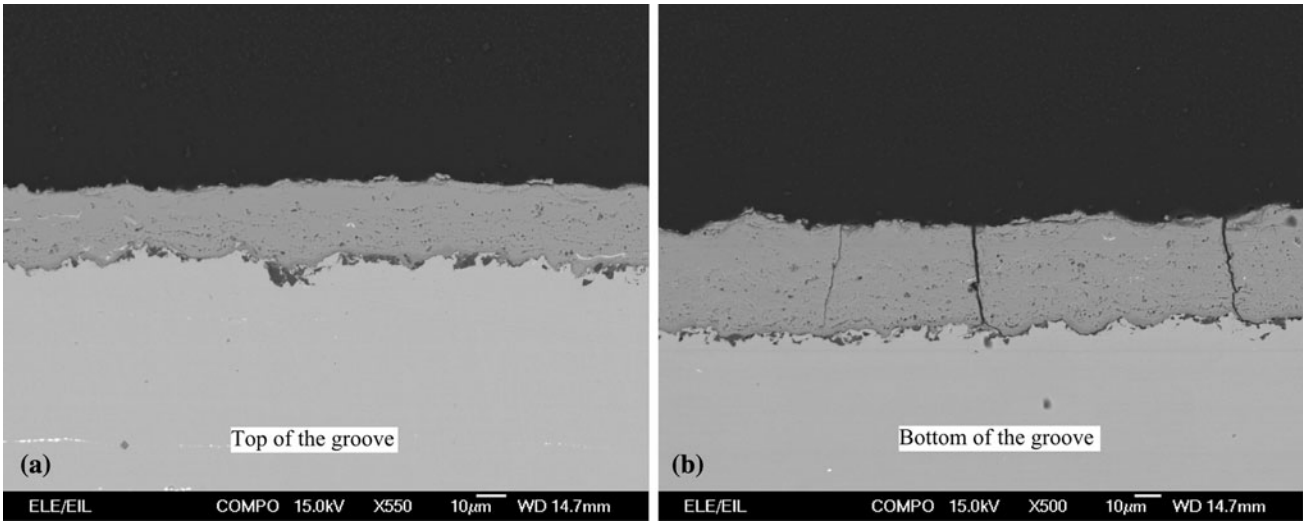

Fig. 8 SEM images from the top (a) and bottom (b) of the corrugated profile exposed to a vertical mechanical load in a high-temperature exposure test with a HVOF $MnCo_2O_4$ coating (1000 h at 700 °C in air)

avoided by adjusting the design of the corrugation and thickness of the interconnect.

3.5 Single-Cell Stack Post-mortem Analysis

Four BSE SEM images of the single-cell stack are presented in Fig. 9. Figure 9(a) shows a low-magnification view of the cathode side of the single-cell stack where the air channel and the contact location between the interconnect and the cathode are visible. It is clear that the coating covers the interconnect completely, including the geometrically challenging features such as the edges of the interconnect ribs. The gap between the cathode and electrolyte and the cracks found in the coating at the air channels are due to sample preparation.

Figure 9(b) shows the contact location between the cathode side of the cell and the coated interconnect with $MnCo_{1.8}Fe_{0.2}O_4$. The micrograph shows good contact between cathode and interconnect. The Cr-oxide scale at the surface of the interconnect metal is about 1 μm in thickness after 6000 h at 700 °C in air. This result can be compared to the exposure tests presented in section 3.2 where the Cr-oxide layer of coated steel was about 0.5 μm thick and the Cr-oxide layer of the unprotected steel was about 2.5-3 μm after 1000 h in air at 700 °C. Therefore, it can be concluded that the coating acts as an effective protection and reduces oxidation of the interconnect in a long-term test in SOFC environment. No cracks are visible in the coating itself, however closed porosity is still present. EDS analysis was performed on the area shown in Fig. 9(b) and no Cr was found neither in the coating nor in the cathode which indicates that Cr diffusion and evaporation through the coating is effectively hindered.

Figure 9(c) shows another micrograph of the coating at an air channel location. The coating presents no cracks but some closed porosity similarly to Fig. 9(b). The Cr-oxide layer under the coating is also about 1 μm thick and no Cr could be detected in the coating. Figure 9(d) illustrates the cathode located at an air channel and a EDS Cr concentration profile. As already mentioned, there is a large gap between cathode and the electrolyte (out of the picture) due to sample preparation and therefore the cathode stands alone in the epoxy. An EDS analysis of the cathode reveals that Cr was present in the cathode at this air channel location. Cr distribution is inhomogeneous and peaks at 2.1 at.%. However, most of the Cr is located away from the active cathode area which is located close to the electrolyte; therefore, the deposited Cr has probably not affected the electrochemical performance of the cathode. The Cr contamination can be either coming from the stainless steel interconnect through the protective coating or from the uncoated Crofer 22 APU air manifold and Inconel 600 air inlet pipe upstream of the cell. However, Cr deposit was located at the air channel (corresponding to Fig. 9d) and not at the contact location with the interconnect (corresponding to Fig. 9b), which supports the hypothesis that Cr has originated from the uncoated air manifold and inlet pipe. Additionally, from the EDS analysis performed across the coating, negligible Cr diffusion appears to take place across the coating. Stainless steel components and manifold upstream of the cells have been previously identified as Cr contamination sources in SOFC stacks (Ref 10, 35). From these results, the coating solution is adequate for steel interconnect protection as it reduces effectively both Cr evaporation and steel interconnect oxidation.

4. Conclusions

Protective $MnCo_2O_4$ and $MnCo_{1.8}Fe_{0.2}O_4$ coatings were manufactured on SOFC steel interconnects by HVOF coating. Exposure tests showed that a 1000 h oxidation in air at 700 °C resulted in a Cr oxide layer of 0.5 μm for the steel protected by HVOF coating. In

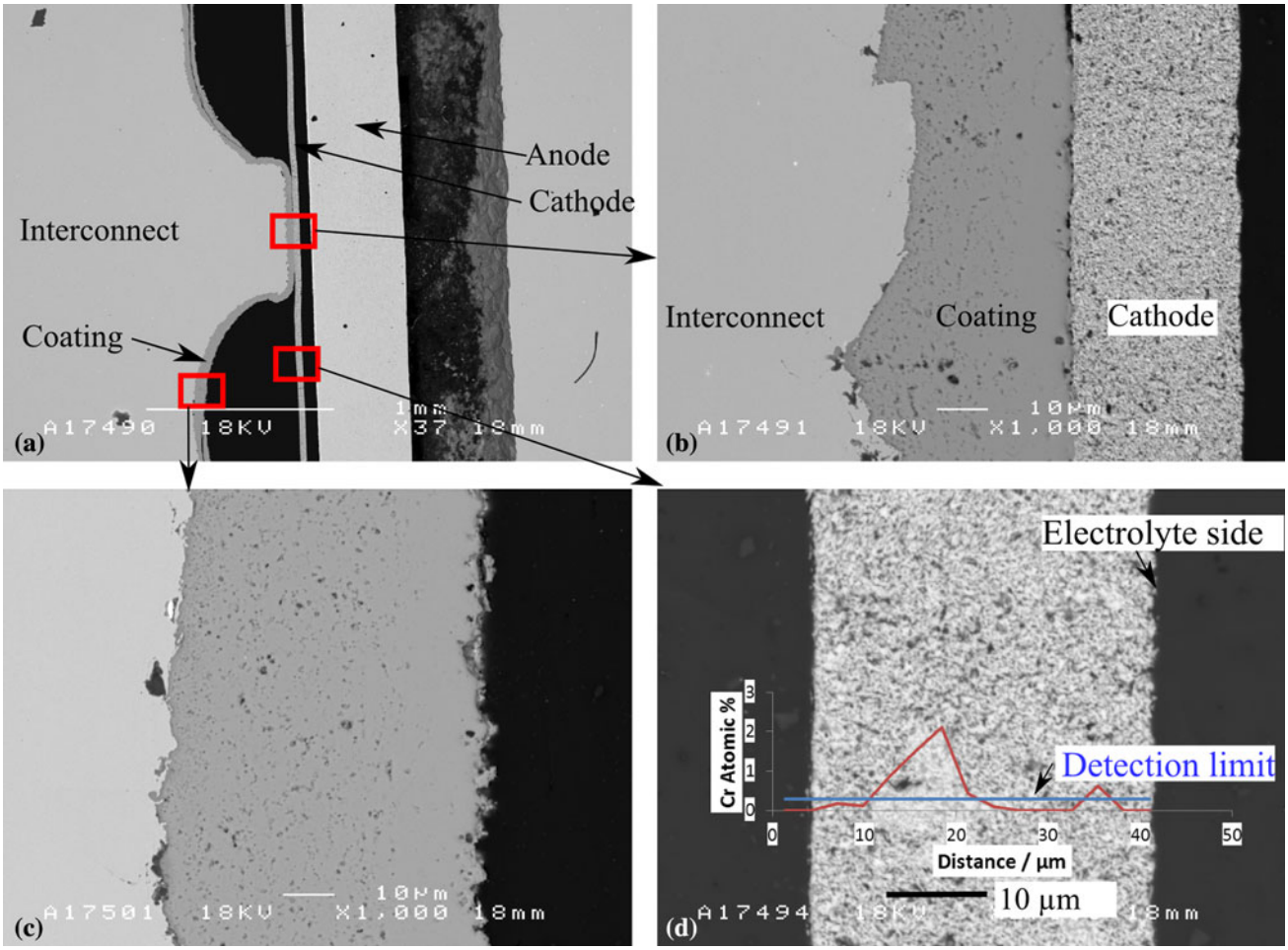

Fig. 9 BSE SEM cross section from the single-cell stack at different locations. (a) Low-magnification image of the air side of the single-cell stack. The interconnect coating composition is $MnCo_{1.8}Fe_{0.2}O_4$. (b) Contact area between coated interconnect and cathode. (c) Surface of the interconnect at an air channel location. (d) Cathode with an EDS Cr profile

comparison, uncoated steel sample developed a 2.5-3 µm Cr oxide layer in the same conditions.

ASR measurements were carried out at 700 °C for 1000 h on coated steel samples in contact with LSM spacers. The results confirmed low ASR values for coated samples of about 20-30 mΩ cm^2 with no degradation over time. These results show that the HVOF coating method developed at VTT is a suitable candidate to be used in SOFC stacks. The mechanical behavior of the coating was evaluated by applying a mechanical load on a coated corrugated thin plate. It was found that the stress arising from deformation of the plate leads to crack formation where the coating is under tension. Therefore, if such corrugated geometry is used for interconnect, more crack-resistant coating solution should be developed.

The protective coating showed adequate corrosion protection and retention of Cr in a single-cell stack test up to 6000 operation hours. The Cr oxide layer was about 1 µm thick and the coating was crack-free and Cr-free. A low concentration of Cr was detected in the fuel cell cathode; however, the uncoated steel manifold and piping upstream of the stack test setup are known to be a source of volatile Cr and are likely to be the origin of the Cr found in the cathode.

Acknowledgments

Financial support from the Finnish Funding Agency for Technology and Innovation, Tekes and the European Commission (Contract 28967, SOFC-Coat) is gratefully acknowledged. Markku Lindberg, Mika Jokipii and Seija Kivi from VTT are acknowledged for sample preparation and Vesa Vuorinen from Aalto University and Risto Parikka from VTT Expert Services Oy are acknowledged for SEM analysis.

References

1. J. Wu and X. Liu, Recent Development of SOFC Metallic Interconnect, *J. Mater. Sci. Technol.*, 2010, **26**(4), p 293-305
2. J.W. Fergus, Metallic Interconnects for Solid Oxide Fuel Cells, *Mater. Sci. Eng. A*, 2005, **397**(1–2), p 271-283

3. W.Z. Zhu and S.C. Deevi, Development of Interconnect Materials for Solid Oxide Fuel Cells, *Mater. Sci. Eng. A*, 2003, **348**(1–2), p 227-243
4. Z. Yang, K.S. Weil, D.M. Paxton, and J.W. Stevenson, Selection and Evaluation of Heat-Resistant Alloys for SOFC Interconnect Applications, *J. Electrochem. Soc.*, 2003, **150**(9), p A1188-A1201
5. M. Stanislowski, E. Wessel, K. Hilpert, T. Markus, and L. Singheiser, Chromium Vaporization from High-Temperature Alloys, *J. Electrochem. Soc.*, 2007, **154**(4), p A295-A306
6. N. Shaigan, W. Qu, D.G. Ivey, and W. Chen, A Review of Recent Progress in Coatings, Surface Modifications and Alloy Developments for Solid Oxide Fuel Cell Ferritic Stainless Steel Interconnects, *J. Power Sources*, 2010, **195**(6), p 1529-1542
7. H. Tu and U. Stimming, Advances, Aging Mechanisms and Lifetime in Solid-Oxide Fuel Cells, *J. Power Sources*, 2004, **127**(1–2), p 284-293
8. M.C. Tucker, H. Kurokawa, C.P. Jacobson, L.C. De Jonghe, and S.J. Visco, A Fundamental Study of Chromium Deposition on Solid Oxide Fuel Cell Cathode Materials, *J. Power Sources*, 2006, **160**(1), p 130-138
9. J.A. Schuler, H. Yokokawa, C.F. Calderone, Q. Jeangros, Z. Wuillemin, A. Hessler-Wyser, and J. Van Herle, Combined Cr and S Poisoning in Solid Oxide Fuel Cell Cathodes, *J. Power Sources*, 2012, **201**, p 112-120
10. O. Thomann, M. Pihlatie, J.A. Schuler, O. Himanen, and J. Kiviaho, Method for Measuring Chromium Evaporation from SOFC Balance-of-Plant Components, *Electrochem. Solid-State Lett.*, 2012, **15**(3), p B35-B37
11. J.W. Fergus, Effect of Cathode and Electrolyte Transport Properties on Chromium Poisoning in Solid Oxide Fuel Cells, *Int. J. Hydrogen Energy*, 2007, **32**(16), p 3664-3671
12. N.H. Menzler, P. Batfalsky, L. Blum, M. Bram, S.M. Groß, V.A.C. Haanappel, J. Malzbender, V. Shemet, R.W. Steinbrech, and I. Vinke, Studies of Material Interaction After Long-Term Stack Operation, *Fuel Cells*, 2007, **7**(5), p 356-363
13. K. Hilpert, D. Das, M. Miller, D.H. Peck, and R. Weiß, Chromium Vapor Species Over Solid Oxide Fuel Cell Interconnect Materials and their Potential for Degradation Processes, *J. Electrochem. Soc.*, 1996, **143**(11), p 3642-3647
14. M. Stanislowski, J. Froitzheim, L. Niewolak, W.J. Quadakkers, K. Hilpert, T. Markus, and L. Singheiser, Reduction of Chromium Vaporization from SOFC Interconnectors by Highly Effective Coatings, *J. Power Sources*, 2007, **164**(2), p 578-589
15. Y. Larring and T. Norby, Spinel and Perovskite Functional Layers Between Plansee Metallic Interconnect (Cr-5 Wt% Fe-1 Wt% Y_2O_3) and Ceramic (La0.85Sr0.15)0.91MnO_3 Cathode Materials for Solid Oxide Fuel Cells, *J. Electrochem. Soc.*, 2000, **147**(9), p 3251-3256
16. X. Chen, P.Y. Hou, C.P. Jacobson, S.J. Visco, and L.C. De Jonghe, Protective Coating on Stainless Steel Interconnect for SOFCs: Oxidation Kinetics and Electrical Properties, *Solid State Ion.*, 2005, **176**(5–6), p 425-433
17. Z. Yang, G. Xia, G.D. Maupin, and J.W. Stevenson, Conductive Protection Layers on Oxidation Resistant Alloys for SOFC Interconnect Applications, *Surf. Coat. Technol.*, 2006, **201**(7), p 4476-4483
18. Y. Fang, C. Wu, X. Duan, S. Wang, and Y. Chen, High-Temperature Oxidation Process Analysis of $MnCo_2O_4$ Coating on Fe-21Cr Alloy, *Int. J. Hydrogen Energy*, 2011, **36**(9), p 5611-5616
19. A. Balland, P. Gannon, M. Deibert, S. Chevalier, G. Caboche, and S. Fontana, Investigation of La_2O_3 and/or (Co, $Mn)_3O_4$ Deposits on Crofer22APU for the SOFC Interconnect Application, *Surf. Coat. Technol.*, 2009, **203**(20–21), p 3291-3296
20. J. Puranen, J. Lagerbom, L. Hyvärinen, T. Mäntylä, E. Levänen, M. Kylmälahti, and P. Vuoristo, Formation and Structure of Plasma Sprayed Manganese-Cobalt Spinel Coatings on Preheated Metallic Interconnector Plates, *Surf. Coat. Technol.*, 2010, **205**(4), p 1029-1033
21. K. Uusi-Esko, E. Rautama, M. Laitinen, T. Sajavaara, and M. Karppinen, Control of Oxygen Nonstoichiometry and Magnetic Property of $MnCo_2O_4$ Thin Films Grown by Atomic Layer Deposition, *Chem. Mater.*, 2010, **22**(23), p 6297-6300
22. L. Mikkelsen, M. Chen, P.V. Hendriksen, Å. Persson, N. Pryds, and K. Rodrigo, Deposition of La0.8Sr0.2Cr0.97V0.03O_3 and $MnCr_2O_4$ Thin Films on Ferritic Alloy for Solid Oxide Fuel Cell Application, *Surf. Coat. Technol.*, 2007, **202**(4–7), p 1262-1266
23. M.J. Lewis and J.H. Zhu, A Process to Synthesize (Mn, $Co)_3O_4$ Spinel Coatings for Protecting SOFC Interconnect Alloys, *Electrochem. Solid-State Lett.*, 2011, **14**(1), p B9-B12
24. V.I. Gorokhovsky, P.E. Gannon, M.C. Deibert, R.J. Smith, A. Kayani, M. Kopczyk, D. Vanvorous, Z. Yang, J.W. Stevenson, S. Visco, C. Jacobson, H. Kurokawa, and S.W. Sofie, Deposition and Evaluation of Protective PVD Coatings on Ferritic Stainless Steel SOFC Interconnects, *J. Electrochem. Soc.*, 2006, **153**(10), p A1886-A1893
25. X. Montero, N. Jordán, J. Pirón-Abellán, F. Tietz, D. Stöver, M. Cassir, and I. Villarreal, Spinel and Perovskite Protection Layers between crofer22APU and La 0.8Sr0.2FeO_3 Cathode Materials for SOFC Interconnects, *J. Electrochem. Soc.*, 2009, **156**(1), p B188-B196
26. J. Puranen, J. Lagerbom, L. Hyvärinen, M. Kylmälahti, O. Himanen, M. Pihlatie, J. Kiviaho, and P. Vuoristo, The Structure and Properties of Plasma Sprayed Iron Oxide Doped Manganese Cobalt Oxide Spinel Coatings for SOFC Metallic Interconnectors, *J. Therm. Spray Technol.*, 2011, **20**(1–2), p 154-159
27. D.P. Lim, D.S. Lim, J.S. Oh, and I.W. Lyo, Influence of Post-Treatments on the Contact Resistance of Plasma-Sprayed La 0.8Sr 0.2MnO_3 Coating on SOFC Metallic Interconnector, *Surf. Coat. Technol.*, 2005, **200**(5–6), p 1248-1251
28. H. Zhai, W. Guan, Z. Li, C. Xu, and W.G. Wang, Research on Performance of LSM Coating on Interconnect Materials for SOFCs, *J. Korean Ceram. Soc.*, 2008, **45**(12), p 777-781
29. M.J. Garcia-Vargas, M. Zahid, F. Tietz, and A. Aslanides, Use of SOFC Metallic Interconnect Coated with Spinel Protective Layers Using the APS Technology, *ECS Trans.*, 2007, **7**, p 2399
30. M. Casteel, P. Willson, T. Goren, P. O'Brien, and D. Lewis, Novel Method for Measuring Chromia Evaporation from SOFC Interconnect Materials, *ECS Trans.*, 2009, **2**(5), p 1411
31. R.N. Basu, F. Tietz, O. Teller, E. Wessel, H.P. Buchkremer, and D. Stöver, LaNi0.6Fe0.4O_3 as a Cathode Contact Material for Solid Oxide Fuel Cells, *J. Solid State Electrochem.*, 2003, **7**(7), p 416-420
32. J. Lagerbom, T. Varis, J. Puranen, M. Pihlatie, O. Himanen, V. Saarinen, J. Kiviaho, and E. Turunen, $MnCo_2O_4$ Spinel Chromium Barrier Coatings for SOFC Interconnect by HVOF, *9th Liège Conference on Materials for Advanced Power Engineering,* 2010, p 925–932
33. J.R. Hoyes and S. Bond, Gaskets for Sealing Solid Oxide Fuel Cells, *Seal. Technol.*, 2007, **8**, p 11-14
34. L. Mikkelsen, K. Neufeld, and P.V. Hendriksen, Interface Resistance Between FeCr Interconnects and La0.85Sr0.15Mn1,1O_3, *ECS Trans.*, 2009, **25**, p 1429
35. J.A. Schuler, Z. Wuillemin, A. Hessler-Wyser, C. Comminges, N.Y. Steiner, and J. Van Herle, Cr-Poisoning in (La, Sr)(Co, Fe)O_3 Cathodes After 10,000 h SOFC Stack Testing, *J. Power Sources*, 2012, **211**, p 177-183

PUBLICATION VI

Post-experimental analysis of a SOFC stack using hybrid seals

Journal of Power Sources. Elsevier.
Vol. 274 (2015), 1009–1015.

Journal of Power Sources 274 (2015) 1009–1015

Contents lists available at ScienceDirect

Journal of Power Sources

journal homepage: www.elsevier.com/locate/jpowsour

Post-experimental analysis of a solid oxide fuel cell stack using hybrid seals

O. Thomann*, M. Rautanen, O. Himanen, J. Tallgren, J. Kiviaho

VTT Technical Research Centre of Finland, P.O. Box 1000, Biologinkuja 5, Espoo, FI-02044 VTT, Finland

HIGHLIGHTS

- Post-experimental analysis of a SOFC stack after 1800 h of operation.
- Microstructural analysis of the glass-coated hybrid seal.
- Materials interactions between glass-coated seals and Crofer 22 APU interconnects.
- Dual exposure of 0.2 mm thin Crofer 22 APU plates in stack operating conditions.

ARTICLE INFO

Article history:
Received 28 July 2014
Received in revised form
8 October 2014
Accepted 16 October 2014
Available online 23 October 2014

Keywords:
SOFC
Seal
Thermiculite 866
Dual exposure
Interconnect
Post-experimental analysis

ABSTRACT

A post-experimental analysis of a SOFC stack is presented. The stack was operated for 1800 h at 700 °C with air and hydrogen and contained hybrid glass-Thermiculite 866 seals. The goal of this work was to investigate the sealing microstructure and possible corrosion during mid-term operation. It was found that hybrid seals could effectively compensate for manufacturing tolerances of cells and other components due to the compliance of the glass layer. Additionally, different interfaces were investigated for corrosion. Corrosion was not observed at two-phase interfaces such as Crofer 22 APU/glass, glass/electrolyte and glass/Thermiculite 866. The three-phase interface between Crofer 22 APU/glass/hydrogen exhibited no corrosion. Some evidence of non-systematic corrosion was found at the Crofer 22 APU/glass/air interface. The possible reasons for the corrosion are discussed. Lastly, dual exposure to humid hydrogen and air of the 0.2 mm Crofer 22 APU interconnect had no detrimental effect on the corrosion compared to air exposure. Overall the hybrid seals used in combination with the thin interconnects were found to be a promising solution due to the low leak rate and limited material interactions.

1. Introduction

Currently, key challenges for successful commercialization of SOFC are to extend their lifetime and to reduce their cost. To achieve that, effective sealing solutions that address all the seals requirements are paramount [1,2]. Seals need to withstand simultaneous exposure to the air side and to the fuel side at temperature between 650 and 850 °C. In addition, they should withstand hundreds to thousands of thermal cycles for stationary and mobile applications respectively. Additionally, seal materials should be chemically compatible with the adjacent components like metallic interconnects and cell materials. Their electrical resistivity should also be high and stable. Lastly, the seals should also be inexpensive, easy to assemble and have to compensate for manufacturing tolerances of the other stack components. Presently, glass ceramic seals are widely used in SOFC stacks. Because they are rigidly bonded to the adjacent surfaces, their coefficient of thermal expansion needs to match closely the one of the neighbouring components. They exhibit very low leak rates [3] but can be prone to degradation with thermal cycling [4]. Compressible seals composed of mica-type paper have been investigated as an alternative [5–7]. The drawback of compressive seals is that in order to achieve acceptable leak rate, a compression stress of the order of several MPa has to be applied on the stack [5]. However, it was found that the leak rate remains significantly higher compared to glass ceramic seals and that the needed level of compression and the necessary compression system becomes technically challenging for large footprint stack. These inherent issues can be addressed by adding compliant layers of glass or metal on both sides of a compressible seal [3,8,9]. The compliant layers block the main leak

* Corresponding author. Tel.: +358 401247497.
E-mail address: olivier.thomann@vtt.fi (O. Thomann).

http://dx.doi.org/10.1016/j.jpowsour.2014.10.100
0378-7753/

path between the seal and the interconnects which leads to a leakage reduction of up to 90% [9]. Additionally, Rautanen et al. showed that a compression stress as low as 0.1 MPa can be used with hybrid seals [9].

Sealing material interaction studies have been previously published but most of the articles have been focusing on glass ceramic seals interaction. Batfalsky et al. performed post-experimental investigation on stacks that had undergone rapid performance degradation [10]. They found that the interconnects had so severely corroded in the vicinity of the glass ceramic seals that the corrosion product had formed electrical bridges between adjacent interconnects and caused short-circuiting after 200 h at 800 °C. They attributed the accelerated corrosion to the presence of PbO in the glass. Menzler et al. presented results of post-experimental investigation of a stack operated for 6400 h at 800 °C [11]. They showed that the corrosion of the interconnects was enhanced in the vicinity of the glass ceramic seals but that the extent of corrosion did not compromise the performance of the stack. Wiener et al. studied interactions between Thermiculite 866 materials (a composite of vermiculite and steatite [12]) and Crofer 22 APU at 800 °C in ex situ experiments [13]. They found that the Crofer 22 APU underwent accelerated corrosion and this was attributed to the decomposition of steatite at 800 °C and transport of Mg to the oxide layer. Bram et al. studied interaction of Thermiculite 866 with Crofer 22 APU in Ref. [14]. They found that the break-away corrosion of Crofer 22 APU took place at temperature as low as 600 °C in ex situ test. They attributed the accelerated corrosion due to the steam emitted by the Thermiculite 866 during heat-up. They found that such a corrosion reaction could be prevented by a pre-oxidation treatment of the interconnects. Interestingly, corrosion was most often found at the three-phase boundary between seal material, interconnect and gas (air or fuel) [10,11,13,14]. Only few material interactions studies have been published on hybrid seals. Chou et al. studied long-term interaction of hybrid seal materials in ex situ experiments [15]. They found that the phlogopite paper was reacting with the glass they used after 500 h at 800 °C, which compromised the performance of the seal during thermal cycling. Interactions between seal materials and ferritic stainless steel were not discussed in that paper. Chou et al. published the results of a post-experimental analysis of a 3-cell stack using hybrid seals operated at 800 °C [16]. They concluded that material interaction was limited and that their material selection for the seal and interconnect material was suitable for long-term operation. However, the three-phase interfaces between seal/interconnect/gases were not discussed.

Dual atmosphere exposure of interconnects has also drawn some attention in the literature. Skilbred et al. and Yang et al. studied the effect of dual atmosphere exposure at 800 and 850 °C on the corrosion of Fe–Cr–Mn steels and they showed that dual exposure affects the oxide scale composition with a higher concentration of Fe in the oxide scale on the air side. Exposure time was limited to 500 h and 300 h [17–19]. Holcomb et al. studied dual exposure of the austenitic steel 316L and found that heavy corrosion was taking place after 100 h at 700 °C. It was caused by the diffusion of oxygen and hydrogen in the alloy and the formation of steam in the metal alloy near the oxide layer, which formed a thick and porous oxide layer [20].

The amount of data available on dual exposure of interconnect steels is presently limited, which is partly explained by the fact that dual exposure tests are more complex than single atmosphere exposure tests. Additionally, the durations of the experiments are typically in the few hundred hours range. The hydrogen atmosphere is often lean with 5% hydrogen in argon for safety reason and the humidity restricted to 3%, whereas these values are typically higher inside a stack.

The thickness of the interconnects is also affecting their lifetime by decreasing the initial reservoir of Cr. Stainless steel alloys are protected from excessive corrosion by the formation of a Cr oxide layer. During operation, the Cr from the protective scale evaporates and is replaced by Cr diffusing from the bulk of the alloy. The Cr is consumed until it reaches a concentration of about 16% in the alloy, when break-away oxidation start to occur [21]. On the one hand, it is interesting to reduce interconnect thickness to reduce the cost associated with the interconnect steel, but on the other hand Asensio-Jimenez et al. showed that the corrosion rate of interconnect steel increases for thinner plate thickness [22]. Therefore data on the corrosion of thin interconnect are valuable.

This present paper contributes to the field with the results of the post-experimental analysis of a SOFC stack using hybrid seal consisting of a Thermiculite 866 compressible core with compliant glass layers. The seal cross-section has been extracted from a single-cell stack that was operated for 1800 h at 700 °C. The in situ nature of the experiment provides exposure conditions to the seals and interconnects that are closer to stack operation compared to ex situ experiments. For example, the steam content in this work was 20% at anode outlet, which is higher compared to ex situ seals (usually maximum 3%). However, even higher steam content is expected in a stack in an actual system environment (from 60 to 80% steam content).

The goals of the post-experimental analysis were: i) to investigate the microstructure of the hybrid seals, ii) to evaluate material interactions between the seal materials and the interconnects and iii) to investigate the effect of dual exposure on thin 0.2 mm interconnects. The stack presented here is a stack prototype developed at VTT Technical Research Centre of Finland in which hybrid seals were used. After this work, the hybrid seal design has been significantly improved by a 10-fold reduction of the amount of glass and the cost associated to it [9].

2. Experimental

The single cell stack used a co-flow configuration. Crofer 22 APU (ThyssenKrupp, Germany) was used for interconnects and end-plates. The interconnects were 0.2 mm in thickness. The anode-supported cell was manufactured by Elcogen AS (Estonia) and is 10×10 cm^2. Hybrid seals were used for all seals located between Crofer 22 APU plates and are made with consolidated Thermiculite 866 (Flexitallic LTd, the United-Kingdom) [12] between two glass tapes of 220 μm green thickness. The glass used belongs to the system MO (M = Mg, Ca)–Al_2O_3–BaO– SiO_2–B_2O_3 (GM31107, Schott, Germany [23]). The Thermiculite 866 is composed in nearly equal amount of vermiculite and steatite, which compositions are $[(K, Mg, Fe)_3(Si,Al)_4O_{10}(OH)_2]$ and $[(Mg_3Si_4(OH)_2]$ respectively. The seal between the cell electrolyte (yttria-stabilized zirconia (YSZ)) and Crofer 22 APU plate was made of glass without Thermiculite 866. 40 kg of weight was added on the stack, which corresponds to a compressive stress of ca. 0.1 MPa assuming that all the weight was carried by the seals and not by the cell.

Dry hydrogen and dry air were used as fuel and oxidant. Pure hydrogen was selected as fuel, which exposes the seals to a worst case condition as it has been shown that the leak rate through hybrid seal increases with the concentration of hydrogen [9]. The stack was operated at 700 °C for 1800 h. Average current density was 0.2 Acm^{-2} and fuel utilisation and air utilisation were 18%. The hydrogen cross leak value corresponded to a loss of 0.9% of the inlet hydrogen flow in these operating conditions, which is low. The cross leak value was calculated according to the method described in Ref. [9].

After the test, the stack was mounted in epoxy and a cross-section was extracted from the area close to the gas outlet for

SEM and EDS analysis. This area was selected because the exposure conditions are expected to be the most challenging due to the increased steam content.

Post-experimental analysis was carried out using SEM observation and energy-dispersive x-ray spectroscopy (EDS) on JSM-6400 Scanning Microscope from JEOL equipped with a Prism 2000 detector and Spirit 1.06.02 Analyzer software from Princeton Gamma-Tech (PGT). The oxide layer thickness was determined by measuring the area on the image corresponding to the oxide phase with ImageJ [24] and dividing it by the picture width according to the method described in Ref. [25].

3. Results and discussion

3.1. Glass compliance

A cross-section of two hybrid seals is illustrated in Fig. 1. It can be seen that the Thermiculite 866 material is significantly deformed by the die-cutting process forming protruding cutting burrs near the edges. Despite the unevenness of the Thermiculite 866, the glass has well accommodated the gap varying between 15 and 150 μm for the upper seal shown in Fig. 1. Pore formation took place only at the location were the Thermiculite 866 is at its thinnest, however these pores are closed and don't form a continuous leak path. Additionally, some excess glass was extruded out of the seal because of the compliance of the glass. This means that the glass tape thickness could be thinner or other methods to apply thinner glass coating could be used. Moreover, the clearances between the Crofer 22 APU plates are 710 and 580 μm at the location of measurement for the two seals shown and this difference in clearance didn't seem to have decreased the quality of the seals at these locations. This demonstrates the benefit of using hybrid seals over purely compressible seals. In short, similar hybrid seals were able to effectively seal gaps between 580 and 710 μm and the glass layer was able to compensate 140 μm thickness variation of the Thermiculite 866. Compressible seals would have required much larger compression stress to flatten the cutting burrs. Additionally, the gap clearance variation would have likely been an issue due to the limited compressibility of Thermiculite 866 [5]. There are many reasons that can lead to a variation of gap clearance in a stack, i.e. differences in cell and interconnect plate thickness, and variation of thickness of the compressible Thermiculite 866. These variations can be decreased to a certain level by more uniform manufacturing methods but cannot be totally avoided. Moreover, generally decreasing the manufacturing tolerance comes with a cost increase. It is therefore of high interest that the seals can accommodate the geometric variation in a stack.

3.2. Materials interactions between seal materials and interconnects

This section presents results of different material interactions, such as Crofer/glass, glass/Thermiculite 866 and glass/electrolyte interfaces. In addition, interactions at the three-phase interfaces such as Crofer/glass/air and Crofer/glass/hydrogen are detailed.

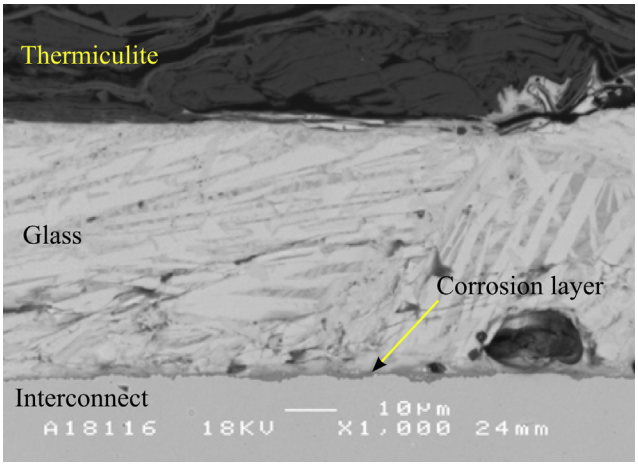

Fig. 2. SEM BSE cross-section of Crofer/glass and glass/Thermiculite 866 interfaces.

3.2.1. Crofer/glass and glass/Thermiculite 866 interfaces

The Crofer/glass and glass/Thermiculite 866 interfaces are illustrated in Fig. 2. This picture has been taken from the middle section of the seal, which means that its exposure to gas is limited to possible leakage through the seal. It appears that the materials have good chemical compatibility and only limited corrosion can be seen between glass and Crofer 22 APU with an oxide layer of less than 1 μm. As a comparison, the oxide layer thickness is thinner in contact with the glass compared to the case when the Crofer 22 APU is exposed to air at the same temperature (see results in Section 3.3). Therefore, it was concluded that the presence of glass did not accelerate the oxidation of the Crofer 22 APU plate at this interface.

3.2.2. Crofer/glass/air interface

Cross-section pictures from the Crofer/glass/air interface are illustrated in Fig. 3 and Fig. 4. The cross-section sample is taken near the air exhaust. The humidity in air downstream of the stack was measured to be ca. 0.4% during stack operation. The cracks present in the glass are due to sample preparation.

The location shown in Fig. 3(a) and (b) corresponds to the upper and lower corners of the seal which is exposed to the same cathode atmosphere, and they are therefore exposed to the same air atmosphere. However, their corrosion behaviour differed significantly. The upper side shows no sign of significant corrosion while the lower side has developed a 20 μm corrosion layer just at the location where the glass layer ends. The corrosion layer does not extend more than 200 μm from the three-phase interface. As it can be seen from the EDS analysis in Fig. 3(d), the oxide layer consists of a first layer of mixed oxide of Cr and

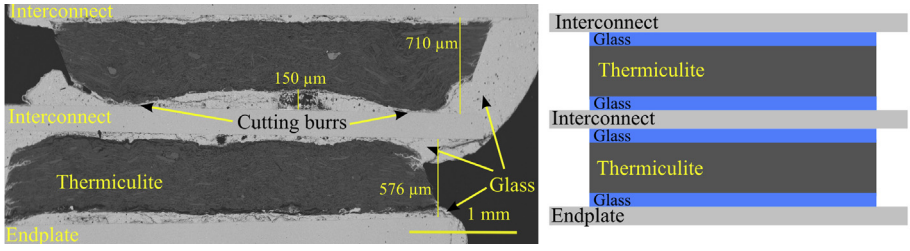

Fig. 1. SEM BSE cross-section of two frame seals. The seals are composed of a Thermiculite 866 core between two glass layers.

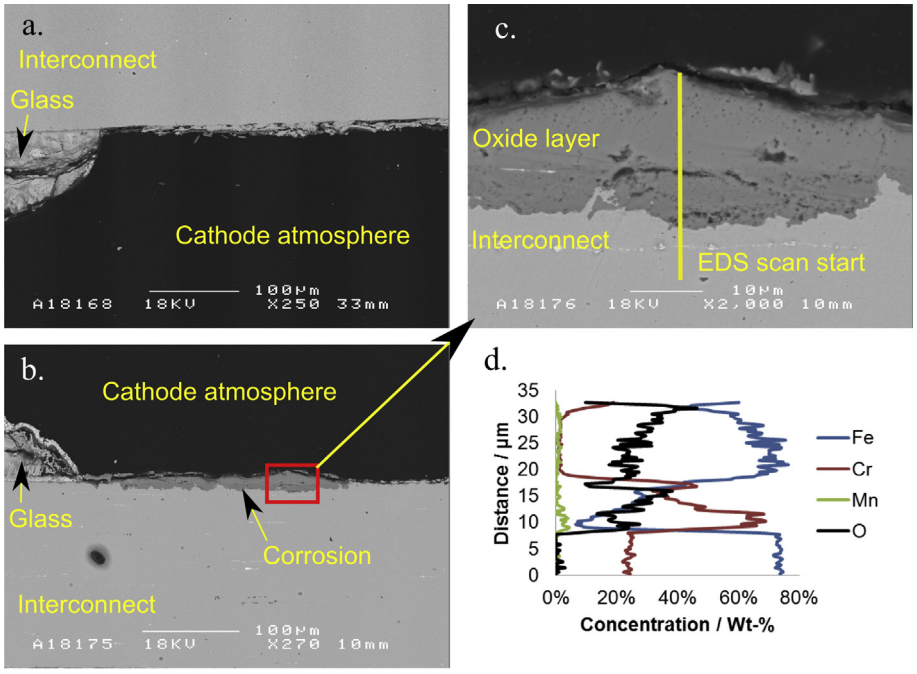

Fig. 3. SEM BSE cross-sections of two Crofer/glass/air interfaces (a and b) that are both exposed to cathode atmosphere. Magnified view of cross-section (c).

Mn and the top layer is mainly composed of Fe oxide. This is a clear example of break-away oxidation, i.e. when the Cr oxide layer cannot anymore protect the stainless steel because of too fast corrosion. It is however surprising that such extent of corrosion takes place only at one corner of the seal (Fig. 3(b)) and not at the other (Fig. 3(a)), despite the exposure condition being identical.

Similarly, pictures shown in Fig. 4(a and b) correspond to two different seals but exposed to the same atmosphere; the air exhaust manifold. Also in this case, no significant corrosion takes place at one side (Fig. 4(a)) and break-away oxidation took place at the other side (Fig. 4(b)), where the oxide layer is 20 µm thick. Accelerated corrosion was found to extend millimetres away from the seals into the air manifold towards the stack air outlet. The oxide layer was thicker 5 mm away from the seal, where it was about 120 µm thick and its top layer was composed mainly of Fe oxide (picture not shown). However, corrosion in the manifold of the thick end plate is not critical for the stack performance.

Different reasons can have caused the Crofer 22 APU to undergo break-away oxidation at some locations. Cr evaporation from the oxide layer is enhanced by the presence of water vapour in air [26,27] and if the evaporation rate of Cr is higher than the rate at which the Cr oxide layer is formed, the stainless steel undergoes break-away oxidation. It is possible that the steam content was locally higher where the break-away oxidation took place. Steam content can be locally higher in case there is a local leak of hydrogen. However this does not appear to be the case here because the seals shown in Figs. 3 and 4 are exposed to air on both sides. The heavy corrosion found deep in the air manifold could be attributed to the presence of contamination from lubricant used during machining of the manifolds. The endplates were heat-treated after machining (800 °C for 12 h) during which possible lubricant was burned, then the plates were polished and then cleaned in laboratory glassware washer and by wiping with ethanol impregnated tissues before use but it is difficult to remove lubricant or burned lubricant residues from the narrow manifolds. This hypothesis is supported by the fact that the heaviest corrosion was found deep in the manifold, several millimetres away from the seal. Lastly, it cannot be excluded that the corrosion could be caused by element evaporating from the glass or Thermiculite 866. Both are made of complex elemental formulations and have potentially many candidates for evaporation and subsequent interactions.

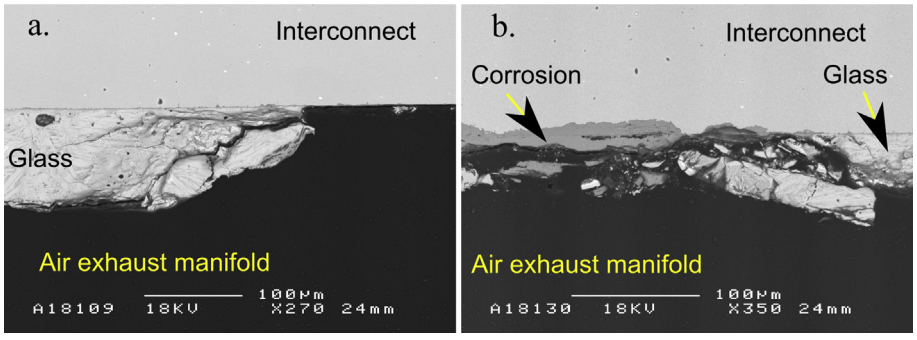

Fig. 4. SEM BSE cross-sections of two Crofer/glass/air interfaces (a and b) that are both exposed to the atmosphere of the air exhaust manifold.

However, if the corrosion mechanism would be from material interaction, one would expect it to happen systematically, which is not the case here.

Bram et al. found similar corrosion behaviour of Crofer 22 APU in their paper on material interactions between Thermiculite 866 and Crofer 22 APU [14]. In their work, they exposed Thermiculite 866 (without any glass) to air and dual atmosphere at 600 °C for 400 h and found that break-away oxidation was taking place at the air side. They attributed the corrosion behaviour of the Crofer 22 APU to the enhanced water concentration near the seal that was originating from vermiculite dehydration and steatite decomposition. This phenomenon was previously described and quantified by Wiener et al. [13]. According to Bram et al., the break-away oxidation behaviour can be suppressed by pre-oxidation of the interconnect plates.

The reason for the accelerated corrosion at the air side remains unclear and is the subject of further research. The main risk associated with the accelerated corrosion found near the seals is the formation of porous Fe oxide all the way through the 0.2 mm thin interconnects and creation of a leak path through the interconnect. Secondarily, in extreme case, accelerated corrosion can form a lump of electrically conductive Fe oxide and creates short-circuiting by connecting adjacent interconnect plates [10]. However, it appears that the corrosion is limited after 1800 h and didn't spread far towards the cathode, therefore it is unlikely that the growth of the oxide layer would affect the area-specific resistance of the interconnect. The most corroded locations were found in the air exhaust manifold on the 2 cm-thick end plate where accelerated corrosion has no consequence for the stack performance. Lastly, it is interesting to notice that corrosion took place near the three-phase boundary and not at the glass/metal (two-phase) interface, which is coherent with findings of several previous studies [10,11,13,14]. As mentioned, dry air was used during the test. In order to subject the materials on the cathode side to a more challenging atmosphere, pre-humidified air (e.g. 1 … 3%) could be used to see the effect of humid air on material corrosion.

3.2.3. Crofer/glass/humid hydrogen interface

A micrograph from the Crofer/glass/humid hydrogen interface is shown in Fig. 5. No significant material interaction could be seen at the interface between seal and humid hydrogen. The humidity of the fuel is also at its highest at this location, about 20%, due to water production from reaction at anode. The cracks in the glass are due to sample preparation.

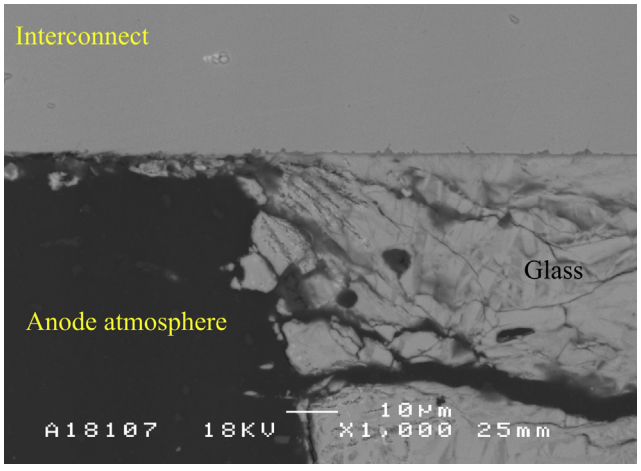

Fig. 5. SEM BSE cross-section at the Crofer/glass/humid hydrogen interface. The visible glass is part of the cell seal which is composed of glass without any Thermiculite 866.

3.2.4. Glass/electrolyte interface

The glass/electrolyte interface is illustrated in Fig. 6. The glass contains little porosity and exhibits a good adherence to the YSZ of the electrolyte. There is no evidence of corrosion between the electrolyte and the glass.

3.3. Corrosion of interconnects exposed to dual atmosphere

The post-experimental analysis of this stack also offers valuable insight into the corrosion of thin interconnects in dual atmosphere compared to exposure to single air atmosphere.

Fig. 7(a and b) show cross-sections from the interconnect plate exposed simultaneously to air and humid hydrogen. The location is near the fuel exhaust and the absolute humidity in the fuel atmosphere was about 20%. Fig. 7(c and d) show cross-sections from an interconnect exposed to air atmosphere on both side. On Fig. 7(a), a crack from sample preparation is present in the oxide layer, splitting it into two layers.

For the single air exposure case shown in Fig. 7(c and d), the oxide layers were 1.4 µm and 1.9 µm in thickness. In case of dual exposure, the oxide layers were found to be of 1.3 µm and 1.2 µm in thickness (Fig. 7(a and b)). The EDS scans suggest that the oxide layer formed in dual exposure is rich in Cr and Mn oxide at both sides. The morphology of the oxide layer depends on the conditions of exposure with a tendency for the oxide layer formed in air to be smoother than the one formed in fuel atmosphere. It was previously shown in the literature that the spinel crystals growing on the surface of ferritic Fe–Cr–Mn steel were dependant on the atmosphere composition [28]. Some limited inwards growth of surface oxide can be seen in Fig. 7(a, b and c) but limited to a depth of 5 µm from the metal surface. It is difficult to find comparable oxide layer thickness data from the literature due to the numerous conditions to be taken into account (temperature, time and atmosphere composition). Linder et al. found that Crofer 22 APU oxide layer thickness was about 5 µm for similar exposure time at 850 °C in air [25]. Sachitanand et al. found that Crofer 22 APU oxide layer thickness was about 12–16 µm at 850 °C in humidified air after 1000 h [29].

The results presented in Fig. 7 lead to three main findings. Firstly, the oxide layers are thin for interconnect without protective coating, showing that the selected interconnect alloy exhibits suitable corrosion-resistance at an operating temperature of 700 °C. Additionally, dual exposure had no detrimental effect on the corrosion rate of the interconnect and the oxide layers were actually thinner in the dual exposure case compared to exposure to air only. Lastly, the interconnect thickness used for this stack (0.2 mm) is relatively thin and therefore the reservoir of Cr in the bulk steel is limited. However, it appears that the low thickness of the interconnects had no significant detrimental effect on their corrosion rate.

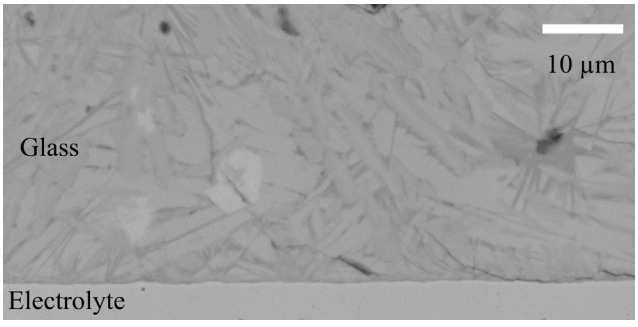

Fig. 6. SEM BSE cross-section at the interface between glass and electrolyte.

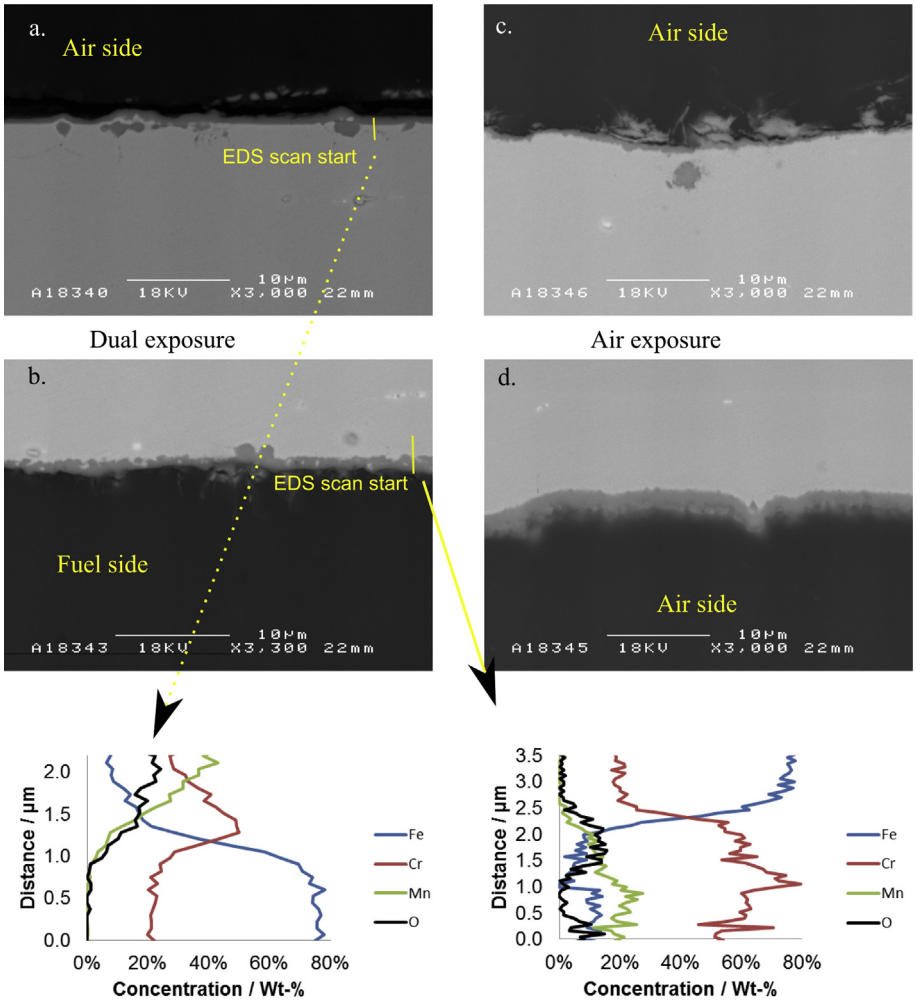

Fig. 7. SEM BSE cross-sections of a 0.2 mm thin interconnect plate exposed simultaneously to air and humid hydrogen (a and b) with two EDS scan. Another interconnect exposed to air on both side (c and d).

4. Conclusions

In this article, post-experimental analysis results of a single-cell stack containing hybrid seals are detailed. The hybrid seal solution was found to work well because it could successfully compensate for thickness variation of stack element of about 150 µm. In addition, the compliant glass layer could well accommodate the unevenness of the Thermiculite 866 caused by the die-cutting process. The hydrogen cross leak value corresponded to a loss of 0.9% of the inlet hydrogen flow, which is very low. Different interfaces and locations inside the stack were investigated for corrosion. Corrosion didn't take place at two-phase interfaces such as Crofer/glass, glass/electrolyte and glass/Thermiculite 866. The three-phase interface between Crofer/glass/hydrogen exhibited no corrosion, whereas some of the locations corresponding to the Crofer/glass/air interface exhibited some non-systematic corrosion. The possible reasons for the corrosion found were discussed and the most likely reason for corrosion is contamination from lubricant that was not properly removed before stack assembly. These results will be the basis of a future study on the corrosion of Crofer 22 APU in contact with sealing materials ex situ, which will aim at improving our understanding of this phenomenon. Lastly, dual exposure of thin Crofer 22 APU interconnect did not cause enhanced corrosion compared to air exposure and the oxide layer thickness was found to be limited below 2 µm. Overall the hybrid seals used in combination with the thin interconnects were found to be a promising solution due to low leak rate and its suitability for long-term operation will be examined further in stack operated for longer period of time.

Acknowledgements

Finnish Funding Agency for Technology and Innovation (TEKES) is acknowledged for financial support. Seija Kivi from VTT is acknowledged for sample preparation, Kai Nurminen, Kari Koskela from VTT and Jorma Stick from SataHitsaus are acknowledged for the experimental part of the work. Risto Parikka from VTT Expert Services Oy is acknowledged for SEM analysis.

References

[1] J.W. Fergus, J. Power Sources 147 (2005) 46–57.
[2] K. Weil, JOM 58 (2006) 37–44.
[3] Y.-S. Chou, J.W. Stevenson, L.A. Chick, J. Power Sources 112 (2002) 130–136.
[4] R.N. Singh, Int. J. Appl. Ceram. Technol. 4 (2007) 134–144.
[5] M. Rautanen, O. Himanen, V. Saarinen, J. Kiviaho, Fuel Cells 9 (2009) 753–759.

[6] Z. Wuillemin, N. Autissier, M. Nakajo, M. Luong, J. Van Herle, D. Favrat, J. Fuel Cell Sci. Technol. 5 (2008).
[7] S.P. Simner, J.W. Stevenson, J. Power Sources 102 (2001) 310–316.
[8] Y.-S. Chou, J.W. Stevenson, L.A. Chick, J. Am. Ceram. Soc. 86 (2003) 1003–1007.
[9] M. Rautanen, O. Thomann, O. Himanen, J. Tallgren, J. Kiviaho, J. Power Sources 247 (2014) 243–248.
[10] P. Batfalsky, V.A.C. Haanappel, J. Malzbender, N.H. Menzler, V. Shemet, I.C. Vinke, R.W. Steinbrech, J. Power Sources 155 (2006) 128–137.
[11] N.H. Menzler, P. Batfalsky, L. Blum, M. Bram, S.M. Groß, V.A.C. Haanappel, J. Malzbender, V. Shemet, R.W. Steinbrech, I. Vinke, Fuel Cells 7 (2007) 356–363.
[12] J.R. Hoyes, S. Bond, Sealing Technol. (2007) 11–14.
[13] F. Wiener, M. Bram, H. Buchkremer, D. Sebold, J. Mater. Sci. 42 (2007) 2643–2651.
[14] M. Bram, L. Niewolak, N. Shah, D. Sebold, H.P. Buchkremer, J. Power Sources 196 (2011) 5889–5896.
[15] Y.-S. Chou, J.W. Stevenson, J. Hardy, P. Singh, J. Power Sources 157 (2006) 260–270.
[16] Y.-S. Chou, J.W. Stevenson, J.-P. Choi, J. Power Sources 250 (2014) 166–173.
[17] Z. Yang, G. Xia, M.S. Walker, C. Wang, J.W. Stevenson, P. Singh, Int. J. Hydrogen Energy 32 (2007) 3770–3777.
[18] B. Skilbred, A. Werner, H. Reidar, Int. J. Hydrogen Energy 37 (2012) 8095–8101.
[19] Z. Yang, M.S. Walker, P. Singh, J.W. Stevenson, T. Norby, J. Electrochem.Soc. 151 (2004).
[20] G.R. Holcomb, M. Ziomek-Horoz, S.D. Cramer, B.S. Covino Jr., S.J. Bullard, J. Mater. Eng. Perform. 15 (2006) 404–409.
[21] P. Huczkowski, V. Shemet, J. Piron-Abellan, L. Singheiser, W.J. Quadakkers, N. Christiansen, Mater. Corros. 55 (2004) 825–830.
[22] C. Asensio-Jimenez, L. Niewolak, H. Hattendorf, B. Kuhn, P. Huczkowski, L. Singheiser, W.J. Quadakkers, Oxid. Met. 79 (2013) 15–28.
[23] D. Goedeke, J. Besinger, Y. Pfluegler, B. Ruedinger, ECS Trans. 25 (2009) 1483.
[24] M.D. Abràmoff, P.J. Magalhães, S.J. Ram, Biophoton. Int. 11 (2004) 36–42.
[25] M. Linder, T. Hocker, L. Holzer, K.A. Friedrich, B. Iwanschitz, A. Mai, J.A. Schuler, J. Power Sources 243 (2013) 508–518.
[26] C. Gindorf, L. Singheiser, K. Hilpert, J. Phys. Chem. Solids 66 (2005) 384–387.
[27] O. Thomann, M. Pihlatie, J.A. Schuler, O. Himanen, J. Kiviaho, Electrochem. Solid State Lett. 15 (2012) B35–B37.
[28] Z. Yang, J.S. Hardy, M.S. Walker, G. Xia, S.P. Simner, J.W. Stevenson, J.Electrochem.Soc. 151 (2004) A1825–A1831.
[29] R. Sachitanand, M. Sattari, J. Svensson, J. Froitzheim, Int. J. Hydrogen Energy 38 (2013) 15328–15334.

Series title and number

VTT Science 97

Title	**Improving sealing, electrical contacts, and corrosion resistance in solid oxide fuel cell stacks**
Author(s)	Markus Rautanen
Abstract	In solid oxide fuel cell systems, the stack is the primary component whose performance and lifetime should be maximized while decreasing the cost. In this thesis, leakages, electrical contact resistance, and corrosion resistance in SOFC stacks were studied and developed. Typically, SOFC stacks are assembled at room temperature, then heated up and conditioned, and then operated at temperatures in the range of 600...900 °C. Therefore, the mechanical properties of seals should be understood from room temperature to operating temperature. Of special interest are the mechanical properties of materials during the first heat up, in which the stack is sealed, reduced, and tested. Mechanical properties of glass and compressible sealing materials were studied with different heat-up procedures. It was noticed that with compressible Thermiculite 866 or CL87 materials, the compressibility is diminished after the first heat up, and therefore it is beneficial to apply compression before heating, to obtain maximum deformation capability of the seal. The progress in manufacturing SOFC cells is leading to an increase in cell area. From the perspective of compressible seals, the increase in cell area presents a challenge: the higher the cell area, the higher the required compressive force for the stack. For this purpose, a hybrid sealing material capable of maintaining leak rates below 1% of the inlet fuel flow below 1 MPa of compressive stress was developed. The material consists of a compressible core of Thermiculite 866, a commercial material consisting of vermiculite and steatite, and a conformable glass-based interlayer. The interlayers seal the mating surfaces, thus diminishing the leakages through the interfaces. Using the coating technique, leak rates were diminished by 60...90% compared to the uncoated seals. Post-mortem analyses of a stack also showed no signs of corrosion caused by the glass-coating. A high operating temperature and exposure to both reducing and oxidizing atmospheres is prone to cause corrosion of materials. One example of these corrosion-related deactivation mechanisms is chromium evaporation from interconnect steel materials. The evaporated chromium is transported in the gas phase to the electrochemically active cell, where it can solidify to chromium oxide, causing loss of performance. These phenomena can be mitigated with chromium barrier coatings on interconnect steels. A MnCo1.8Fe0.2O4 coating deposited by a high-velocity oxygen flame (HVOF) method was prepared and tested both with ex-situ and stack tests. The prepared coating showed good stability and low area-specific resistivity, and was found to hinder chromium transport to the electrochemical cell.
ISBN, ISSN	ISBN 978-951-38-8313-3 (Soft back ed.) ISBN 978-951-38-8314-0 (URL: http://www.vtt.fi/publications/index.jsp) ISSN-L 2242-119X ISSN 2242-119X (Print) ISSN 2242-1203 (Online)
Date	June 2015
Language	English, Finnish abstract
Pages	68 p. + app. 59 p.
Name of the project	
Commissioned by	
Keywords	SOFC, stack, seal, leak, corrosion, contact, chromium
Publisher	VTT Technical Research Centre of Finland Ltd P.O. Box 1000, FI-02044 VTT, Finland, Tel. 020 722 111

Julkaisun sarja ja numero

VTT Science 97

Nimeke	**Kiinteäoksidipolttokennostojen tiivisteiden, sähköisten kontaktien ja korroosiosuojauksen kehittäminen**
Tekijä(t)	Markus Rautanen
Tiivistelmä	Kiinteäoksidipolttokennojärjestelmän tärkein komponentti on kennosto, jonka suorituskyky ja elinikä pyritään maksimoimaan samalla kun kustannukset pyritään minimoimaan. Tässä väitöskirjassa tutkittiin ja kehitettiin kiinteäoksidipolttokennoston tiivisteitä sekä keskityttiin parantamaan kennoston sisäistä sähköistä kontaktia ja korroosiokestävyyttä. Kiinteäoksidipolttokennostojen kokoonpano tapahtuu huoneenlämpötilassa, minkä jälkeen ne lämmitetään ja esikäsitellään tyypillisesti 600...900 °C lämpötila-alueella. Tämän vuoksi tiivistemateriaalien mekaaniset ominaisuudet tulee tuntea koko lämpötila-alueella huoneenlämpötilasta käyttölämpötilaan saakka. Erityisen tarkastelun kohteena ovat mekaaniset ominaisuudet ensimmäisessä lämmityksessä, jonka aikana kennosto tiivistetään, pelkistetään ja testataan. Erilaisten puristus- ja lämmitystapojen vaikutusta tiivisteiden mekaanisiin ominaisuuksiin tutkittiin kokeellisesti. Testattujen kokoonpuristuvien tiivisteiden (Thermiculite 866 & CL87) kokoonpuristuvuuden havaittiin vähentyvän lämmityksen jälkeen. Näin ollen kennoston kannalta optimaalista on suorittaa kennoston ensimmäinen puristus huoneenlämpötilassa. SOFC-kennojen pinta-alan kasvu tuottaa haasteita kokoonpuristuville tiivisteille, koska pinta-alan kasvaessa kennoston puristamiseksi tarvitaan suurempi voima. Työssä kehitettiin hybriditiiviste, jolla voidaan saavuttaa alle 1% vuototaso suhteessa polttoainevirtaukseen pienilläkin, alle 1 MPa, puristuspaineilla. Kehitetty tiivisteratkaisu koostuu kokoonpuristuvasta Thermiculite 866 substraatista, joka pinnoitettiin lasia sisältävällä seoksella. Pinnoitetun tiivisteen vuototasojen mitattiin olevan 60...90% pienemmät suhteessa pinnoittamattomaan tiivisteeseen. Pinnoitteen ja virtauskanavalevyjen tai kennojen välillä ei myöskään havaittu tiivisteistä johtuvaa korroosiota. Kiinteäoksidipolttokennojen korkea käyttölämpötila ja kaksoiskaasukehä aiheuttavat helposti materiaalien välistä korroosiota. Ehkä merkittävin korroosioilmiö on kromin höyrystyminen virtauskanavalevyjen teräksistä ja kulkeutuminen sähkökemiallisesti aktiivisiin kennoihin, joihin kiteytyessään se vähentää suorituskykyä. Tämän ilmiön pienentämiseksi työssä valmistettiin $MnCo_{1.8}Fe_{0.2}O_4$-pinnoitettuja virtauskanavalevyjä ja testattiin niitä sekä ex-situ-kokeilla että kennostossa. Pinnoitteen havaittiin ehkäisevän kromin höyrystymistä ja siten parantavan kennoston elinikää.
ISBN, ISSN	ISBN 978-951-38-8313-3 (nid.) ISBN 978-951-38-8314-0 (URL: http://www.vtt.fi/publications/index.jsp) ISSN-L 2242-119X ISSN 2242-119X (Painettu) ISSN 2242-1203 (Verkkojulkaisu)
Julkaisuaika	Kesäkuu 2015
Kieli	Englanti, suomenkielinen tiivistelmä
Sivumäärä	68 s. + liitt. 59 s.
Projektin nimi	
Rahoittajat	
Avainsanat	SOFC, stack, seal, leak, corrosion, contact, chromium
Julkaisija	Teknologian tutkimuskeskus VTT Oy PL 1000, 02044 VTT, puh. 020 722 111

Improving sealing, electrical contacts, and corrosion resistance in solid oxide fuel cell stacks

Solid oxide fuel cells are high temperature electrochemical devices for direct conversion of fuel and oxidant to electricity and heat. The high temperature and dual atmosphere creates challenges for the materials in solid oxide fuel cell stacks. In this thesis SOFC stack materials were studied and developed.

SOFC stacks are assembled at room temperature, then heated up, conditioned and operated at 600...900 °C. Therefore, the mechanical properties of seals should be understood from room temperature to operating temperature. Mechanical properties of SOFC sealing materials were studied with different heat-up procedures.

Increasing cell footprint presents a challenge for the sealing: the higher the cell area, the higher the required compressive force for the stack. To diminish the required compressive force, a hybrid sealing material consisting of a compressible core and a conformable glass-based interlayer was developed. This hybrid sealing material decreased leak rates by 60...90% compared to the conventional compressible seals.

High operating temperature and exposure to both reducing and oxidizing atmospheres is prone to cause corrosion of materials. One example of these corrosion-mechanisms is chromium evaporation from interconnect steel materials. The evaporated chromium is transported in the gas phase to the electrochemically active cell, where it can solidify to chromium oxide, causing loss of performance. A chromium barrier coating based on $MnCo_{1.8}Fe_{0.2}O_4$ was developed and deposited by a high-velocity oxygen flame method on the interconnect steel. The coating showed good stability and low area-specific resistivity, and effectively hindered chromium transport to the electrochemical cell.

ISBN 978-951-38-8313-3 (Soft back ed.)
ISBN 978-951-38-8314-0 (URL: http://www.vtt.fi/publications/index.jsp)
ISSN-L 2242-119X
ISSN 2242-119X (Print)
ISSN 2242-1203 (Online)